Doctoral theses at NTNU, 2020:342

Gunnar Håkonseth

Transient Electric Field Distribution Estimates for Layered Paper-Oil High Voltage Direct Current Insulation

Effects of Slow Polarization and Applicability of Dielectric Response Theory

Doctoral thesis

NTNU
Norwegian University of Science and Technology
Thesis for the Degree of Philosophiae Doctor
Faculty of Information Technology and Electrical Engineering
Department of Electric Power Engineering

NTNU
Norwegian University of Science and Technology

Gunnar Håkonseth

Transient Electric Field Distribution Estimates for Layered Paper-Oil High Voltage Direct Current Insulation

Effects of Slow Polarization and Applicability of Dielectric Response Theory

Thesis for the Degree of Philosophiae Doctor

Trondheim, November 2020

Norwegian University of Science and Technology
Faculty of Information Technology and Electrical Engineering
Department of Electric Power Engineering

NTNU
Norwegian University of
Science and Technology

NTNU
Norwegian University of Science and Technology

Thesis for the Degree of Philosophiae Doctor

Faculty of Information Technology and Electrical Engineering
Department of Electric Power Engineering

© Gunnar Håkonseth

ISBN 978-82-326-5030-9 (printed ver.)
ISBN 978-82-326-5031-6 (electronic ver.)
ISSN 1503-8181

Doctoral theses at NTNU, 2020:342

Printed by NTNU Grafisk senter

Contents

List of Figures vii

List of Tables x

Lists of Symbols and Abbreviations xi

Abstract xv

Preface xvii

1 Introduction 1
- 1.1 Background . . . 1
  - 1.1.1 Long Distance Energy Transmission . . . 1
  - 1.1.2 Mass-Impregnated Cables . . . 1
  - 1.1.3 Increasing the Transmission Capacity of HVDC cables . . . 3
  - 1.1.4 Challenges due to Operation of HVDC Cables . . . 4
- 1.2 Common Approach to Assessing Electric Fields in HVDC Cables . 4
  - 1.2.1 Factors Affecting Electric Fields in HVDC Cables . . . 4
  - 1.2.2 Effect of Cylindrical Geometry . . . 5
  - 1.2.3 Effect of Field-Dependent Conductivity . . . 5
  - 1.2.4 Effect of Temperature Gradient . . . 5
  - 1.2.5 Effect of Changing the Voltage . . . 6
- 1.3 Aim of This Work . . . 7
- 1.4 Outline of the Thesis . . . 8
- 1.5 Terminology . . . 10

2 Theory 11
- 2.1 Basis for Estimating Electric Fields in Layered Insulation . . . 12
- 2.2 El. Fields in Two Materials with Only Instantaneous Polarization 12
- 2.3 Dielectric Response . . . 15
  - 2.3.1 Contribution from Fast Polarization Mechanisms . . . 15

2.3.2 Contribution from Slow Polarization Mechanisms 16
2.3.3 Polarization and Depolarization Currents 18
2.4 Electric Fields in Two Materials with Dielectric Response 19
2.4.1 Two-Material-Input Method 20
2.4.2 One-Material-Input Method 21

3 Experimental Methods **23**
3.1 Electrical Experiments 23
3.1.1 Test Objects 23
3.1.2 Experimental Setup 26
3.1.3 Test Procedure 29
3.2 Scanning Electron Microscopy 30

4 Estimation Methods **31**
4.1 Estimation of Electrical Properties from Measurements 31
4.1.1 Estimation of Permittivities 31
4.1.2 Estimation of Conductivities 32
4.1.3 Estimation of Dielectric Response Functions 34
4.1.4 Interpretation of Time-Dependent Conduction 35
4.2 Estimation of Time-Dependent Electric Fields 37
4.2.1 Ordinary Diff. Eqs. for the Two-Material-Input Method . 37
4.2.2 Ordinary Diff. Eqs. for the One-Material-Input Method . . 39
4.2.3 Type of Numerical Solver for Ordinary Differential Eqs. . 41
4.3 Estimation of Current Density 41
4.4 Measure of Rate of Change of Electric Fields 42

5 Results from Materials Characterization **43**
5.1 Permittivity of Paper 43
5.2 Permittivity of Oil 44
5.3 Conductivity of Paper 45
5.3.1 Results 45
5.3.2 Discussion 47
5.4 Conductivity of Oil 48
5.4.1 Results 48
5.4.2 Discussion 48
5.5 Dielectric Response Function for Paper 51
5.5.1 Results 51
5.5.2 Discussion 53
5.6 Dielectric Response Function for Oil 55
5.6.1 Results 55
5.6.2 Discussion 57

5.7 Structure of Paper 58
5.7.1 Results 58
5.7.2 Discussion 59

6 Results from Estimates and Measurements on a Series Connection Test Object 64
6.1 Results 65
6.1.1 Results from the Two-Material Input Method 65
6.1.2 Results from One-Material-Input Method 68
6.2 Discussion 70
6.2.1 Sensitivity to Dielectric Response Functions 70
6.2.2 Verification of the Two-Material-Input Method 72
6.2.3 Considerations regarding the One-Material-Input Method 74
6.2.4 Comparison with Literature 75
6.2.5 Other Estimation Approaches 75

7 Application to Mass-Impregnated Cables 76
7.1 Considerations regarding Application 76
7.1.1 Cylindrical Geometries and Temperature Gradients 76
7.1.2 Challenges with the One-Material-Input Method 77
7.1.3 Edge Effects 77
7.2 Case Studies 78
7.2.1 Description of Cases 78
7.2.2 Results 80
7.2.3 Discussion 85

8 Main Conclusions 89

9 Suggestions for Further Work 91

Appendix A Approximation to Plane-Parallel Geometry 93

Appendix B Derivation of Equations (4.9)–(4.11) and (5.1)–(5.2) 95
B.1 Derivation of Equations (4.9)–(4.11) 95
B.2 Derivation of Equations (5.1)–(5.2) 97

Appendix C Curve Fitting Technique 98

Appendix D Derivation of Systems of Ordinary Differential Equations 99
D.1 Two-Material-Input Method 99
D.2 One-Material-Input Method 100

Appendix E Equivalence of Integrodiff. and Ordinary Diff. Equations 101
E.1 Two-Material-Input Method 101
E.2 One-Material-Input Method 106

Appendix F Article on Effects of Paper Edges 108

Appendix G List of Publications 115

Bibliography 117

Figures

1.1 Sketch of of cable insulation with four layers of paper tapes . . . 3
1.2 Steady-state electric field distribution in a cable 6

2.1 Equivalent circuit for a series connection of two materials, each characterized by its own permittivity and conductivity 14
2.2 Example of electric field distributions in two-material insulation with constant permittivities and conductivities 14
2.3 Impulse response for polarization 16
2.4 Principle for derivation of equation (2.15) 17
2.5 Equivalent circuit for a series connection of two materials with permittivities, conductivities, and dielectric response functions . 21

3.1 Expanded views of the series connection test objects 25
3.2 Reference plane used for thickness measurements 26
3.3 Expanded views of the single-guard electrode arrangement . . . 27
3.4 Expanded view of the double-guard electrode arrangement . . . 27
3.5 Measurement circuit for polarization and depolarization currents 28

4.1 Determination of median dielectric response functions 35
4.2 Migration of space charge from position x_1 to position x_2 36
4.3 Equivalent electric circuit for a series connection of two insulation materials with dielectric response represented by RC branches . 38
4.4 Equivalent circuit for a series connection of layered insulation where some materials are represented by a “black box” 40

5.1 Conductivity of paper test objects with various numbers of sheets 46
5.2 Conductivity of ten-sheet paper test objects read at different times 46
5.3 Conductivity of paper reported by others 48
5.4 Conductivity of oil 49
5.5 Dielectric response function for paper 52
5.6 Dielectric response function for paper, electric field strengths shown 53

5.7 Dielectric response function for paper measured by others 54
5.8 Dielectric response function for oil 56
5.9 Dielectric response function for oil, electric field strengths shown, polarization 56
5.10 Dielectric response function for oil, electric field strengths shown, depolarization 57
5.11 Scanning electron micrograph of cable paper surface 59
5.12 Scanning electron micrograph of cable paper surface 60
5.13 Scanning electron micrograph of cable paper cross section 60
5.14 Scanning electron micrograph of cable paper cross section 60
5.15 Scanning electron micrograph of cable paper cross section 61
5.16 Scanning electron micrograph of cable paper cross section 61

6.1 Electric fields, series connection test object, voltage on, two-material-input method 66
6.2 Current densities corresponding to figure 6.1 66
6.3 Electric fields, series connection test object, grounding, two-material-input method 67
6.4 Current densities corresponding to figure 6.3 67
6.5 Electric fields, series connection test object, voltage on, one- and two-material-input methods 68
6.6 Electric fields, series connection test object, grounding, one- and two-material-input methods 69
6.7 Electric fields, series connection test object, voltage on, two-material-input method, sensitivity analysis 71
6.8 Current densities corresponding to figure 6.7 71

7.1 Cable insulation model, 15 paper tapes between each butt gap . 79
7.2 Cable insulation model, 2 paper tapes between each butt gap. . 79
7.3 Electric fields in cable insulation, $d_{\mathrm{pap}}/d_{\mathrm{oil}} = 2$, $\overline{E} = 12\,\mathrm{kV/mm}$. 81
7.4 Electric fields in cable insulation, $d_{\mathrm{pap}}/d_{\mathrm{oil}} = 2$, $\overline{E} = 40\,\mathrm{kV/mm}$. 81
7.5 Electric fields in cable insulation, $d_{\mathrm{pap}}/d_{\mathrm{oil}} = 15$, $\overline{E} = 12\,\mathrm{kV/mm}$ 82
7.6 Electric fields in cable insulation, $d_{\mathrm{pap}}/d_{\mathrm{oil}} = 15$, $\overline{E} = 40\,\mathrm{kV/mm}$ 82
7.7 Electric fields in cable insulation, $d_{\mathrm{pap}}/d_{\mathrm{oil}} = 2$, $\overline{E} = 12\,\mathrm{kV/mm}$, polarity reversal 83
7.8 Electric fields in cable insulation, $d_{\mathrm{pap}}/d_{\mathrm{oil}} = 15$, $\overline{E} = 40\,\mathrm{kV/mm}$, polarity reversal 83
7.9 The value t_{90} corresponding to figures 7.3–7.6 84
7.10 The value t_{90} corresponding to figures 7.7–7.8 84

A.1 Closed surface of a sector in a cylindrical symmetric cable 94
A.2 Approximately plane-parallel detail of a cylindrical arrangement 94

Tables

5.1 Thicknesses and capacitances for paper test objects 44
5.2 Relative permittivity of oil 45

6.1 Values of t_{90}, series connection test object, one- and two-material-input methods 69
6.2 Values of t_{90}, series connection test object, voltage on, two-material-input method, sensitivity analysis 70

7.1 Electric fields at steady state. 85

Symbols and Abbreviations

Indices that are used together with several symbols are listed below the list of symbols. Most symbols and indices that only occur close to where they are defined are excluded from the lists. Some of the symbols and indices in appendix F deviate from those in the lists. Units follow the *International System of Units* and are not listed here. Minutes (symbol: min) and hours are used in addition to seconds as units of time.

Symbols

0^+	a value infinitesimally larger than zero
A_i	fitting parameter for the dielectric response function
C	capacitance
D	electric displacement in one dimension
d	thickness
E	electric field strength
$\overline{E}$	mean electric field strength (average over a distance, not time)
E_0	constant electric field strength
$\lvert E_{\mathrm{pap}} \rvert$	absolute value of electric field strength in paper
f	dielectric response function
J	total current density (conduction plus displacement) in one dimension
J_{st}	total current density at steady state
N	number of terms in a linear combination of exponential functions
P	electric polarization
R	resistance
r	radial position
S	effective electrode area
t	time
t_{90}	parameter defined in section 4.4
t_{gnd}	value of t at grounding
t_i	fitting parameter for the dielectric response function
U	voltage
U_0	magnitude of step voltage, constant voltage

$V_{0,\mathrm{a}}$	electric potential above material “a” (see fig. 4.3)
$V_{0,\mathrm{b}}$	electric potential between materials “a” and “b” (see fig. 4.3)
$V_{i,\mathrm{a}}$	electric potential between resistor $R_{i,\mathrm{a}}$ and capacitor $C_{i,\mathrm{a}}$ (see fig. 4.3)
$V_{i,\mathrm{b}}$	electric potential between resistor $R_{i,\mathrm{b}}$ and capacitor $C_{i,\mathrm{b}}$ (see fig. 4.3)
W	Lambert W function
z	argument of the Lambert W function
α	defined in equation (2.29)
β	defined in equation (2.30)
γ	defined in equation (2.31)
ε	permittivity (relating only to fast polarization mechanisms)
ε_0	vacuum permittivity
ε_r	relative permittivity (relating only to fast polarization mechanisms)
η	parameter for the conductivity’s dependency on the electric field
ϑ	Heaviside step function
ξ	integration variable with dimension of time
σ	conductivity
σ_0	parameter for the conductivity’s dependency on the electric field
τ	time constant for approach towards steady state
χ	electric susceptibility (relating only to fast polarization mechanisms)

Indices

$_1$	in position 1
$_2$	in position 2
$_\mathrm{a}$	across/in/of material a
$_\mathrm{b}$	across/in/of material b
$_\mathrm{fast}$	relating to fast (i.e., instantaneous) polarization mechanisms
$_i$	index of summation, term number
$_k$	across/in/of material k, which may be any material
$_\mathrm{mea}$	measured value
$_\mathrm{oil}$	across/in/of oil
$_\mathrm{pap}$	across/in/of impregnated paper
$_\mathrm{slow}$	relating to slow (i.e., not instantaneous) polarization mechanisms

Abbreviations

DC	direct current
HVDC	high voltage direct current
IDE	integrodifferential equation
IEEE	The Institute of Electrical and Electronics Engineers, Incorporated
ODE	ordinary differential equation
ODEs	ordinary differential equations (plural)
PDC	polarization and depolarization currents
PTFE	polytetrafluoroethylene (Teflon)

Abstract

The aim of this work is to contribute to an increased capacity of mass-impregnated, high voltage direct current (HVDC) cables. This has been done by providing a better understanding of the transient electric field distribution between impregnated paper and oil-filled butt gaps. The focus is in particular how this field distribution is affected by the dielectric response functions of oil and impregnated paper.

In this work, mass-impregnated HVDC insulation was modeled mathematically as a series connection of two materials, namely oil and impregnated paper. The model was based on linear dielectric response theory. A system of differential equations for estimating the time-dependent electric field distribution and the current density was established as part of the model. The input parameters to the model were thickness, high-frequency permittivity, steady-state conductivity, and dielectric response function for each material separately, as well as the applied voltage across the whole series connection. The dielectric response functions were here used to represent any polarization and conduction processes that were not represented by the high-frequency permittivities or steady-state conductivities. The model was used to estimate electric field distributions in plane-parallel, mass-impregnated insulation with and without dielectric response functions considered.

An air-tight, temperature-controlled container was equipped with necessary piping, bushing, and electrodes for vacuum drying, impregnating, and electrical testing of plane-parallel test objects. The test objects were made of paper and oil of qualities typically used for mass-impregnated cables. Some of the test objects contained impregnated paper, some contained only oil, and some contained an oil gap between stacks of paper. A test circuit for applying step voltages and measuring the resulting polarization and depolarization currents was built and connected to the electrodes via the bushing. Dielectric response functions and steady-state conductivities were determined from the polarization and depolarization currents for oil and impregnated paper separately. This was done at 50 °C with electric field strengths ranging from 0.3 to 7 kV/mm for oil and from

0.2 to 40 kV/mm for impregnated paper. The permittivity for each material was determined from measurements at 1 kHz and 0.7 V_{rms}. The measured electrical properties were used as input to the abovementioned model. Furthermore, polarization and depolarization currents were measured in a 2.5 mm thick plane-parallel series connection, i.e. an oil gap between stacks of paper, at 30.6 kV. The measured currents in the series connection were compared with currents estimated by the model. To ensure that the comparison was relevant, the currents in the series connection and the electrical properties used as input to the model were measured under as similar conditions as possible. Paper without impregnation was studied with scanning electron microscopy to assess its internal, porous structure.

The agreement observed between measured and estimated currents indicates that linear dielectric response theory is adequate for estimating the transient electric field distribution between layers of oil gaps and impregnated paper. Further, it was found that the dielectric response functions strongly affect how fast steady state is approached. For example, in a particular piece of insulation at 50 °C, the estimated time needed for ninety percent of the change from initial to steady-state electric field distribution to take place was at least twice as long when dielectric response functions were taken into account than when they were neglected. Further, it was observed a trend that the time needed for this change to take place decreases and becomes less affected by the dielectric response functions as the ratio of total paper thickness to total oil gap thickness in the insulation is increased. The scanning electron microscopy showed that typical thicknesses of interstices between paper fibers were less than 15 % of the paper sheet thicknesses. This confirmed that oil gaps in such interstices are much smaller than butt gaps and thus can be modeled as part of the impregnated paper.

Preface

This thesis is submitted in partial fulfillment of the requirements for the degree of Philosophiae Doctor (PhD) at the Norwegian University of Science and Technology (NTNU).

This work is part of the project *Mass Impregnated Non-Draining HVDC Submarine Cables*, led by Nexans Norway AS. The project is financially supported by The Research Council of Norway (Norges forskningsråd), Nexans Norway AS, Statnett SF, Affärsverket svenska kraftnät, and Fingrid Oyj. The project has project number 256405 within the ENERGIX program of The Research Council of Norway.

The majority of my time working on this PhD project was spent in Halden, at the premises of my employer, Nexans Norway AS. I also spent a year on campus in Trondheim, approximately 600 km north of Halden. It was in Trondheim that most of my compulsory coursework was conducted.

I would like to thank Nexans for allowing me to undertake this work. I would also like to thank my main supervisor at the Norwegian University of Science and Technology (NTNU), Erling Ildstad, and my co-supervisors, Frank Mauseth (NTNU) and Knut Magne Furuheim (Nexans), for their guidance and encouragement. Furthermore, I would like to thank people at NTNU and SINTEF Energy Research (SINTEF Energi AS) for their valuable discussions and practical help. Special thanks go to Lars Erik Pettersen, who performed some of the electrical experiments as part of his work for his master's thesis at NTNU.

One person who has worked very hard throughout this project is my dear wife Lillian. You even moved with me and our three children (Now we have four!) from Halden to Trondheim and back again for this project. You deserve the greatest thanks for all your encouragement, flexibility, and support.

Halden, June 2020

Gunnar Håkonseth

Chapter 1

Introduction

1.1 Background

1.1.1 Long Distance Energy Transmission

High voltage direct current (HVDC) cables transport large amounts of electric energy over long distances. A typical HVDC cable carries several hundred megawatts across several hundred kilometers [1]. Some examples of HVDC cable links are from Norway to Denmark [1]–[3], Norway to the Netherlands [4], Great Britain to the Netherlands [5], Sweden to Germany [6], Sweden to Poland [7], Sardinia to the Italian mainland [8], Greece to Italy [8], and Tasmania to the Australian mainland [9]. The longest of these is the 580 km link between Norway and the Netherlands [4].

Across wide and deep bodies of water, overhead transmission lines are not feasible, and the use of cables is the only solution. Cables are sometimes preferred to overhead lines onshore as well, in attempt to reduce public objections to power grid expansion [10].

Long alternating current transmission lines involves high losses due to large capacitive charging and discharging currents. Use of direct current (DC) avoids this problem, and is therefore preferred for long distances. Another advantage of DC is that it enables the interconnection of power grids whose frequencies are not synchronized with one another [4], [11], [12].

1.1.2 Mass-Impregnated Cables

A much used HVDC cable insulation type is mass-impregnated paper. It is believed that a pair of mass-impregnated cables put in service in Lyon in 1907 were the world's first truly commercial HVDC cables [13], [14]. The first subsea

mass-impregnated HVDC cable was installed between Gotland and the Swedish mainland in 1954 [3]. All of the HVDC links indicated in section 1.1.1 have cables of this type [1]–[9].

Mass-impregnated paper insulation is made by wrapping approximately 2 cm wide, pre-dried paper tapes helically around the conductor. The paper tapes consist solely of electrotechnical paper that is cut to the desired tape with. The lay length of the paper tapes is slightly larger than the tape width so that a 1–4 mm wide gap is left between the tapes. This gap is called a *butt gap* and accommodates the bending of the cable without jamming the paper tapes. Typically a few hundred layers of paper tapes are wrapped around each other. Each layer is staggered with respect to the layer it surrounds so that the butt gaps of adjacent layers do not coincide with each other. The lay direction is reversed at certain radial positions of the insulation, typically every twelve to sixteen layers, to avoid torsion in the cable. The inner- and outermost layers consist of conductive paper to ensure an electrically smooth transition from conductive metal to insulating paper. After additional drying under vacuum, the paper-wrapped conductor is impregnated with *mass*, a high-viscosity compound based on mineral oil [4], [5]. The mass will henceforth be called *oil*.

The internal structure of the paper tapes is irregular with fibers that were originally hollow but have collapsed and fibrillated from the pulp refinement process. There is thus a network of "channels" in between the fibers. When the paper is impregnated, these channels are filled with oil. Moreover, the paper surface roughness causes contact to occur at discrete spots [15], creating further room for oil between these spots. The room between such spots and the oil therein are henceforth called *intersheet gap* and *intersheet oil*, respectively. The oil also fills the butt gaps. The impregnated paper and the oil-filled butt gaps constitute the electrical insulation. A sketch of such cable insulation is demonstrated in figure 1.1.

A lead sheath encompasses the electrical insulation in mass-impregnated cables and acts as a water barrier. It also acts as grounding. Various components are applied outside of the metallic sheath, mainly for mechanical and anti-corrosion purposes.

Mass-impregnated cables are referred to as "nondraining", since the high viscosity prevents the oil from draining to lower sections of the cable [17].[1] In reality, production constraints and thermal contraction prevents this ideal. The cable is impregnated while being warm (typically around 120 °C). When the cable cools, the oil contracts more than the paper due to different thermal

[1] Other types of paper-insulated cables make use of low-viscosity oil that is kept pressurized by onshore pressurizing units. In such cables, the oil is allowed to flow in and out of the cable at the pressurizing units as the oil expands or contracts due to temperature variations [4].

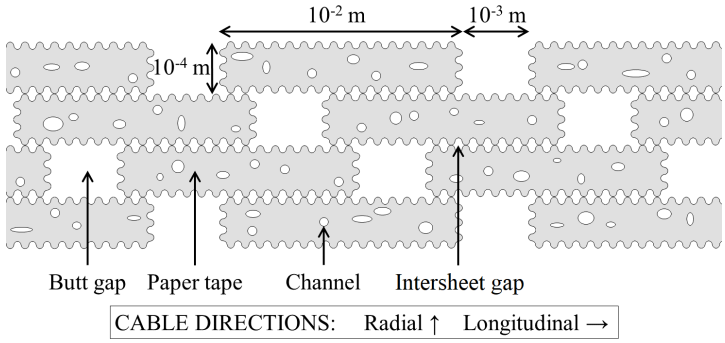

Figure 1.1: Skecth of cable insulation with four layers of paper tapes. The sketch is not to scale. Original figure published in [16], ©2019 IEEE, reproduced in modified form with permission.

expansion coefficients, and the oil cavitates. Cavities decrease the breakdown strength of the cable. Some or all of the cavities disappear when the temperature is raised again [4]–[6], [18], [19].

Mass-impregnated insulation is regarded to be a proven technology [20]. The insulation system is durable. A dissection of a piece of cable after forty-five years of service displayed no significant change in degree of polymerization (an ageing indicator) of the insulation paper [21].

1.1.3 Increasing the Transmission Capacity of HVDC cables

There are two basic ways of increasing the transmission capacity of mass-impregnated cables: increasing the voltage capacity or increasing the current capacity. An increased voltage leads to higher electric field strengths in the insulation. An increased current leads to more heat being generated in the conductor, unless the conductor resistance is lowered by increasing its cross-sectional area. The temperature has an effect on the electric field distribution in the insulation. An increased temperature gradient will typically lead to a larger difference between the maximum and minimum electric field strength, with the highest field strength in the coldest part of the insulation [22].

If all other parameters are constant, an increased insulation thickness lowers the electric field strengths. Therefore, the effects of increasing the voltage or current can to some extent be compensated for by increasing the diameter of the insulation. However, this increases raw materials consumption, production costs, and installation costs.

This means that, in many cases, an increased transmission capacity will involve an increased electric field strength in the insulation. This again means

that the insulation will operate closer to its limit in terms of breakdown strength. Knowledge about the electric fields is therefore important when increasing the transmission capacity of HVDC cables.

1.1.4 Challenges due to Operation of HVDC Cables

Normal operation of HVDC cables involves changing the voltage in several ways: switching the voltage on, switching it off, and reversing its polarity. Such changes in voltage results in transients in the electric field strength distribution. Large electric field transients are critical situations for the insulation.

The polarity occasionally is reversed in order to reverse the direction of power flow in the cable.[2] The desired direction of power flow in HVDC cables typically depends on supply and demand in the interconnected grids. With an increased share of renewable sources in the energy mix, the energy supply is likely to change frequently due to the intermittent nature of wind and solar power. Where HVDC links connect areas of renewable power generation with areas of balancing power generation, frequent changes to the supply–demand situation leads to a frequent need for reversing the power flow in the HVDC link [29]–[31].

1.2 Common Approach to Assessing Electric Fields in HVDC Cables

When assessing electric fields in HVDC cables, a common approach is to model the insulation as a single material and neglect any inhomogeneities except those due to temperature gradients [22], [32]–[34]. Some major concepts in such assessments are presented in the following sections (i.e., sections 1.2.1–1.2.5).

1.2.1 Factors Affecting Electric Fields in HVDC Cables

The electric field distribution in a HVDC cable is dependent on voltage, the insulation's geometry, the insulation's electrical properties, and time. Immediately after a step voltage is applied across the insulation (i.e., the voltage is turned on), the electric field distribution is governed by the permittivities of the various regions of the insulation and is called a *capacitive* field distribution. It then

[2] The power flow direction can be reversed either by reversing the voltage or by reversing the current. Which of these techniques is used depends on the type of converter stations that feed the HVDC cable [23], [24]. All of the HVDC links mentioned in chapter 1.1.1 have converter stations that depend on voltage polarity reversal for reversing power flow [25]–[27], except for one of the four cables between Norway and Denmark [28].

approaches a steady-state distribution that is governed by the conductivities of the insulation's various regions and is called a *resistive* field distribution [35].

1.2.2 Effect of Cylindrical Geometry

When the electrical properties of the insulation in cylindrical cables are homogeneous, the electric field distribution depends on the voltage and the cylindrical geometry alone, and the electric field E as a function of radial position r is [35]

$$E(r) = \frac{U}{r \ln \frac{r_{\text{out}}}{r_{\text{in}}}}. \tag{1.1}$$

Here, U is the voltage, r_{out} is the outer radius of the insulation, and r_{in} is the inner radius of the insulation.

1.2.3 Effect of Field-Dependent Conductivity

The conductivity increases when the electric field strength is raised. If the conductivities at two radial positions r_1 and r_2 are σ_1 and σ_2, respectively, the ratios between the electric fields E_1 and E_2 in those positions can be expressed as [36]

$$\frac{E_1}{E_2} = \frac{\sigma_2 r_2}{\sigma_1 r_1}. \tag{1.2}$$

This reduces the dependency described by equation (1.1) [22].

1.2.4 Effect of Temperature Gradient

When a cable carries a current, resistive heating in the conductor and cooling from the cable's surroundings create a temperature gradient across the insulation. Since the conductivity for typical insulation materials (such as paper and oil) increases with increasing temperature, the temperature gradient results in a conductivity gradient that points in the same direction. The higher conductivity in the warm region close to the conductor reduces the steady-state electric field strength in that region. Conversely, the lower conductivity close to the insulation screen increases the steady-state electric field there. Depending on the temperature gradient, this may cause the electric field strength to be highest near the insulation screen where the temperature and conductivity are lowest [22], [32], [35]. This phenomenon is called field inversion [37] and is illustrated in figure 1.2.

The permittivity of mass-impregnated paper insulation is hardly influenced by temperature [38] and is often assumed homogeneous even in the presence of a temperature gradient [22], [39].

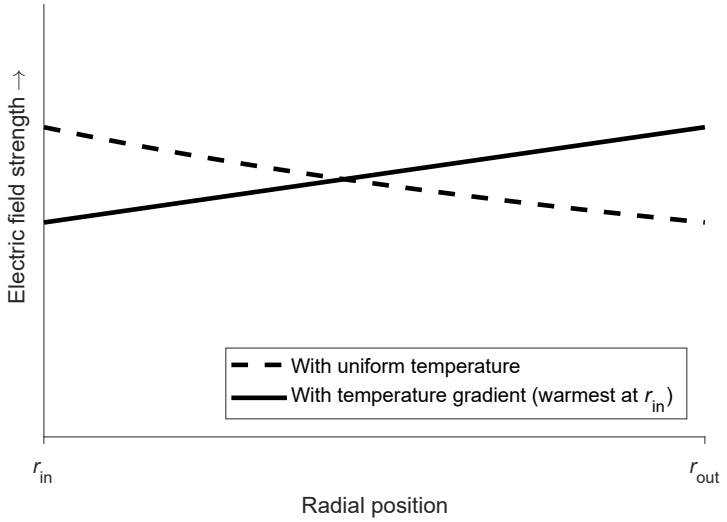

Figure 1.2: Steady-state electric field distribution in a cable with and without temperature gradient.

1.2.5 Effect of Changing the Voltage

In the capacitive field distribution, which occurs immediately after the voltage is turned on, equation (1.2) is valid with the conductivities replaced [35] by permittivities ε:

$$\frac{E_1}{E_2} = \frac{\varepsilon_2 r_2}{\varepsilon_1 r_1}. \tag{1.3}$$

In the case of uniform permittivity across the insulation (which is the normal assumption [22], [39]), equation (1.3) is in agreement with equation (1.1). The electric field distribution will then gradually transition to a resistive distribution as explained above.

During the transition from capacitive to resistive field distribution, space charge accumulates in the insulation due to the conductivity gradient.[3] When the voltage is subsequently turned off, the space charges are still present and need some time to dissipate [22]. In practice, turning off the voltage can be considered to superimpose a negative capacitive field distribution on the resistive field distribution. If the resistive electric field as a function of the radial position r is $E_{\text{res}}(r)$ and the capacitive electric field is $E_{\text{cap}}(r)$, the resulting, total electric field immediately after the voltage is turned off is [22]

$$E(r) = E_{\text{res}}(r) - E_{\text{cap}}(r). \tag{1.4}$$

[3] A conductivity gradient caused by a temperature gradient is here assumed. In the case of uniform permittivity and conductivity, the electric field obeys equation (1.1) continuously.

The electric field throughout the cable subsequently approaches zero.

Also a polarity reversal superimposes a capacitive field distribution onto the existing distribution, but with a magnitude twice as large as when the voltage is turned off. Immediately after the reversal,

$$E(r) = E_{\text{res}}(r) - 2E_{\text{cap}}(r). \tag{1.5}$$

The maximum value of the absolute value of the electric field is typically higher immediately after polarity reversal than at steady state or immediately after turning on or off the voltage. The maximum absolute value immediately after polarity reversal is found close to the conductor [22].

The electric field distribution in the intermediate period from when the voltage is turned on, reversed, or turned off until steady state is reached is more complicated. Other authors have studied this transient electric field for mass-impregnated cable insulation that, apart from temperature gradients and resulting gradients in electrical properties, has been considered homogeneous. This has involved solving the current continuity equation and Gauss's law numerically [22], [32].

1.3 Aim of This Work

The aim of this work is to obtain a better understanding of the time-dependent electric field distribution between butt gaps and impregnated paper. The focus is on modeling slow polarization mechanisms and their importance for the electric field distribution.

Impregnated paper will be considered a homogeneous material whose electrical properties are given by the combined action of the paper fibers and the oil in between those fibers. Intersheet oil (see section 1.1.2) will also be regarded as part of the impregnated paper, whereas the oil in the butt gaps will not. This limits the scope to include two materials only: oil in butt gaps and impregnated paper elsewhere.

The primary research questions are as follows:

- How can linear dielectric response theory be utilized for estimating transient electric field distributions between the materials in layered, two-material HVDC insulation?
- Is the answer to the question above applicable to cases where the two materials are oil and impregnated paper?
- What is the effect of dielectric response functions on the time-dependent electric field distribution between oil and impregnated paper?

1.4 Outline of the Thesis

The thesis is organized as follows:

Chapter 1 (Introduction) gives an introduction to HVDC cables in general and mass-impregnated HVDC cables in particular, with emphasis on the structure of the insulation. It points out that knowledge about the electric fields in the insulation is important when the transmission capacity of such cables is to be increased. Chapter 1 provides in this way the background for the research that is presented in the rest of the thesis. Further, it presents common ways of assessing the electric fields when the structure of the insulation is neglected. Subsequently, this chapter states the aim and the research questions for the work, as well as an outline of the thesis. It ends with an important note about the terminology used in the rest of the thesis.

Chapter 2 (Theory) provides the theory upon which this work is based. In particular, it reviews the basics of linear dielectric response theory and explains how dielectric response functions represent slow polarization mechanisms. Furthermore, it establishes equations for estimating electric fields and current densities in series connections of two materials—with and without dielectric response functions taken into account. These equations are the basis for the model for the electric fields and current densities in the two materials. The model includes two slightly different methods for estimating the electric fields, differing in which input parameters are required for the equations.

Chapter 3 (Experimental Methods) describes the test objects and experimental procedures used in this work. The experiments served three purposes:

- to provide the model with the necessary input (i.e., properties of the materials)
- to provide measured current densities for a series connection of oil and impregnated paper to compare with estimated current densities for verification of the model
- to investigate the internal, porous structure of paper to assess whether or not it is reasonable to consider oil-filled butt gaps without also considering the oil inside the paper

Chapter 4 (Estimation Methods) starts by detailing how the electrical properties were determined, based on the electrical measurements. This includes

explicating how the dielectric response functions represent not only slow polarization but also other phenomena. This is an important concept in the model for estimating electric fields and current densities. The chapter moves on to describe how the equations of chapter 2 were converted to a more convenient form and solved, and how electric fields as well as current densities were obtained from the solutions. Finally, it establishes a measure of how fast steady-state electric field distributions are approached.

Chapter 5 (Results from Materials Characterization) presents the measured electrical properties for oil and impregnated paper, as well as the results from the assessment of the internal structure of the paper. The electrical properties are in subsequent chapters used as input for the model for estimating electric fields and current densities.

Chapter 6 (Results from Estimates and Measurements on a Series Connection Test Object) has two primary purposes: demonstrate the effects of the dielectric response functions and to demonstrate the reliability of the methods used to estimate electric fields. All the estimates and measurements presented in chapter 6 relate to a plane-parallel test object in which an oil gap is situated between two stacks of impregnated paper (i.e., a *series connection test object*). The first purpose is fulfilled by presenting estimates of electric fields and current densities with and without dielectric response functions taken into account, as well as presenting a sensitivity analysis where the dielectric response functions used as input are varied. The second purpose is fulfilled by comparing estimated and measured current densities in the series connection test object (see the second bullet point for chapter 3 above).

Chapter 7 (Application to Mass-Impregnated Cables) outlines how these methods can be applied to mass-impregnated cables under test or operating conditions. The chapter also presents case studies of transient electric field distributions in series connections of the same type as the one used in chapter 6, but where values of the ratio between the thicknesses of the paper section and the oil gap are relevant to mass-impregnated cables. The chapter gives an account of how fast steady state is approached in various cases and discusses the implications of these results for mass-impregnated cables.

Chapter 8 (Main Conclusions) lists the main conclusions of the thesis.

Chapter 9 (Suggestions for Further Work) lists suggestions for further investigating the electric field distributions between oil and impregnated paper, in particular in mass-impregnated HVDC cables, based on the principles presented in this thesis.

1.5 Terminology

The term *paper* is henceforth used for *impregnated paper*, and the terms *field* and *field strength* for *electric field (strength)*, unless otherwise stated. The term *current* (or *current density*) is used for the sum of the conduction current (density) and the displacement current (density).

Chapter 2

Theory

This chapter presents theory relating to electric fields and dielectric response in layered insulation. The layers are here considered to be plane-parallel.[1] Edge effects are not considered. The vectors of current density, electric field, and electric displacement are thus assumed parallel to the radial direction and perpendicular to the interfaces [35]. Only the radial dimension is hence considered. Furthermore, each layer is assumed to be homogeneous and in perfect electrical contact (i.e., there is no transition resistance) with its neighboring layers. Propagation times for electromagnetic waves are assumed to be negligible. These assumptions imply that the electric field is assumed to be homogeneous within each layer and that the electric field is equal in all materials of the same material [35]. Therefore, several layers of the same material can be treated as a single layer whose thickness is the sum of the thicknesses of the individual layers of that material—even if those layers are separated by other materials. It is thus possible to refer *materials* instead of *layers*, and each material can be considered as a component in a series connection. This will be implemented in the following.

[1] As explicated in appendix A, plane-parallelism is a good approximation when considering a few adjacent, thin layers in a cylindrically symmetric cable.

2.1 Basis for Estimating Electric Fields in Layered Insulation

The time-dependent electric fields in layered insulation can be established from the principles that the current density J is equal in[2] all materials and that the sum of voltages across all materials equals the applied voltage across the whole series connection [40]. This presupposes that an expression for the current density as a function of electric field and time is known for each material. The current density is commonly expressed as

$$J = \sigma E + \frac{\mathrm{d}D}{\mathrm{d}t}. \tag{2.1}$$

The displacement D is defined as [41]

$$D = \varepsilon_0 E + P, \tag{2.2}$$

where ε_0 is the vacuum permittivity, and where the polarization P is generally dependent on both the electric field and time [42].

2.2 Electric Fields in Two Materials with Only Instantaneous Polarization

A commonly used relation between the displacement and the electric field is

$$D(t) = \varepsilon E(t), \tag{2.3}$$

which is valid and consistent with the definition (equation (2.2)) in cases where all the polarization is regarded as instantaneous.[3] This transforms equation (2.1) into

$$J(t) = \sigma E(t) + \varepsilon \frac{\mathrm{d}E}{\mathrm{d}t}. \tag{2.4}$$

A system of two materials (i.e., “a” and “b”) where this is the case is here considered. Each material has a total thickness of d_a and d_b, respectively. The current densities are the same in both materials, so

$$\sigma_\mathrm{a} E_\mathrm{a}(t) + \varepsilon_\mathrm{a} \frac{\mathrm{d}E_\mathrm{a}(t)}{\mathrm{d}t} = \sigma_\mathrm{b} E_\mathrm{b}(t) + \varepsilon_\mathrm{b} \frac{\mathrm{d}E_\mathrm{b}(t)}{\mathrm{d}t}. \tag{2.5}$$

[2] The current density J is the sum of the conduction current density and the displacement current density. Although part of the displacement current in the case of a changing electric field does not actually flow *inside* the material (there is a net charge accumulation at the boundaries of the insulation), the preposition *in* is used for brevity both here and in similar contexts throughout the thesis.

[3] Details are given in section 2.3.1.

Since the total voltage is the sum of voltages across each material,

$$E_{\mathrm{b}}(t) = \frac{U(t) - d_{\mathrm{a}} E_{\mathrm{a}}(t)}{d_{\mathrm{b}}}. \tag{2.6}$$

The combination of equations (2.5) and (2.6) provides the ordinary differential equation [43], [44]

$$\frac{\mathrm{d}E_{\mathrm{a}}(t)}{\mathrm{d}t} = \frac{\sigma_{\mathrm{b}} U(t) + \varepsilon_{\mathrm{b}} \frac{\mathrm{d}U}{\mathrm{d}t}}{d_{\mathrm{a}}\varepsilon_{\mathrm{b}} + d_{\mathrm{b}}\varepsilon_{\mathrm{a}}} - \frac{d_{\mathrm{a}}\sigma_{\mathrm{b}} + d_{\mathrm{b}}\sigma_{\mathrm{a}}}{d_{\mathrm{a}}\varepsilon_{\mathrm{b}} + d_{\mathrm{b}}\varepsilon_{\mathrm{a}}} E_{\mathrm{a}}(t). \tag{2.7}$$

In cases where the permittivities and conductivities are constant (i.e., independent of both time and electric field), the system can be represented by the equivalent electric circuit shown in figure 2.1. A step voltage of magnitude U_0 applied at $t = 0$ can be described as

$$U(t) = U_0 \vartheta(t), \tag{2.8}$$

where $U(t)$ is the time-dependent voltage and $\vartheta(t)$ is the Heaviside step function. When the voltage is a step voltage, as indicated, and the conductivities and permittivities are constant, the solution to equation (2.7) is [43]

$$E_{\mathrm{a}}(t) = \frac{\sigma_{\mathrm{b}} U_0}{d_{\mathrm{a}}\sigma_{\mathrm{b}} + d_{\mathrm{b}}\sigma_{\mathrm{a}}} \left(1 - \mathrm{e}^{-t/\tau}\right) + \frac{\varepsilon_{\mathrm{b}} U_0}{d_{\mathrm{a}}\varepsilon_{\mathrm{b}} + d_{\mathrm{b}}\varepsilon_{\mathrm{a}}} \mathrm{e}^{-t/\tau} \quad \text{for} \quad t > 0, \tag{2.9}$$

where the time constant

$$\tau = \frac{d_{\mathrm{a}}\varepsilon_{\mathrm{b}} + d_{\mathrm{b}}\varepsilon_{\mathrm{a}}}{d_{\mathrm{a}}\sigma_{\mathrm{b}} + d_{\mathrm{b}}\sigma_{\mathrm{a}}}. \tag{2.10}$$

The electric field in the other material, $E_{\mathrm{b}}(t)$, can be determined by using equation (2.6) or by simply swapping the indices $_{\mathrm{a}}$ and $_{\mathrm{b}}$. Equation (2.9) indicates that the electric field distribution goes from being dominated by the permittivities to being dominated by the conductivities. Electric fields according to this equation are shown in the "voltage on" segment of figure 2.2. The other parts of figure 2.2 exhibit the electric fields after polarity reversal and grounding; these sections are also solutions to equation (2.7). As is evident in equation (2.10), increasing the ratio $d_{\mathrm{a}}/d_{\mathrm{b}}$ brings the time constant closer to the limit $\varepsilon_{\mathrm{b}}/\sigma_{\mathrm{b}}$. Furthermore, it can be demonstrated from equation (2.9) that when $d_{\mathrm{a}}/d_{\mathrm{b}}$ increases, the ratio between the initial and steady-state values of E_{a} becomes closer to unity.[4]

[4]This can be achieved by demonstrating both that the ratio $G = E_{\mathrm{a}}(0^+)/E_{\mathrm{a}}(\infty)$ is either strictly increasing or strictly decreasing (i.e., G does not oscillate) as the ratio $K = d_{\mathrm{a}}/d_{\mathrm{b}}$ increases and that $G \to 1$ as $K \to \infty$. The former can be accomplished by showing that $\mathrm{d}G/\mathrm{d}K \neq 0$ unless $\sigma_{\mathrm{a}}\varepsilon_{\mathrm{b}} = \sigma_{\mathrm{b}}\varepsilon_{\mathrm{a}}$. (In the case of $\sigma_{\mathrm{a}}\varepsilon_{\mathrm{b}} = \sigma_{\mathrm{b}}\varepsilon_{\mathrm{a}}$, $G = 1$ regardless the value of K.) The latter can be accomplished by showing that $G = \varepsilon_{\mathrm{b}}(K\sigma_{\mathrm{b}} + \sigma_{\mathrm{a}})/\sigma_{\mathrm{b}}(K\varepsilon_{\mathrm{b}} + \varepsilon_{\mathrm{a}})$ and applying l'Hôpital's rule [45] to that expression.

A similar approach can be employed to demonstrate that increasing K always brings τ closer to $\varepsilon_{\mathrm{b}}/\sigma_{\mathrm{b}}$.

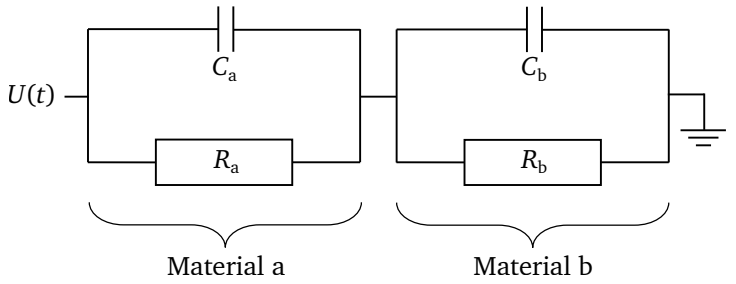

Figure 2.1: Equivalent circuit for a series connection of two materials, each characterized by its own permittivity and conductivity. The permittivities and conductivities are here represented by capacitances C and resistances R, respectively.

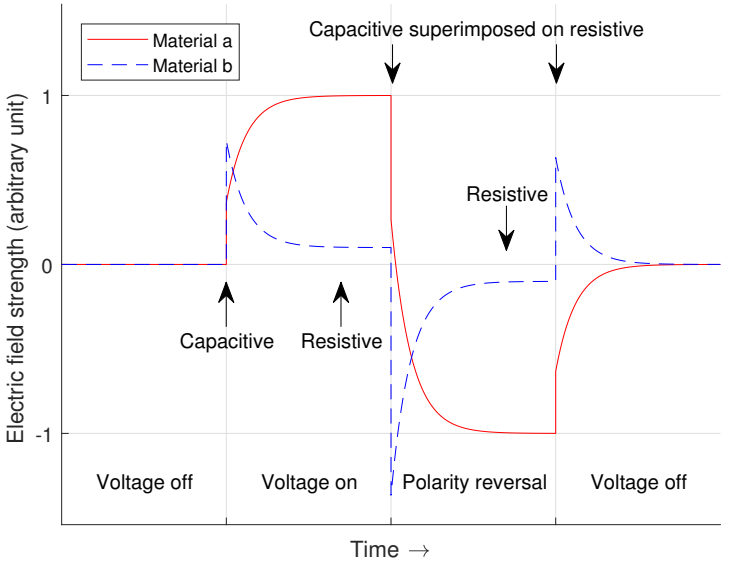

Figure 2.2: Electric fields caused by voltage application, polarity reversal, and grounding of a two-material insulation. Example with constant permittivities and conductivities, $\varepsilon_b = \frac{1}{2}\varepsilon_a$, $\sigma_b = 10\sigma_a$, and $d_b = d_a$. Capacitive, resistive, and superimposed electric field distributions are indicated.

For any layered system of two insulation materials (not only those where all the polarization is instantaneous), charges accumulate at the interface(s) between the materials as steady state is approached. When the voltage is suddenly changed, the interface charges remain and contribute to the electric field distribution. The interface charge density then gradually adjusts to the new voltage and establishes a new steady state. When the voltage is turned off, the total voltage becomes zero, but the voltage across each of the two materials is nonzero, equal in magnitude but with polarities that are opposite each other. The voltage across each of the materials eventually decays to zero; so too does the interface charge density [43]. This is the scenario displayed in the rightmost section of figure 2.2.

2.3 Dielectric Response

Some polarization mechanisms are fast enough to be considered as instantaneous (henceforth called *fast*), whereas other polarization mechanisms (henceforth called *slow*) require a considerable amount of time to complete. It is useful to account for fast and slow polarization separately [40]. The total, time-dependent polarization $P(t)$ can be expressed as

$$P(t) = P_{\text{fast}}(t) + P_{\text{slow}}(t), \tag{2.11}$$

where $P_{\text{fast}}(t)$ and $P_{\text{slow}}(t)$ are the contributions from the fast and slow polarization mechanisms, respectively. Where to set the limit between fast and slow is a question of which time scale is of interest. It may also be a question of experimental limitations [46]. In high voltage engineering, polarization mechanisms that are able to follow the electric fields at power frequencies are often regarded as fast [40], [47], [48].

2.3.1 Contribution from Fast Polarization Mechanisms

Fast polarization can be accounted for by a susceptibility χ [48]:

$$P_{\text{fast}}(t) = \varepsilon_0 \chi E(t). \tag{2.12}$$

The susceptibility χ, the permittivity ε, and the relative permittivity ε_{r} relate to each other as follows:

$$1 + \chi = \frac{\varepsilon}{\varepsilon_0} = \varepsilon_{\text{r}}. \tag{2.13}$$

Since χ in the following relates to fast polarization, ε and ε_{r} also relate to fast polarization. This principle is maintained throughout this thesis.

In cases where all the polarization is fast, such as the case considered in section 2.2, equations (2.2), (2.12), and (2.13) together imply that $D(t) = \varepsilon_0 E(t) + P(t) = \varepsilon_0 E(t) + \varepsilon_0 \chi E(t) = \varepsilon_0(1+\chi)E(t) = \varepsilon_0 \varepsilon_r E(t) = \varepsilon E(t)$.

2.3.2 Contribution from Slow Polarization Mechanisms

Slow polarization has a time-dependency beyond the time-dependency of the electric field. The *dielectric response function* $f(t)$ describes this time-dependency, and can be defined for a dielectric material that satisfies the following criteria:

- The material is homogeneous.
- The polarization is linear with respect to the electric field that causes the polarization.

A corollary to the second assumption is that the superposition principle holds: the response to consecutive excitations is the sum of the response to the individual excitations.

An electric field impulse can be described by the electric field strength E and the short time period $\mathrm{d}t$ over which the electric field is acting. The dielectric response function can be defined in terms of the vacuum permittivity ε_0 and the response of the slow polarization $P_{\text{slow,imp}}$ to an impulse of strength $E\,\mathrm{d}t$ applied at the time $t = 0$:

$$P_{\text{slow,imp}}(t) = \varepsilon_0 f(t) E\,\mathrm{d}t. \tag{2.14}$$

This is illustrated in figure 2.3. The linearity implies that f is independent of E [42].

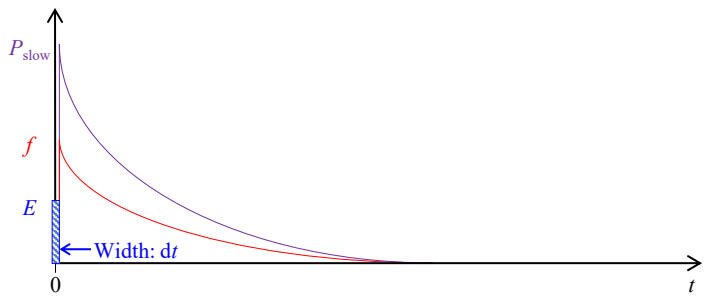

Figure 2.3: Impulse response for polarization.

The polarization at a time t due to an electric field impulse of width $\mathrm{d}\xi$ that occurred at the time $t-\xi$ can then be written as $P_{\text{slow,imp}}(t) = \varepsilon_0 f(\xi) E(t-\xi)\mathrm{d}\xi$ as illustrated in figure 2.4. A time-dependent electric field can be viewed as

many consecutive impulses whose values of E differ from each other. Because of the superposition principle, $P_{\text{slow}}(t)$ at a time t is the sum of the contributions from all those impulses and can be found by integrating $\varepsilon_0 f(\xi)E(t-\xi)\,\mathrm{d}\xi$ over all times. Because of causality, $f(\xi) = 0$ for $\xi < 0$, so the lower integration limit can be set to zero instead of $-\infty$. It will henceforth be assumed that there is no electric field before $t = 0$, so $E(t-\xi)$ vanishes when ξ exceeds t, and the upper integration limit can be set to t instead of ∞. The integral then becomes

$$P_{\text{slow}}(t) = \varepsilon_0 \int_0^t f(\xi)E(t-\xi)\,\mathrm{d}\xi, \tag{2.15}$$

which is mathematically equivalent to[5] to

$$P_{\text{slow}}(t) = \varepsilon_0 \int_0^t E(\xi)f(t-\xi)\,\mathrm{d}\xi. \tag{2.16}$$

The choice of which of these two equations to use is a matter of convenience.

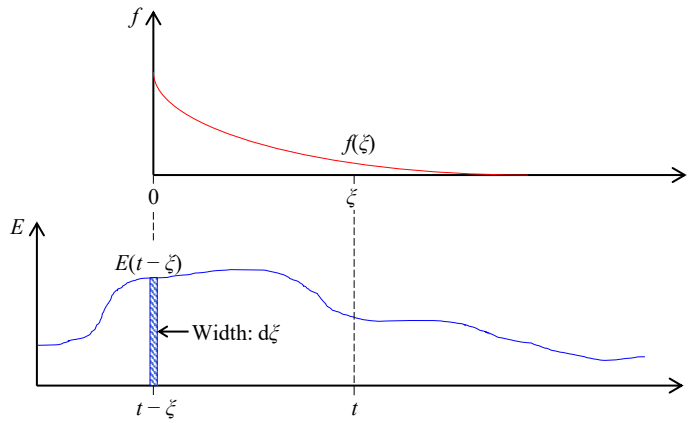

Figure 2.4: Principle for derivation of equation (2.15). At the time t, the total dielectric response function has had the time ξ to act on the impulse at $t-\chi$. Illustration idea from [42].

The integral in equation (2.16) is referred to as the *convolution* of E and f.[6]

[5]The equivalence can be proved by substituting ζ for $t-\xi$ in the integrand, writing the integration limits in terms of ζ instead of ξ so that $\int_{\xi=0}^{\xi=t}$ becomes $\int_{\zeta=t}^{\zeta=0}$, then using that $\mathrm{d}\zeta = -\mathrm{d}\xi$ and that $-\int_t^0 \ldots = \int_0^t \ldots$, and lastly renaming ζ to ξ.

[6]The lower integration limit of a convolution is often $-\infty$ and the upper limit ∞, but, as previously indicated, the integrand is 0 both for $\xi < 0$ and for $\xi > t$, so extending the limits to $\pm\infty$ does not change the value of the integral.

The physical implication of this convolution integral is that the dielectric system has a "memory"; its state in the present depends on its state in the past [42].

In materials where the polarization is induced only by the applied electric field, namely where there is no permanent polarization, $f(t) \to 0$ when $t \to \infty$ [42]. Such behavior will be assumed in the following.

2.3.3 Polarization and Depolarization Currents

When the contributions from both fast and slow polarization are considered, equation (2.2) takes the form

$$D(t) = \underbrace{\varepsilon_0 \overbrace{(1+\chi)}^{\varepsilon_\mathrm{r}}}_{\varepsilon} E(t) + \varepsilon_0 \int_0^t E(\xi) f(t-\xi)\,\mathrm{d}\xi, \tag{2.17}$$

and equation (2.1) takes the form [40], [46]

$$J(t) = \sigma E(t) + \varepsilon \frac{\mathrm{d}E(t)}{\mathrm{d}t} + \varepsilon_0 \frac{\mathrm{d}}{\mathrm{d}t} \int_0^t E(\xi) f(t-\xi)\,\mathrm{d}\xi. \tag{2.18}$$

By the Leibniz integral rule [49], the latter is equivalent with

$$J(t) = \sigma E(t) + \varepsilon \frac{\mathrm{d}E(t)}{\mathrm{d}t} + \varepsilon_0 f(0) E(t) + \varepsilon_0 \int_0^t E(\xi) \frac{\partial f(t-\xi)}{\partial t}\,\mathrm{d}\xi. \tag{2.19}$$

Note that although the use of the dielectric response function in this way demands it be independent of the electric field strength, the conductivity may depend on the electric field strength, which again may depend on the time.[7]

A step voltage of magnitude U_0 applied at $t = 0$ across a slab of a single insulation material creates a step field

$$E(t) = E_0 \vartheta(t) = \frac{U_0}{d} \vartheta(t), \tag{2.20}$$

where d is the thickness of the material and $\vartheta(t)$ is the unit step function. Equation (2.19) for this piece of insulation material then becomes [42]

$$J(t) = \sigma E_0 + \varepsilon_0 E_0 f(t), \quad t > 0. \tag{2.21}$$

This current is referred to in the following as a *polarization current*. As $t \to \infty$, $f(t) \to 0$, and equation (2.21) becomes Ohm's law:

$$J(\infty) = \sigma E_0. \tag{2.22}$$

[7] The notation $\sigma[E(t)]$ could have been used to indicate this dependency. However, the symbol σ is used alone for ease of reading.

If the material is grounded at a time $t = t_{\mathrm{gnd}}$ when $f(t)$ has decayed to practically zero, equation (2.21) becomes

$$J(t) = -\varepsilon_0 E_0 f(t - t_{\mathrm{gnd}}), \quad t > t_{\mathrm{gnd}}. \tag{2.23}$$

This current is henceforth called a *depolarization current* [40]. The sum of the polarization and depolarization current is as follows:

$$\underbrace{J(t)}_{\substack{\text{pol.}\\ \text{current}}} + \underbrace{J(t + t_{\mathrm{gnd}})}_{\substack{\text{depol.}\\ \text{current}}} = \sigma E_0, \quad 0 < t < t_{\mathrm{gnd}}. \tag{2.24}$$

2.4 Electric Fields in Two Materials with Dielectric Response

As established in section 2.2, expressions for current densities can be used to estimate electric fields in layered insulation of two materials “a” and “b” when only instantaneous (“fast”) polarization is considered. In the following, this is modified to account also for the slow polarization mechanisms by using dielectric response functions. Slow polarization mechanisms affect neither the initial nor the steady-state field distribution after the application of a step voltage. They do, however, affect the transient period between initial and steady-state.

As in section 2.2, the principle that the current density is equal in both materials, namely

$$J_{\mathrm{a}}(t) = J_{\mathrm{b}}(t), \tag{2.25}$$

can be used as a starting point for estimating the time-dependent electric fields. Expressions for the current densities as functions of electric properties, electric fields, and time, as well as the relationship between the electric fields in the two materials (equation (2.6)), are thus required. However, instead of using equation (2.25), it is possible to use the principle that the current density in any of the materials, say, material “a”, equals the current density $J_{\mathrm{mea}}(t)$ that is measurable in the external circuit and flows to the insulation:

$$J_{\mathrm{a}}(t) = J_{\mathrm{mea}}(t). \tag{2.26}$$

By using this above equation, an expression for J_{b} is not needed for estimating the electric fields.

Thus, the presented theory allows for two methods for estimating the time-dependent electric fields in two layered materials, mainly differing in the input parameters that are needed:

- The first method needs electrical properties (ε, σ, and f) for both materials as input.
- The other method needs electrical properties (ε, σ, and f) for one of the materials as input, in addition to measured values of the current density $J_{\text{mea}}(t)$ that flows to the system.

These two methods will henceforth be referred to as the *two-material-input method* and the *one-material-input method*, respectively.

The same principles can be used to derive equations for estimating time-dependent electric fields in insulation with more than two materials.

2.4.1 Two-Material-Input Method

Equation (2.25) is the starting point of the two-material-input method. Inserting equation (2.19) into this gives

$$\begin{aligned}&\sigma E_{\text{a}}(t)+\varepsilon_{\text{a}}\frac{\mathrm{d}E_{\text{a}}(t)}{\mathrm{d}t}+\varepsilon_0 f_{\text{a}}(0)E_{\text{a}}(t)+\varepsilon_0\int_0^t E_{\text{a}}(\xi)\frac{\partial f_{\text{a}}(t-\xi)}{\partial t}\,\mathrm{d}\xi\\ &=\sigma E_{\text{b}}(t)+\varepsilon_{\text{b}}\frac{\mathrm{d}E_{\text{b}}(t)}{\mathrm{d}t}+\varepsilon_0 f_{\text{b}}(0)E_{\text{b}}(t)+\varepsilon_0\int_0^t E_{\text{b}}(\xi)\frac{\partial f_{\text{b}}(t-\xi)}{\partial t}\,\mathrm{d}\xi.\end{aligned} \tag{2.27}$$

Applying equation (2.6) and rearranging gives

$$\begin{aligned}\frac{\mathrm{d}E_{\text{a}}(t)}{\mathrm{d}t}=\alpha(t)-\beta E_{\text{a}}(t)-\gamma\int_0^t E_{\text{a}}(\xi)\frac{\partial f_{\text{a}}(t-\xi)}{\partial t}\,\mathrm{d}\xi\\ +\gamma\int_0^t\frac{U(\xi)-d_{\text{a}}E_{\text{a}}(\xi)}{d_{\text{b}}}\frac{\partial f_{\text{b}}(t-\xi)}{\partial t}\,\mathrm{d}\xi,\end{aligned} \tag{2.28}$$

where the coefficients $\alpha(t)$, β, and γ are defined as follows:

$$\alpha(t)=\frac{(\varepsilon_0 f_{\text{b}}(0)+\sigma_{\text{b}})U(t)}{d_{\text{a}}\varepsilon_{\text{b}}+d_{\text{b}}\varepsilon_{\text{a}}}+\frac{\varepsilon_{\text{b}}}{d_{\text{a}}\varepsilon_{\text{b}}+d_{\text{b}}\varepsilon_{\text{a}}}\frac{\mathrm{d}U(t)}{\mathrm{d}t}, \tag{2.29}$$

$$\beta=\frac{d_{\text{a}}\sigma_{\text{b}}+d_{\text{b}}\sigma_{\text{a}}+\varepsilon_0 d_{\text{a}}f_{\text{b}}(0)+\varepsilon_0 d_{\text{b}}f_{\text{a}}(0)}{d_{\text{a}}\varepsilon_{\text{b}}+d_{\text{b}}\varepsilon_{\text{a}}}, \tag{2.30}$$

$$\gamma=\frac{\varepsilon_0 d_{\text{b}}}{d_{\text{a}}\varepsilon_{\text{b}}+d_{\text{b}}\varepsilon_{\text{a}}}. \tag{2.31}$$

Equation (2.28) is an *integrodifferential equation* (IDE).[8] Such equations can often be solved numerically as initial value problems [50]. Field-dependent conductivities can be supported by equation (2.28) by inserting appropriate relationships for the conductivities in the expressions for α and β. After having estimated the electric field, the current density in the material (and thereby in the whole system) can be estimated from equation (2.19).

The equivalent circuit in figure 2.5 illustrates the system.

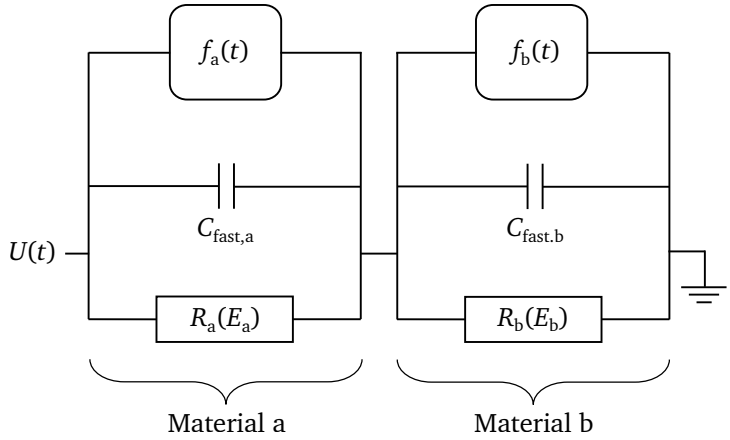

Figure 2.5: Equivalent circuit for a series connection of two materials, each characterized by its own permittivity, field-dependent conductivity, and dielectric response function $f(t)$. The permittivities and field-dependent conductivities are here represented by capacitances C_{fast} and resistances $R(E)$, respectively.

2.4.2 One-Material-Input Method

The starting point for the one-material-input method is that the current density in the one material (i.e., material "a") equals the measured current density. Combining equations (2.26) and (2.19) and gives [32]

$$\frac{\mathrm{d}E_\mathrm{a}(t)}{\mathrm{d}t} = \frac{J_\mathrm{mea}(t)}{\varepsilon_\mathrm{a}} - \frac{\sigma_\mathrm{a} + \varepsilon_0 f_\mathrm{a}(0)}{\varepsilon_\mathrm{a}} E_\mathrm{a}(t) - \frac{\varepsilon_0}{\varepsilon_\mathrm{a}} \int_0^t E_\mathrm{a}(\xi) \frac{\partial f_\mathrm{a}(t-\xi)}{\partial t} \mathrm{d}\xi. \quad (2.32)$$

Like equation (2.28), equation (2.32) is an IDE that often can be solved numerically as an initial value problem [50].

[8] In an integrodifferential equation, the unknown function appears in the integrand as well as outside the integral. This particular integrodifferential equation is a *Volterra* equation since the region of integration is variable (the upper integration limit here is the variable t). This is as opposed to *Fredholm* equations where the regions of integration are fixed [50].

In the case where $f_\mathrm{a}(t) = f_\mathrm{b}(t) = 0$ for all values of t, equation (2.28) becomes identical to equation (2.7), which is a first-order ordinary differential equation [45].

Although electrical properties for materials other than material “a” are not needed as input for this equation, permittivities for all the materials in the system are needed for determining the initial value $E_{\mathrm{a}}(0^{+})$ in case of an applied step voltage.[9]

[9] In theory, a measured current and the electrical properties of material “a” are still sufficient. In practice, accurate measurements of currents immediately after voltage steps can be impossible to obtain [48]. Therefore, the permittivities are needed for determining initial values.

Chapter 3

Experimental Methods

3.1 Electrical Experiments

The electrical measurements in this study comprised of polarization and depolarization current (PDC) measurements and capacitance measurements. The PDC measurements were collected to determine dielectric response functions and conductivities in paper and oil and to verify estimates for series connections. The capacitance measurement were used to determine permittivities.

3.1.1 Test Objects

Materials

One paper type and one oil type were used for the experiments. The paper (before impregnation) was taken from a roll of HVDC cable insulation paper manufactured by Ahlstrom-Munksjö AB. The nominal thickness[1] of the unimpregnated paper was 90 µm. The oil was of the type *T 2015* manufactured by H&R ChemPharm (UK) Limited. This is a mineral oil with additives for obtaining a sufficiently high viscosity. It is commonly used as impregnation compound (i.e., a "cable mass") for mass-impregnated HVDC cables. Before use, the oil was degassed by being circulated in a vacuum chamber at 100–120 °C for four hours.

[1] The single sheet thickness was specified to be within ±5 µm of the nominal thickness, measured according to the International Standard ISO 534:2011. This standard [51] calls for measurements with a micrometer that measures a circular region of 2 cm^2 under a static load corresponding to (100 ± 10) kPa.

Types of Test Objects

Three types of test objects were used, which are henceforth referred to as *oil test objects*, *paper test objects*, and *series connection test objects*. The test objects were circular with sufficiently large diameters to utilize the active areas of the relevant electrode arrangements (as described in section 3.1.2) and were created as follows:[2]

Oil test objects were produced using Teflon (i.e., polytetrafluoroethylene [PTFE]) spacers to form an oil gap between electrodes that were submerged in oil. For the polarization and depolarization measurements, the oil gap was 1 mm thick. For the capacitance measurements, the oil gap was 0.21–5.8 mm thick.

Paper test objects were created by placing stacks of 2–18 impregnated paper sheets between the electrodes. The thicknesses of the paper test objects were assumed to be the nominal thickness of each paper sheet (90 μm) multiplied by the number of sheets.

Series connection test objects were produced in the same way as paper test objects, but spacers were used to create an oil gap in the middle of the paper stack. Both a large and a small series connection test object were made. The thicknesses of the oil gaps were large compared with the thicknesses of the paper parts. This was to make it easier to detect the effects of the oil gaps in the results and to mitigate the effects from undesirable thickness variations.

Large. The spacers for the large series connection test object were assembled using paper glued together with a dextrin adhesive. Such spacers were placed both around the periphery and in the center of the test object, as illustrated in figure 3.1a. This was to mitigate the oil gap's tendency to collapse due to the lack of mechanical strength in the upper paper stack. There were five paper sheets on each side of the oil gap. The total paper thickness d_{pap} (i.e., the sum of the thicknesses of the two paper stacks) was assumed to be the nominal thickness of each paper sheet multiplied by the number of sheets. The thickness of the oil gap d_{oil} was assumed to be the total test object thickness minus the thickness of the paper stacks. (The total test object thickness was estimated as described later in this section 3.1.1.) This was calculated as $d_{\text{pap}} = 0.90\,\text{mm}$ and $d_{\text{oil}} = 1.6\,\text{mm}$.

[2] The paper test objects and the large series connection test object were made by Lars Erik Pettersen in cooperation with the author of this thesis. This was done as part of Pettersen's work with his master's thesis [52].

Small. The small series connection test object did not have any central spacer but a 1 mm thick PTFE peripheral spacer with two paper sheets on each side, as illustrated in figure 3.1b. The total paper thickness d_{pap} was assumed to be the nominal thickness of each paper sheet multiplied by the number of sheets. The thickness of the oil gap d_{oil} was assumed to equal the thickness of the spacer. This was calculated as $d_{\text{pap}} = 0.36\,\text{mm}$ and $d_{\text{oil}} = 1.0\,\text{mm}$.

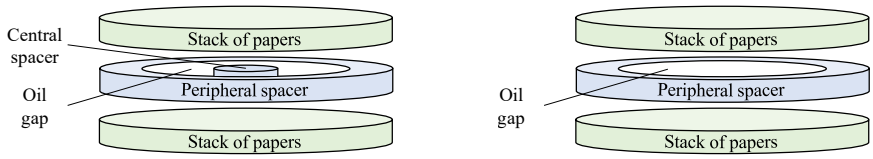

(a) Large (b) Small

Figure 3.1: Expanded views of the series connection test objects. Sketches not to scale.

Impregnation, Handling, and Storage of Test Objects

An airtight, temperature-controlled container with necessary piping and bushing was used for holding the test objects during drying, impregnation, and measurements. The paper test objects and series connection test objects were dried in a vacuum for at least two days at 100–120 °C. After drying, degassed oil of approximately the same temperature was piped into the container so that the dried paper became submerged in oil without being exposing to air. When the paper was fully impregnated, the temperature was lowered to allow handling with gloved hands. The container was opened and the desired test object was placed between the electrodes in the middle of the container. The other test objects remained submerged elsewhere in the container. The oil covered the lower electrode and part of the upper electrode, so although impregnated paper could be exposed to air in the process of placing it between the electrodes, it was not exposed when resting between the electrodes. After positioning the test objects, the container was closed and its atmosphere flushed with dry nitrogen gas to keep the oil dry.[3] After flushing, dry nitrogen at a pressure of 10^5 Pa remained over the oil. Such flushing was done whenever a test object had been repositioned.

[3]Moisture can heavily affect the electric properties of paper and oil [53].

Determination of Total Thicknesses

The total test object thickness was determined by measuring the distance from a reference plane to the top of the upper electrode (figure 3.2) with a vernier depth gauge both with and without the test object mounted between the electrodes. This was done for several points on the upper electrode, and the mean distance was calculated. The difference between the mean height with and without the test object was accepted as the total test object thickness.

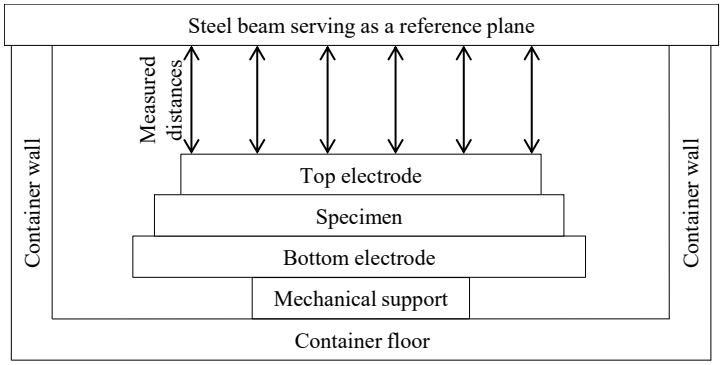

Figure 3.2: Reference plane used for thickness measurements. Sketch not to scale.

The measured total test object thickness was heavily affected by varying amounts of oil between the paper sheets due to test object handling and thus had low reproducibility. Measurements before and after squeezing out excess intersheet oil could differ by up to a factor 1.9. Typically, different measurements of the same test object differed by a factor 1.2 or less.

3.1.2 Experimental Setup

Electrodes

A single-guard and a double-guard electrode arrangement were used. All electrodes were made of brass. When test objects with spacers were used, the spacers aligned with the guards.[4]

The single-guard electrode arrangement (figure 3.3) had a disk-shaped effective area of 49 cm^2, with a guard encompassing the effective area. The single-guard electrode arrangement was used for the PDC measurements on oil test objects, paper test objects, and the small series connection test object.

[4]Each oil test object had only one spacer, even when used together with the double-guard electrode arrangement.

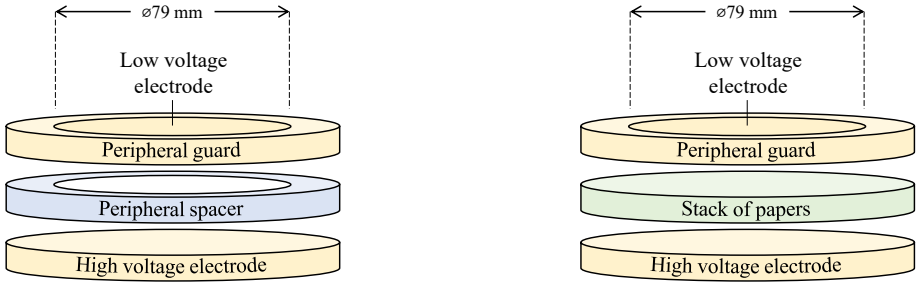

(a) With oil test object. (b) With paper test object.

Figure 3.3: Expanded views of the single-guard electrode arrangement. Sketches not to scale. There was 2 mm of guard insulation between the electrode and the guard (not shown in the figure). The indicated diameter relates to the middle of the guard insulation.

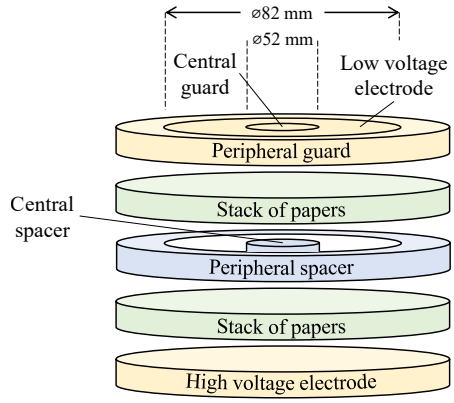

Figure 3.4: Expanded view of the double-guard electrode arrangement, illustrated with the large series connection test object. Sketch not to scale. There was 2 mm of guard insulation between the low voltage electrode and the guards. The indicated diameters relate to the middle of the guard insulation.

The double-guard electrode arrangement (figure 3.4) had an annular effective area of 32 cm^2, with a guard around its periphery and an additional guard in its center. The purpose of the central guard was to prevent the central spacer from affecting the results. The double-guard electrode arrangement was used for the large series connection test object, as well as for all the capacitance measurements.

Test Circuit

The electrical circuit for the PDC measurements is exhibited in figure 3.5. The test circuit was designed for applying a step voltage across the test object, measuring the resulting polarization current, and, after a predetermined period of time, grounding the test object and measuring the resulting depolarization current.[5] The HVDC voltage source was a *Fug HCN 140 – 35 000*, capable of supplying up to 35 kV with a stability of $\pm 10^{-5}$ per eight hours. Currents were measured with a *Keithley 6485* picoammeter with a resolution in the sub-picoampere range. Switching and data logging was aided by *LabVIEW* software.[6] Protective resistors limited the current in case of faults.

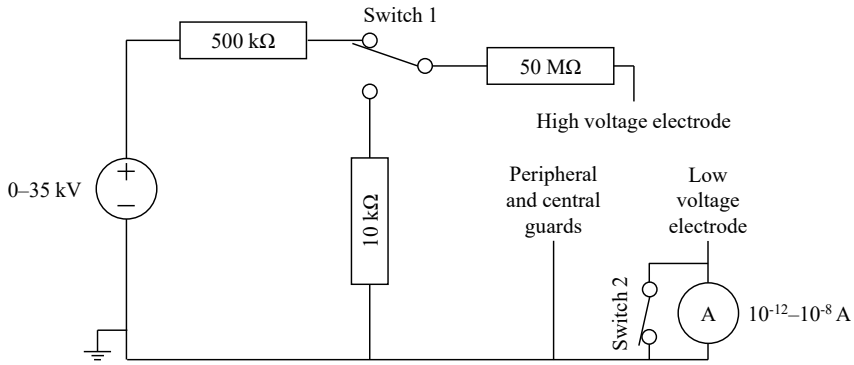

Figure 3.5: Measurement circuit for polarization and depolarization current measurements. For details on the electrode arrangements, see figures 3.3–3.4.

The voltage application and grounding were done by allowing switch 1 (figure 3.5) to connect to high voltage and ground, respectively. The picoammeter was protected against the large initial currents by closing keeping switch 2 closed for a short period around the energizing and grounding events. Switch 2 was opened one second after each such event, and it was then kept open for the duration of the current measurement.

[5] The circuit was based on the design used in [54].

[6] The *LabVIEW* program (i.e., the "virtual instrument" [VI]) was developed by SINTEF Energy Research.

High-frequency capacitances for determining permittivities were measured with an Agilent U1732C capacitance meter with the abovementioned circuit disconnected from the electrodes.

3.1.3 Test Procedure

Test Temperature

All electrical measurements were conducted done at 50 °C. This is a typical service temperature for mass-impregnated cables [5]. Using a lower temperature would be impractical due to the high oil viscosity at low temperatures. Moreover, lower temperatures would decrease the rate of dielectric relaxation [55] and thus cause the collection of the measurements to be more time-consuming.

Polarization and Depolarization Current Measurements

A step voltage was applied across the test object. The resulting polarization current was measured until it had practically reached steady state. Then the test object was grounded and the resulting depolarization current was measured.

For the paper and series connection test objects, the polarization time was 2.5–36 hours. The grounding time between successive voltage applications was at least as long as the preceding polarization time. The voltage was increased for each successive experiment so that the influence on the currents from the remaining polarization would be as small as possible. The applied voltage was up to 35 kV.

For oil test objects, the voltage was limited to a maximum of 7 kV due to signs of discharges or breakdown at higher voltages. The polarization time was 0.5–5 hours. The test objects were grounded for a sufficiently long time in order for the depolarization current to decay to the noise level (about 1 pA). This happened within 10 minutes.

Capacitance Measurements

High-frequency capacitances C_{fast} for paper test objects and oil test objects were measured at 1 kHz and approximately 0.7 V (root mean square) [56]. The test objects were mounted in the double-guard electrode arrangement during the capacitance measurements. Oil test objects with thicknesses from 0.2 to 5.8 mm and paper test objects with 4–11 sheets were used. Excess oil between paper sheets was squeezed out from some but not all of the test objects prior to measuring. This was done with a gloved finger.

3.2 Scanning Electron Microscopy[7]

Paper without impregnation was used for surface and cross-section analysis.

Paper surfaces were examined by scanning electron microscopy without any preparation other than a sputter coating of gold to ensure that the specimens were conductive. The microscope was operated in secondary electron mode.

Specimens for examining cross sections were prepared in the following way: Pieces of paper were impregnated with epoxy in casting molds. The epoxy was subsequently cured in the molds to fixate the paper fibers. The epoxy casts containing the paper were cut and polished to achieve smooth cross-sections. The specimens were rendered conductive by coating them with a thin layer of carbon. The microscope was operated in back-scattered electrons mode to distinguish between the paper fibers and the epoxy that surrounded the fibers. It was assumed that the epoxy wetted the paper fibers in the same way that oil does. When paper tapes are wound with a certain tension around a conductor, radial and tangential mechanical stresses occur [57]. The effects of such stresses were not considered in this analysis. The cross-section specimens were examined with angle of view both in machine direction and in cross direction.[8]

[7] Most of the text in section 3.2 is a verbatim excerpt from reference [16], ©IEEE, 2019, used with permission. The specimens for the scanning electron microscope were prepared by Per Olav Johnsen at RISE PFI AS. The scanning electron microscope was operated by him in cooperation with the author of this thesis.

[8] *Machine direction* is the direction that is parallel to the direction of the paper's travel through the paper making machine. *Cross direction* is the direction that is parallel to the plane of the paper and at the same time perpendicular to the machine direction [58].

Since the lay length of paper tapes in cables is usually short, the machine direction corresponds approximately to the circumferential direction of the cable, whereas the cross direction corresponds approximately to the longitudinal direction of the cable [16].

Chapter 4

Estimation Methods

4.1 Estimation of Electrical Properties from Measurements

4.1.1 Estimation of Permittivities

For parallel-plane insulation, the high-frequency capacitance C_{fast} at "infinitely" high frequencies (where only fast polarization mechanisms are active) is expressed as

$$C_{\text{fast}} = \frac{\varepsilon S}{d} = \frac{\varepsilon_0 \varepsilon_{\text{r}} S}{d}, \tag{4.1}$$

where S denotes the effective electrode area, and d is the thickness of the insulation. This equation was used to estimate permittivities from measurements of high-frequency capacitances of each of the two materials, though in different ways for oil and paper.

Permittivity of oil

For the permittivity in oil, equation (4.1) was used in the form

$$\varepsilon_{\text{r}} = \frac{C_{\text{fast}} d}{\varepsilon_0 S} \tag{4.2}$$

together with measured capacitances and test object thicknesses. The permittivity was taken as the average of five permittivities obtained from oil test objects of various thicknesses.

Permittivity of Paper

When measuring the high-frequency capacitance of paper test objects, excess intersheet oil contributed to the result. The contribution from excess intersheet oil (i.e., oil that, if desired, could have been squeezed out from the test object with a gloved finger) was eliminated from the paper permittivity estimates in the following manner: Total thicknesses (see section 3.1.1) and capacitances were measured on several paper test objects containing various numbers of sheets. Excess intersheet oil had, to varying extents, been squeezed out from some but not all of the test objects. The thickness of the paper was assumed to equal the nominal thickness as per section 3.1.1. In the following, the index $_{\mathrm{mea}}$ indicates measured values, while the indices $_{\mathrm{pap}}$ and $_{\mathrm{ex}}$ indicate values for paper and excess intersheet oil, respectively. The difference between the measured thicknesses and the nominal paper thicknesses for each of the test objects was assumed to equal the thickness of excess intersheet oil:

$$d_{\mathrm{ex}} = d_{\mathrm{mea}} - d_{\mathrm{pap}}. \tag{4.3}$$

Furthermore, neglecting all edge effects, the measured capacitance was assumed to be the total capacitance of the series connection of paper and the excess intersheet oil, so

$$\frac{1}{C_{\mathrm{mea}}} = \frac{1}{C_{\mathrm{pap}}} + \frac{1}{C_{\mathrm{ex}}}. \tag{4.4}$$

By combining equations (4.1), (4.3), and (4.4), the following relation was obtained:

$$\underbrace{d_{\mathrm{mea}} C_{\mathrm{mea}}}_{y} = \underbrace{\left(1 - \varepsilon_{\mathrm{r,ex}}/\varepsilon_{\mathrm{r,pap}}\right)}_{a} \underbrace{d_{\mathrm{pap}} C_{\mathrm{mea}}}_{x} + \underbrace{\varepsilon_0 \varepsilon_{\mathrm{r,ex}} S}_{b}. \tag{4.5}$$

For convenience, terms are here named y, a, x, and b as indicated. Equation (4.5) is a linear equation $y = ax + b$. Both y and x are products of known (i.e., measured or assumed) values, so for all measurements of capacitance and corresponding thickness, y could be plotted versus x. The value for $\varepsilon_{\mathrm{r,oil}}$ that was estimated with equation (4.2) as described above was taken as $\varepsilon_{\mathrm{r,ex}}$ and used to calculate b. Then the slope a was found from linear regression (method of least squares). Lastly, $\varepsilon_{\mathrm{r,pap}}$ was calculated from the slope a.

4.1.2 Estimation of Conductivities

Conductivity of Paper

A PDC measurement was performed by applying a step voltage $U(t) = U_0 \vartheta(t)$ across a paper test object at $t = 0$ and subsequently grounding at it $t = t_{\mathrm{gnd}}$

after steady-state was reached. It follows from equations (2.24) that

$$\sigma = \frac{J(t) + J(t + t_{\text{gnd}})}{E_0} \quad \text{for} \quad 0 < t < t_{\text{gnd}}. \tag{4.6}$$

As usual, $E_0 = U_0/d$ with d being the nominal thickness of the test object.[1] The highest available values of t (while still less than t_{gnd}) were used for the estimation. This procedure was repeated for several field strengths E_0. The commonly used relation [55], [59]

$$\sigma_{\text{pap}}(E_{\text{pap}}) = \sigma_0 \mathrm{e}^{\eta |E_{\text{pap}}|} \tag{4.7}$$

was curve fitted to the results for paper, with σ_0 and η as fitting parameters.

Conductivity of Oil

The conductivity of oil σ_{oil} has been estimated with both bare electrodes and paper-covered electrodes. By comparing both methods, it was possible to discern if the presence of paper between the electrodes and the oil gap affected the conductivity. Covered electrodes resemble the conditions in butt gaps more than bare electrodes.

With bare electrodes. Polarization currents were measured on oil test objects and the conductivity was calculated with equation (2.22) (Ohm's law), using the values for the highest available values of t (i.e., when $f(t)$ had decayed to practically zero).

With paper-covered electrodes. PDC measurements were performed on series connection test objects. The paper parts of the test objects served as electrode covering. The conductivity of the paper was assumed to follow equation (4.7). The steady-state value J_{st} was obtained from

$$J_{\text{st}} = J(t) + J(t + t_{\text{gnd}}) \tag{4.8}$$

at the highest available values for t that were still smaller than t_{gnd} (cf. equation (4.6)). As illustrated in appendix B, the exponential relationship between

[1] Possible excess intersheet oil would scarcely affect the estimated conductivity. For example, if excess intersheet oil amounted to 10 % of the paper thickness and σ_{oil} were five times larger than σ_{pap}, the estimated paper thickness be 2 % lower than the true value. If the ratio between σ_{oil} and σ_{pap} were larger, the estimate would be even closer to the true value.

electric field and conductivity of paper allows the steady-state electric field in the oil be expressed as

$$E_{\text{oil}} = \frac{U_0\eta - d_{\text{pap}}\mathrm{W}_0(z)}{d_{\text{oil}}\eta} \tag{4.9}$$

where W_0 is the principal branch of the Lambert W function [60] and its argument

$$z = \frac{\eta J_{\text{st}}}{\sigma_0}. \tag{4.10}$$

Furthermore,

$$\sigma_{\text{oil}} = \frac{d_{\text{oil}}\eta J_{\text{st}}}{\eta U_0 - d_{\text{pap}}\mathrm{W}_0(z)}. \tag{4.11}$$

This was used to determine the oil conductivity at various electric field strengths.

4.1.3 Estimation of Dielectric Response Functions

The dielectric response functions were calculated from measured polarization or depolarization currents together with equations (2.21) or (2.23), respectively.

For each material, the median of several measurements of the dielectric response function was used for further calculations. The median was identified on the basis of the measured value at $t = 2\,\text{s}$. This is illustrated in figure 4.1. The value $t = 2\,\text{s}$ was chosen for median determination as the dielectric response functions at this time had not had much time to decrease, and it was considered practical to choose a time somewhat after the start of the measurements. The maximum and minimum dielectric response functions were also identified and used for sensitivity analysis. The measurements with the largest and smallest value for the largest amount of time before $t = 50\,\text{s}$ were identified as the maximum and minimum dielectric response functions, respectively.

Curve fitting was conducted to express the median, maximum, and minimum dielectric response functions as linear combinations of exponential functions on the form

$$f(t) = \sum_{i=1}^{N} A_i \mathrm{e}^{-t/t_i}. \tag{4.12}$$

The term with the largest time constant t_i was fitted first, then the term with the second largest time constant, and so on. Details on this procedure are described in appendix C. Each term was fitted with the least squares method. No information on the currents were recorded the first second after voltage application or grounding. The dielectric response functions were extrapolated backwards to $t = 0$ by using the mentioned curve fitting.

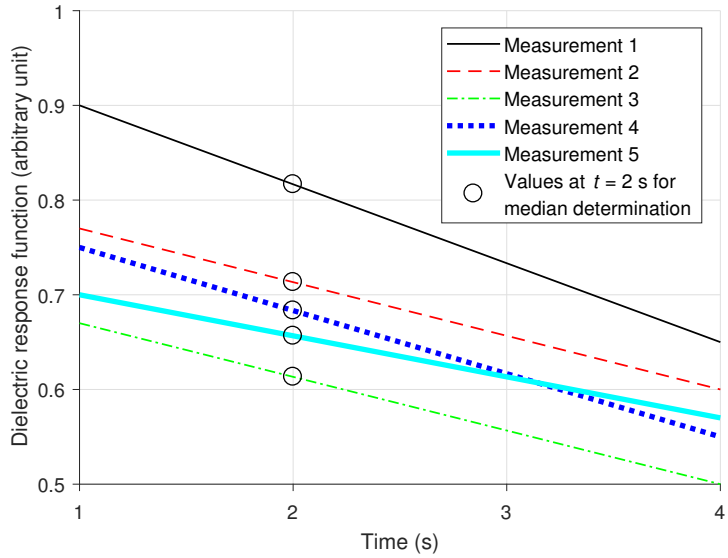

Figure 4.1: Illustration of how the median dielectric response functions was determined. In this example with five measurements of the dielectric response function, the median of the values at $t = 2\,\mathrm{s}$ is that of measurement 4. Hence, measurement 4 is identified as the median of the dielectric response functions. The values in the figure are for illustration—not real measurements.

Expressing dielectric response function as linear combination of exponential functions is a purely mathematical construct and has no physical interpretation regarding the polarization mechanisms involved. The curve fitting was implemented because it proved convenient, as will be evident in section 4.2.

4.1.4 Interpretation of Time-Dependent Conduction

A steady-state conductivity may well be field-dependent. Thus, a changing electric field will lead to a changing conductivity with

$$\frac{\mathrm{d}\sigma}{\mathrm{d}t} = \frac{\mathrm{d}\sigma}{\mathrm{d}E}\frac{\mathrm{d}E}{\mathrm{d}t}. \tag{4.13}$$

Since only steady-state conductivities were used in this work, any time-dependent charge transport that was not due to $\frac{\mathrm{d}}{\mathrm{d}t}(\sigma E)$ was accounted for by the dielectric response function and was thereby interpreted as polarization. The materials were considered to be homogeneous. Consequently, charge was assumed to accumulate only at the interfaces between the materials and at the electrode surfaces.

This is illustrated in the following example: A slab of dielectric with thickness d and permittivity ε is placed between a pair of parallel electrodes, as illustrated in figure 4.2. To keep the example simple, the dielectric is homogeneous in the directions parallel to the electrode surfaces and has no slow polarization mechanisms. The dielectric is subjected to a step voltage $U(t) = U_0\vartheta(t)$. After application of the voltage, a very thin layer of positive charge migrates from the position x_1 to the position x_2. This reduces the net charge at x_1 and increases it at x_2, as indicated in figure 4.2. Since the migrating space charge layer is thin, it can be described by a surface charge density κ_{sc}. If it were not compensated for, the space charge migration would lower the electric field between x_1 and x_2 by $\Delta E = \kappa_{sc}/\varepsilon$. This would reduce the voltage between the electrodes by $\Delta U = (x_2 - x_1)\Delta E$. However, to maintain the voltage between the electrodes, a compensating charge density

$$\kappa_{comp} = \kappa_{sc}\frac{x_2 - x_1}{d} \tag{4.14}$$

is added to the positive electrode and subtracted from the negative electrode. The migration of space charge is interpreted as an increase ΔP in polarization, with $\Delta P = \kappa_{comp}$. The flow of this compensating charge is measured as a current in the external circuit. If the velocity of the space charge layer migrating from x_1 to x_2 is $v_{sc}(t)$, the measured compensating current is

$$J_{comp} = \frac{\mathrm{d}\kappa_{comp}}{\mathrm{d}t} = \frac{\kappa_{sc}v_{sc}(t)}{d}. \tag{4.15}$$

Since this is a transient current, it is here interpreted as part of the dielectric response function. Its contribution to the dielectric response function is

$$f_{sc}(t) = \frac{\kappa_{sc}v_{sc}(t)}{\varepsilon_0 U_0}. \tag{4.16}$$

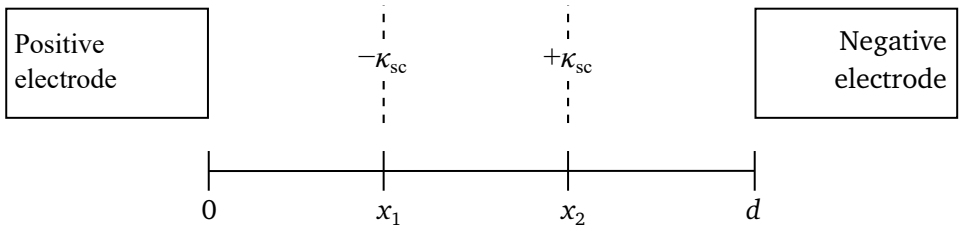

Figure 4.2: Migration of a thin layer of space charge from position x_1 to position x_2. This changes the net surface charge density at x_1 and x_2 by $-\kappa_{sc}$ and κ_{sc}, respectively.

4.2 Estimation of Time-Dependent Electric Fields

Time-dependent electric fields in oil and impregnated paper were estimated with the two-material-input method and the one-material-input method.

Writing and verifying effective algorithms for numerically solving the integrodifferential equations (IDEs; i.e., equations (2.28) and (2.32)) can be demanding. However, if the dielectric response functions are in the form of equation (4.12), i.e., linear combinations of exponential functions, it is possible to convert the IDEs to systems of ordinary differential equations (ODEs).[2] Although such systems of ODEs in general must still be solved numerically, the main advantage of the conversion is that the ODE systems can be solved with existing commercial or free ODE software. Such conversions were used for estimating electric fields in this work, both for the two-material-input method and for the one-material-input method.

Conversion from an IDE to a system of ODEs is a mathematical exercise, and the equivalence between the IDE and the system of ODEs can be shown in a purely mathematical fashion. This is undertaken in appendix E for both the two-material-input method and the one-material-input method.

However, the same systems of ODEs can also be obtained by constructing an equivalent circuit for the system and using Kirchhoff's laws to derive equations for the potentials in the equivalent circuit. This is perhaps more illustrative than the pure mathematics of appendix E, and is shown below.

4.2.1 Ordinary Differential Equations for the Two-Material-Input Method[3]

For each material k in the insulation, the dielectric response function is expressed as a linear combination of N_k exponential functions,

$$f_k(t) = \sum_{i=1}^{N_k} A_{i,k} \mathrm{e}^{-t/t_{i,k}}, \tag{4.17}$$

where $A_{i,k}$ and $t_{i,k}$ are constants (cf. section 4.1.3). This makes it possible to represent the series connection of the two materials "a" and "b" with the equivalent circuit shown in figure 4.3 (cf. fig. 2.5) [40], [62].The circuit parameters of

[2] Exponential functions (as in equation (4.12)) were selected as basis functions for $f(t)$ because it was convenient. Other types of basis functions (i.e., curve fitting to other types of functions, cf. section 4.1.3) may also potentially facilitate conversion to ODEs.

[3] The essence of this section has been published in [61].

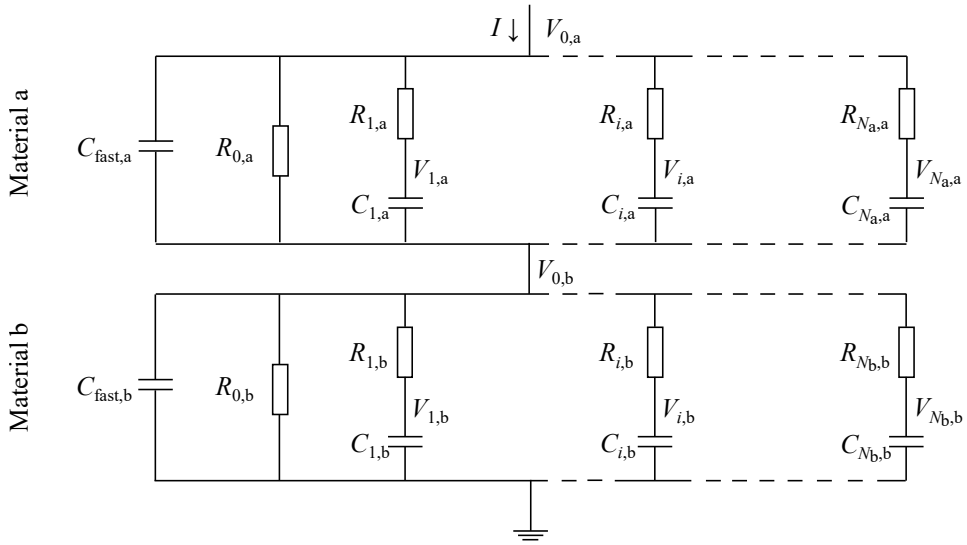

Figure 4.3: Equivalent electric circuit for a series connection of two insulation materials where the dielectric response of the two materials are represented by N_a and N_b resistance-capacitance branches, respectively. Potentials at various places in the equivalent circuit are denoted by $V_{0,\mathrm{a}}$, $V_{i,\mathrm{a}}$, $V_{0,\mathrm{b}}$, and $V_{i,\mathrm{b}}$.

the equivalent circuit are as follows [40], [46]:

$$C_{\mathrm{fast},k} = \varepsilon_k S/d_k, \tag{4.18}$$

$$R_{0,k} = d_k/(\sigma_k S), \tag{4.19}$$

$$R_{i,k} = d_k/\left(A_{i,k}\varepsilon_0 S\right), \qquad i \in \{1,2,\ldots,N_k\}, \tag{4.20}$$

$$C_{i,k} = t_{i,k}/R_{i,k}, \qquad i \in \{1,2,\ldots,N_k\}. \tag{4.21}$$

The symbol S denotes the area of the layers of the series connection. The potentials $V_{0,\mathrm{a}}(t)$, $V_{i,\mathrm{a}}(t)$, $V_{0,\mathrm{b}}(t)$, and $V_{i,\mathrm{b}}(t)$ are defined in figure 4.3. Since the ground potential is zero, the known, applied voltage $U(t)$ determines the potential $V_{0,\mathrm{a}}(t)$:

$$V_{0,\mathrm{a}}(t) = U(t). \tag{4.22}$$

Therefore,

$$E_{\mathrm{a}}(t) = \frac{V_{0,\mathrm{a}}(t) - V_{0,\mathrm{b}}(t)}{d_{\mathrm{a}}}, \tag{4.23}$$

and

$$E_{\mathrm{b}}(t) = V_{0,\mathrm{b}}(t)/d_{\mathrm{b}}. \tag{4.24}$$

As shown in appendix D, Kirchhoff's laws can be used to derive the following system of coupled ODEs for the potentials $V_{i,\mathrm{a}}(t)$, $V_{0,\mathrm{b}}(t)$, and $V_{i,\mathrm{b}}(t)$:

$$\frac{\mathrm{d}V_{0,\mathrm{b}}(t)}{\mathrm{d}t} = \frac{1}{C_{\mathrm{fast,a}} + C_{\mathrm{fast,b}}} \left(\frac{V_{0,\mathrm{a}}(t) - V_{0,\mathrm{b}}(t)}{R_{0,\mathrm{a}}} + \sum_{i=1}^{N_\mathrm{a}} \frac{V_{0,\mathrm{a}}(t) - V_{i,\mathrm{a}}(t)}{R_{i,\mathrm{a}}} - \frac{V_{0,\mathrm{b}}(t)}{R_{0,\mathrm{b}}} - \sum_{i=1}^{N_\mathrm{b}} \frac{V_{0,\mathrm{b}}(t) - V_{i,\mathrm{b}}(t)}{R_{i,\mathrm{b}}} + C_{\mathrm{fast,a}} \frac{\mathrm{d}V_{0,\mathrm{a}}(t)}{\mathrm{d}t} \right), \tag{4.25}$$

$$\frac{\mathrm{d}V_{i,\mathrm{a}}(t)}{\mathrm{d}t} = \underbrace{\frac{\mathrm{d}V_{0,\mathrm{b}}(t)}{\mathrm{d}t}}_{\text{See Eq. (4.25)}} + \frac{V_{0,\mathrm{a}}(t) - V_{i,\mathrm{a}}(t)}{R_{i,\mathrm{a}} C_{i,\mathrm{a}}}, \tag{4.26}$$

$$\frac{\mathrm{d}V_{i,\mathrm{b}}}{\mathrm{d}t} = \frac{V_{0,\mathrm{b}}(t) - V_{i,\mathrm{b}}(t)}{R_{i,\mathrm{b}} C_{i,\mathrm{b}}}. \tag{4.27}$$

The system of ODEs can be solved for $V_{0,\mathrm{b}}(t)$, $V_{i,\mathrm{a}}(t)$, and $V_{i,\mathrm{b}}(t)$ as an initial value problem. The electric fields can then be found from equations (4.23) and (4.24).

As appendix E shows, the system of ODEs (4.25)–(4.27) is mathematically equivalent to the IDE (2.28), provided that appropriate initial values for $V_{0,\mathrm{b}}(t)$, $V_{i,\mathrm{a}}(t)$, and $V_{i,\mathrm{b}}(t)$ are used.

Since both the electric fields and the polarization are zero before $t = 0$, the initial values for all the potentials must be zero. However, in the case of U being a step voltage of magnitude U_0, the system of ODEs can be evaluated from $t = 0^+$ with initial values as follows:

$$V_{i,\mathrm{a}}(0^+) = V_{0,\mathrm{b}}(0^+) = U_0 \frac{C_{\mathrm{fast,a}}}{C_{\mathrm{fast,a}} + C_{\mathrm{fast,b}}}, \tag{4.28}$$

$$V_{i,\mathrm{b}}(0^+) = 0. \tag{4.29}$$

This method was used to estimate time-dependent electric fields in this work.

The same approach can be extended for systems of more than two different layered materials, but the equation systems then become more complex.

4.2.2 Ordinary Differential Equations for the One-Material-Input Method

ODEs for the one-material-input method can be derived in a similar manner as for the two-material-input method described above. However, information on

electrical properties from material "b" is not needed, so the equivalent circuit (fig. 4.3) can be simplified, as illustrated in figure 4.4. The circuit parameters as defined in equations (4.18)–(4.21) still apply, and they still require that the dielectric response function (for material "a" only) be expressed as a linear combination of exponential functions as in equation (4.17). Kirchhoff's current

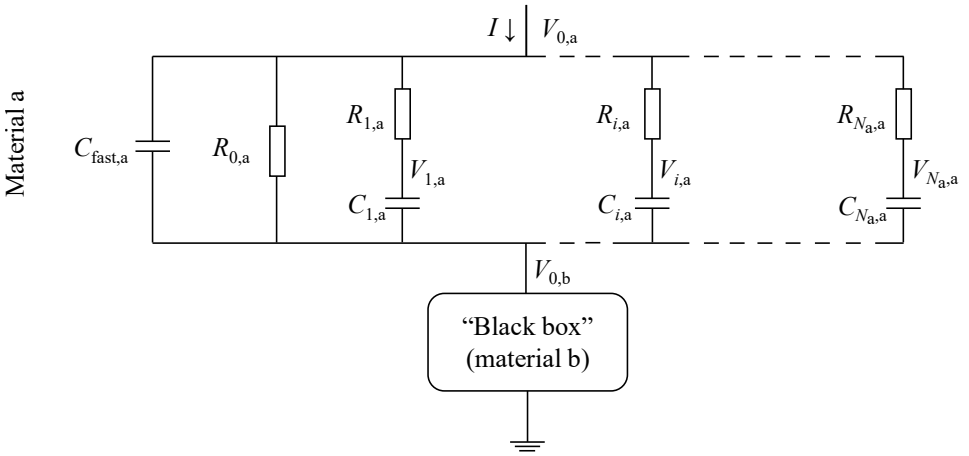

Figure 4.4: Equivalent circuit for a series connection of layered insulation where all materials but material "a" are represented by a "black box", cf. figure 4.3. Potentials at various places in the equivalent circuit are denoted by $V_{0,a}$, $V_{i,a}$, and $V_{0,b}$.

law applied on the equivalent circuit leads to the following system of ODEs:

$$\frac{\mathrm{d}V_{0,b}(t)}{\mathrm{d}t} = \frac{\mathrm{d}V_{0,a}(t)}{\mathrm{d}t} - \frac{I(t)}{C_{fast,a}} + \frac{V_{0,a}(t) - V_{0,b}(t)}{R_{0,a}C_{fast,a}} + \sum_{i=1}^{N_a} \frac{V_{0,a}(t) - V_{i,a}(t)}{R_{i,a}C_{fast,a}}, \tag{4.30}$$

$$\frac{\mathrm{d}V_{i,a}(t)}{\mathrm{d}t} = \underbrace{\frac{\mathrm{d}V_{0,b}(t)}{\mathrm{d}t}}_{\text{See Eq. (4.30)}} + \frac{V_{i,a}(t) - V_{0,b}(t)}{R_{i,a}C_{i,a}}. \tag{4.31}$$

Appendix E shows that, with appropriate initial values, the system of ODEs (4.30)–(4.31) is mathematically equivalent to the IDE (2.32).

As with the two-material-input method, the assumption that the piece of insulation is completely discharged before $t = 0$ dictates the initial conditions as for the system of ODEs:

$$V_{0,b}(0) = V_{i,a}(0) = 0. \tag{4.32}$$

However, in the case of a step voltage $U(t) = U_0\vartheta(t)$ across the insulation, the values of the potentials immediately after $t = 0$ (i.e., at $t = 0^+$) can be used as

initial values:

$$V_{0,\mathrm{b}}(0^+) = \frac{U_0 C_{\mathrm{fast,b}}}{C_{\mathrm{fast,a}} + C_{\mathrm{fast,b}}}, \tag{4.33}$$

$$V_{i,\mathrm{a}}(0^+) = 0. \tag{4.34}$$

This has been implemented in this work.

4.2.3 Type of Numerical Solver for Ordinary Differential Equations

The systems of ODEs (both for the two-material-input method and for the one-material-input method) were solved with the software Matlab R2017a [63]. The Matlab scripts utilized Matlab's "ode45" function, which is based on a Runge-Kutta method [64]. These ode45-utilizing scripts were tested with other Matlab scripts that solved the corresponding IDEs.[4]

4.3 Estimation of Current Density

From the solutions for $V_{0,\mathrm{a}}(t)$, $V_{i,\mathrm{a}}(t)$, and $V_{i,\mathrm{b}}(t)$ in the two-material-input method, it was possible to calculate not only the time-dependent electric fields but also the time-dependent current in the insulation. This was done with the following relation [61]:

$$\begin{aligned} I(t) = {} & \frac{C_{\mathrm{fast,b}}}{C_{\mathrm{fast,a}} + C_{\mathrm{fast,b}}} \left(\frac{V_{0,\mathrm{a}}(t) - V_{0,\mathrm{b}}(t)}{R_{0,\mathrm{a}}} + \sum_{i=1}^{N_\mathrm{a}} \frac{V_{0,\mathrm{a}}(t) - V_{i,\mathrm{a}}(t)}{R_{i,\mathrm{a}}} \right) \\ & + \frac{C_{\mathrm{fast,a}}}{C_{\mathrm{fast,a}} + C_{\mathrm{fast,b}}} \left(\frac{V_{0,\mathrm{b}}(t)}{R_{0,\mathrm{b}}} + \sum_{i=1}^{N_\mathrm{b}} \frac{V_{0,\mathrm{b}}(t) - V_{i,\mathrm{b}}(t)}{R_{i,\mathrm{b}}} + C_{\mathrm{fast,b}} \frac{\mathrm{d}V_{\mathrm{a}}(t)}{\mathrm{d}t} \right). \end{aligned} \tag{4.35}$$

The derivation of this equation is explicated in appendix D. The current density was found by dividing the current by the effective area S.

With the one-material-input method, the current could not be calculated since it was used as input parameter.

[4] The IDE-solving scripts were based on a script that was written and verified by Jon Vegard Venås, who was with the Department of Mathematical Sciences at the Norwegian University of Science and Technology at the time.

4.4 Measure of Rate of Change of Electric Fields

For comparison of the results from the estimations of the time-dependent electric fields, the parameter t_{90} was used. The parameter t_{90} is here defined as the time when 90 % of the change from initial to steady state has occurred, namely the time at which

$$E(t) = E(0^+) + 0.9\Big[E(\infty) - E(0^+)\Big]. \tag{4.36}$$

The value of t_{90} is identical when considering both the electric field in paper and the electric field in oil.[5]

For series connections of two materials with constant electric properties and no slow polarization mechanisms, the transition from initial to steady-state electric fields is an exponential function of time for which the time constant τ is well-defined (equation (2.10)). For such series connections, $t_{90} = 2.3\tau$.

[5]Equation (4.36) for paper can be rewritten as $E_{\text{pap}}(t) = 0.1E_{\text{pap}}(0^+) + 0.9E_{\text{pap}}(\infty)$. From equation (2.6), it is evident that $E_{\text{pap}} = (U_0 - d_{\text{oil}}E_{\text{oil}})/d_{\text{pap}}$. Inserting this in the first equation of this footnote gives $[U_0 - d_{\text{oil}}E_{\text{oil}}(t)]/d_{\text{pap}} = 0.1[U_0 - d_{\text{oil}}E_{\text{oil}}(0^+)]/d_{\text{pap}} + 0.9[U_0 - d_{\text{oil}}E_{\text{oil}}(\infty)]/d_{\text{pap}}$. Subtracting U_0/d_{pap} from both sides and thereafter multiplying by $-d_{\text{pap}}/d_{\text{oil}}$ gives $E_{\text{oil}}(t) = 0.1E_{\text{oil}}(0^+) + 0.9E_{\text{oil}}(\infty)$. This is equation (4.36) for oil. Since $t = t_{90}$ satisfies the first equation in this footnote, it also satisfies the last equation. Therefore, the same value of t_{90} satisfies equation (4.36) for both paper and oil. In other words, t_{90} is the same for the electric fields in both paper and oil.

Chapter 5

Results from Materials Characterization

This chapter presents and discusses results from the estimation of permittivity, conductivity, and dielectric response function for paper and oil, and from the scanning electron microscopy study of paper structure.[1]

5.1 Permittivity of Paper

Table 5.1 displays the results from the capacitance and thickness measurements that were the basis for estimating the paper permittivity. By using the method described in section 4.1.1 for eliminating the contribution from excess intersheet oil (i.e., oil that caused the measured test object thickness to exceed nominal paper thickness), the relative permittivity of paper was estimated to be $\varepsilon_{\mathrm{r,pap}} = 3.14$.

Examples of values for the relative permittivity of paper used for calculations on mass-impregnated paper insulation in literature are 3.5 [34], [65], 4.0 [32], and 4.1 [66]. Typical values for impregnated pressboard (for transformers) are between 3.6 and 4.4 [67]. The value found in this study ($\varepsilon_{\mathrm{r,pap}} = 3.14$) is lower than those values. Since oil has a relative permittivity of 2.25 (see section 5.2), the low value of paper permittivity found here indicates that the share of oil in the paper test objects was relatively high, even though excess intersheet oil was eliminated from the estimate. The large uncertainty in the total thickness

[1] The current measurements on which the results in sections 5.3 and 5.5 are based were performed by Lars Erik Pettersen in cooperation with the author of this thesis. The same applies to the measurements on which the circles in figure 5.4 are based. Data from the measurements are published in Pettersen's master's thesis [52].

Table 5.1: Thicknesses and capacitances for paper test objects

Total thickness d_{mea} (mm)	Capacitance C_{mea} (pF)
FOUR SHEETS ($d_{\mathrm{pap}} = 0.36\,\mathrm{mm}$):	
0.34	215.7
0.41	220.0
EIGHT SHEETS ($d_{\mathrm{pap}} = 0.72\,\mathrm{mm}$):	
0.88	104.3
0.91	106.4
1.14	73.6
0.99	90.3
1.11	56.0
0.90	80.8
TEN SHEETS ($d_{\mathrm{pap}} = 0.90\,\mathrm{mm}$):	
1.27	60.7
0.87	89.5
0.95	67.0
0.89	90.1
THIRTEEN SHEETS ($d_{\mathrm{pap}} = 1.2\,\mathrm{mm}$):	
1.25	75.8
EIGHTEEN SHEETS ($d_{\mathrm{pap}} = 1.6\,\mathrm{mm}$):	
1.78	54.7

measurements could have also been a major contributor to the deviation from the aforementioned literature values.

5.2 Permittivity of Oil

Measured permittivities of oil test objects are indicated in table 5.2. The average relative permittivity was $\varepsilon_{\mathrm{r,oil}} = 2.25$ and was used in the further calculations. This corresponds to what the manufacturer states as the “typical value” for this particular oil at 60 °C [68]. The source does not state which frequency this value relates to. The range from 2.2 to 2.3 is typical for the permittivity of mineral oils at power frequency (50 Hz or 60 Hz) and room temperature [35].

Table 5.2: Relative permittivity of oil

Test object thickness[a] (mm)	Capacitance (F)	Relative permittivity
0.21	216.6	1.62
1.08	53.5	2.06
3.22	20.5	2.36
4.33	20.5	2.36
5.82	13.6	2.83
		2.25[b]

[a] Measured with the "total test object thickness" method described in section 3.1.1, page 26.
[b] Average of the entries above.

5.3 Conductivity of Paper

5.3.1 Results

Figure 5.1 indicates steady-state conductivity as a function of electric field strength in paper test objects with various numbers of paper sheets. The conductivities were calculated from the difference between polarization currents and depolarization currents 2.5 hours after voltage application and grounding; this corresponds to equation (4.6) with $t = 2.5$ hours. The lowest electric field strength in these measurements was 0.2 kV/mm.

Figure 5.2 displays measured conductivity as a function of electric field strength in paper test objects with ten paper sheets. These conductivities were calculated with currents measured 5 and 36 hours after voltage application and grounding. The conductivities have the exponential characteristic of equation (4.7) above approximately 10 kV/mm. Curve fitting of equation (4.7) gave $\sigma_0 = 7.75 \times 10^{-15}$ S/m and $\eta = 2.52 \times 10^{-8}$ m/V, and the fitted curve is indicated in the figure. Furthermore, the figure illustrates that the differences between the results from the five-sheet and the fourteen-sheet test objects were less than the variations in results from the various measurement series with ten-sheet test objects. There was thus no observed difference due to test object thickness. It indicates that with as few as five sheets, effects from the bulk already dominates over effects from the electrode-paper interfaces.

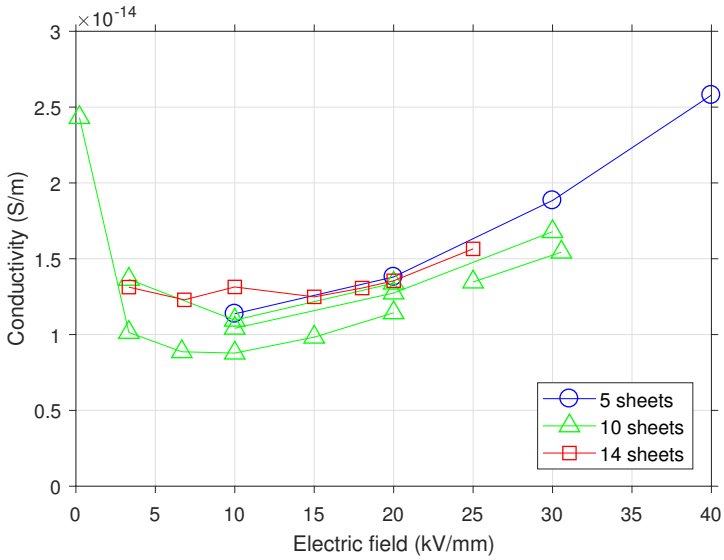

Figure 5.1: Conductivity of paper test objects with various numbers of paper sheets, calculated from polarization and depolarization currents. There were four measurement series with ten sheets. Readings 2.5 hours after voltage application and grounding.

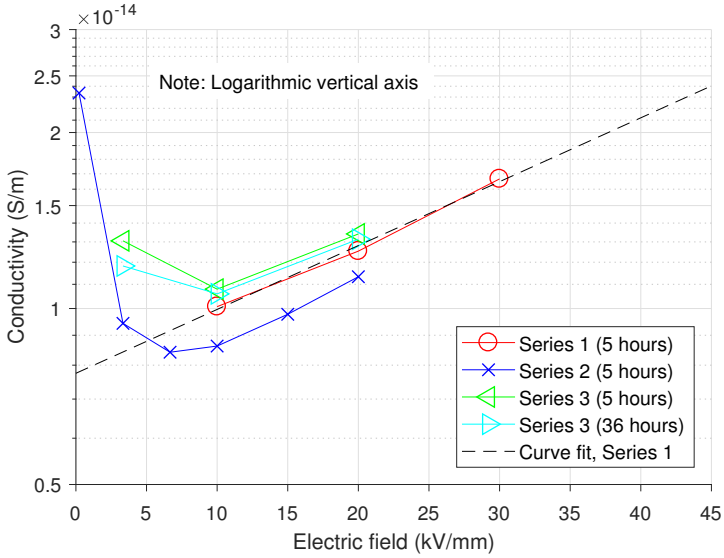

Figure 5.2: Conductivity of paper test objects with ten paper sheets, calculated from polarization and depolarization currents. Three measurement series, all with readings 5 hours after voltage application, one of them with an additional reading 36 hours after voltage application. Curve fit of equation (4.7), $\sigma_{\mathrm{pap}}(E_{\mathrm{pap}}) = \sigma_0 \exp(\eta |E_{\mathrm{pap}}|)$, to Series 1.

5.3.2 Discussion

Because multi-layered test objects were used, the effects from inhomogeneities both due to the internal structure of each sheet and due to paper-paper interfaces (either in the form of charge traps and barriers or other phenomena [22], [69], [70]) were averaged out. The similarity between the results obtained with five- and ten-sheet test objects indicates that if injected charge from the electrodes caused the conductivity to be higher in some of the sheets than in the rest of the test object, the higher conductivity was mainly restricted to the paper sheet closest to each electrode. This is supported by space charge measurements [22] that has showed that injected charge in mass-impregnated paper at room temperature is restricted to only the sheet closest to the electrode.[2]

Figure 5.2 illustrates that waiting 36 hours instead of 5 hours between voltage application and current reading did not affect the results more than the variation between different measurement series. Five hours was thus considered as a sufficient polarization time.

The curve fit in figure 5.2 was selected as conductivity for further calculations. Series 1 was chosen for the curve fit as it lies well within the spread of results, and it covers most of the range of electric field strengths relevant to the electric field estimates. For electric field strengths under 10 kV/mm, the exponential curve does not fit the measured conductivity well. Thus, the choice of using this particular curve fit cause the conductivity to be underestimated below approximately 10 kV/mm. However, as will become apparent later, those field strengths are less relevant for the electric field estimates in this work.

Figure 5.3 facilitates comparison of the steady-state conductivity of paper test objects and cable insulation at 50 °C reported by other authors. The electric field dependency η (cf. equation (4.7)) in the present work is 0.0252 mm/kV. This is close to 0.03 mm/kV, which is a typical value in the literature [5], [55], [59].

[2] Information on the temperature was obtained from the author of reference [22] via e-mail on November 19, 2019.

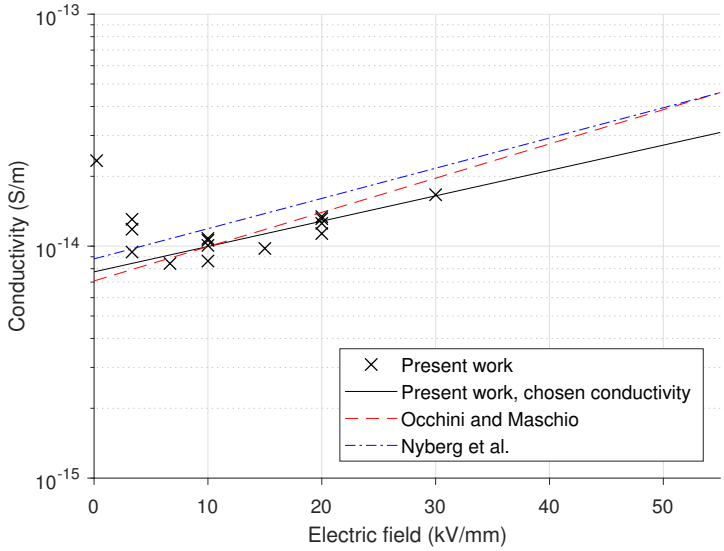

Figure 5.3: Conductivity of mass-impregnated HVDC paper test objects or cable insulation as a function of electric field strength at 50 °C in various works.
"Present work": results presented in figure 5.2; plane-parallel laboratory test objects.
Occhini and Maschio [55]: plane-parallel laboratory test objects.
Nyberg et al. [71]: cable, including butt gaps.

5.4 Conductivity of Oil

5.4.1 Results

Results from conductivity measurements with bare and paper-covered electrodes are presented in figure 5.4. The results from bare electrodes are largely within the same range as those from paper-covered electrodes. The two test objects used for paper-covered electrodes were the large and small series connection test objects, as defined in section 3.1.1.

5.4.2 Discussion

Bare Electrodes

The repeatability of the measurements were low. Handling of the PTFE spacer that created the oil gap seem to have impaired the repeatability, possibly due to redistribution of impurities in the oil. Furhtermore, current fluctuations rendered determination of steady-state values difficult. The maximum attainable electric field strength with bare electrodes was 7 kV/mm before current fluctuations or discharges that overwhelmed the experimental equipment occurred. Current

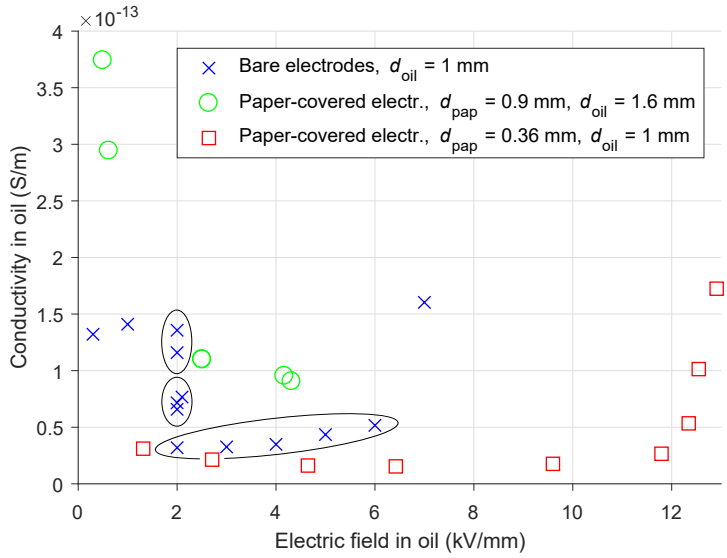

Figure 5.4: Conductivity of oil with bare and paper-covered electrodes. For bare electrodes, the test object was not repositioned between measurements plotted within the same ellipse in the figure. For paper-covered electrodes, each test object remained untouched between all of the measurements. The data for bare electrodes are previously pulished in [72].

fluctuations, poor repeatability and poor breakdown strength for conductivity of liquids with bare electrodes are common phenomena, attributed to impurities in the liquid or adsorbed layers at the electrodes [73].

Paper-Covered Electrodes

Since the conductivity of a material depends on the concentration of charge carriers [74], the extent to which charge carriers are neutralized or immobilized at the electrode surfaces affects the conductivity. The neutralization and immobilization are affected by the electrode material and the conditions at the surfaces [73]. For an oil gap surrounded by paper, the papers act as electrodes for the oil. The paper surfaces provide sites for the trapping of charge carriers [75], which affects the charge carrier concentration in the oil. Furthermore, the electrode material and condition affect the ability to inject charges into the oil [73]. For these reasons, paper-covered electrodes are more relevant than bare electrodes when conductivities in oil gaps surrounded by paper are to be determined. However, this study's results from bare and paper-covered electrodes overlapped each other. The variations within each method were approximately as large as the variations between the methods.

When plotted versus electric field strength as in figure 5.4, the conductivities form a U-shaped curve. This is consistent with ionic conduction in insulation liquids: The conductivity is constant at low electric field strengths. At intermediate field strengths, the conductivity decreases with increasing field strength. At high field strengths, charge injection from the electrodes become significant and causes the conductivity to increase with increasing field strengths [35], [73], [76].

With bare electrodes, four parameters are required to estimate the oil conductivity: applied voltage, measured current, effective electrode area, and oil gap thickness. With paper-covered electrodes, the values of paper thickness and the relationship between electric field strength and conductivity in paper are needed as well. This introduces additional sources of error. As asserted in section 5.3.2, the relation used for $\sigma_{\mathrm{pap}}(E_{\mathrm{pap}})$ underestimates E_{pap} at low electric field strengths. Equation (4.9) can be re-written as

$$E_{\mathrm{oil}} = \frac{U_0 - \overbrace{d_{\mathrm{pap}} J_{\mathrm{st}}/\sigma_{\mathrm{pap}}}^{U_{\mathrm{pap}}}}{d_{\mathrm{oil}}}, \tag{5.1}$$

and equation (4.11) can be rewritten as

$$\sigma_{\mathrm{oil}} = \frac{d_{\mathrm{oil}} J_{\mathrm{st}}}{U_0 - \underbrace{d_{\mathrm{pap}} J_{\mathrm{st}}/\sigma_{\mathrm{pap}}}_{U_{\mathrm{pap}}}}, \tag{5.2}$$

where U_{pap} indicates the estimated voltage drop across the paper part of the test object (see appendix B). The underestimated σ_{pap} leads to an underestimated E_{oil} and an overestimated σ_{oil}. This can be compensated for by using equations (5.1) and (5.2) with E_{pap} from Series 2 or 3 (cf. fig. 5.2) for the lowest electric field strengths. The plot of σ_{oil} versus E_{oil} will then still be U-shaped, though for the smaller of the two test objects, the left part of the U shape will be less steep, with $E_{\mathrm{oil}} = 0.23 \times 10^{-13}\,\mathrm{S/m}$ at $E_{\mathrm{oil}} = 1.8\,\mathrm{kV/mm}$ and $E_{\mathrm{oil}} = 0.19 \times 10^{-13}\,\mathrm{S/m}$ at $E_{\mathrm{oil}} = 3.0\,\mathrm{kV/mm}$. For the lowest applied voltages, the estimated values for E_{oil} and σ_{oil} were negative. This indicates that the difference between the true σ_{pap} and the input σ_{pap} was so large that U_{pap} in equations (5.1) and (5.2) became larger than the applied voltage U_0. The negative results are excluded from figure 5.4 since they are clearly erroneous.

Values from Literature

Various values have been found in literature for the conductivity of oil for mass-impregnated cables:

- 1×10^{-12} S/m measured at 50 °C, electric field strength not reported [55].
- 1×10^{-13} S/m to 5×10^{-13} S/m for new oil at 60 °C, electric field less than 10 kV/mm [77].
- 0.5×10^{-11} S/m to 2×10^{-11} S/m for oil extracted from cycled (assumingly *temperature* cycled) cables, measured at 60 °C, electric field less than 10 kV/mm [77].

Further details on measurement techniques were not disclosed. The large range of these values confirms that oil conductivity is a parameter that varies considerably.

Value Chosen for Further Calculations

The field-dependent "curves" obtained with the two different series connection test objects (i.e., paper-covered electrodes) differ from each other by a factor five or more (fig. 5.4). Many of the results from the bare electrodes are between those curves. None of the results are prominent as more accurate than the others, and the field-dependency of the oil conductivity is not clear from the results. For these reasons, the average (mean) conductivity from bare electrodes, $\sigma_{\text{oil}} = 8.4 \times 10^{-14}$ S/m, was used for further calculations, and the oil conductivity was regarded as independent of the electric field strength.

5.5 Dielectric Response Function for Paper

5.5.1 Results

Results from several measurements of the dielectric response function for paper are illustrated in figure 5.5. The median dielectric response function determined from polarization is highlighted in the figure. The median was used for further calculations after curve fitting of equation (4.12), which is a linear combination of exponential functions. The curve fit was conducted with eight exponential functions (i.e., $N = 8$). The median was determined from the current measurements at polarization, not depolarization.

Figure 5.5 reveals that for the first approximately six hundred seconds, the results from depolarization had generally larger values than the results from polarization. For each of the thirteen PDC measurements presented in the figure, the difference between $f_{\text{pap}}(t = 2\,\text{s})$ determined from the depolarization current and $f_{\text{pap}}(t = 2\,\text{s})$ determined from the polarization current was calculated. The mean of these differences was $5.5 \times 10^{-3}\,\text{s}^{-1}$, and the standard deviation was $5.2 \times 10^{-3}\,\text{s}^{-1}$. This implies that the difference between $f_{\text{pap}}(t)$ determined

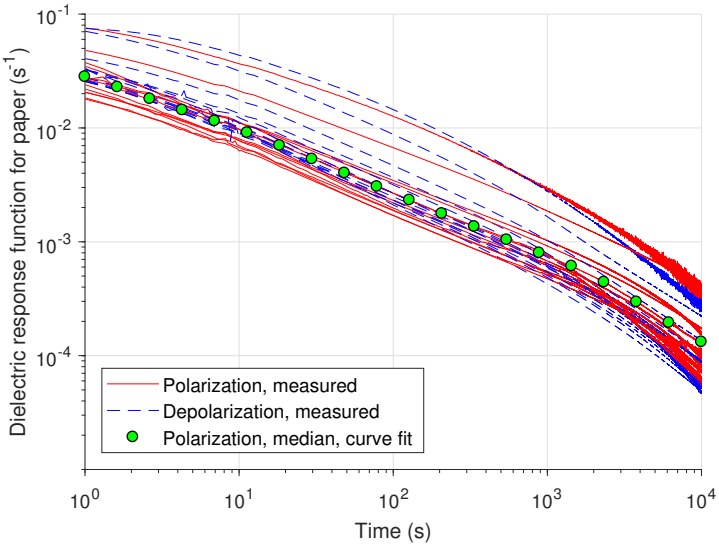

Figure 5.5: $f_{\mathrm{pap}}(t)$ estimated from several measurements of polarization ("pol") and depolarization ("depol") currents in paper test objects with ten paper sheets.

from depolarization and $f_{\mathrm{pap}}(t)$ determined from polarization was statistically significant for $t = 2\,\mathrm{s}$. The corresponding difference for $t = 1000\,\mathrm{s}$ was not significant.[3]

Not only the difference but also the ratio between $f_{\mathrm{pap}}(t = 2\,\mathrm{s})$ determined from the depolarization current and $f_{\mathrm{pap}}(t = 2\,\mathrm{s})$ determined from the polarization current was calculated for each of the thirteen PDC measurements. The maximum, mean, and minimum of these ratios were 1.5, 1.3, and 0.9, respectively. Corresponding values for $t = 1000\,\mathrm{s}$ were 1.1, 0.9, and 0.7, respectively. In comparison, the maximum and minimum dielectric response functions determined from polarization differed from each other by a factor of 4.6–7.5. This illustrates that the spread in the results was larger than the differences between depolarization and polarization.

No clear dependency on the applied electric field were observed. This is illustrated by figure 5.6, which displays an excerpt from figure 5.5 with the applied electric field strengths indicated.

[3]It was constructed a null hypothesis stating that the mean difference was zero. A two-sided test of the null hypothesis was performed with a significance level of 0.5 % and twelve degrees of freedom, assuming Student's t distribution [44]. The sample mean was $5.5 \times 10^{-3}\,\mathrm{s}^{-1}$ for $t = 2\,\mathrm{s}$ and $-6.7 \times 10^{-5}\,\mathrm{s}^{-1}$ for $t = 1000\,\mathrm{s}$. The sample standard deviations were $5.2 \times 10^{-3}\,\mathrm{s}^{-1}$ and $1.3 \times 10^{-4}\,\mathrm{s}^{-1}$, respectively. This resulted in rejection of the null hypothesis for $t = 2\,\mathrm{s}$ but not for $t = 1000\,\mathrm{s}$. The p values were 0.0025 and 0.0572, respectively.

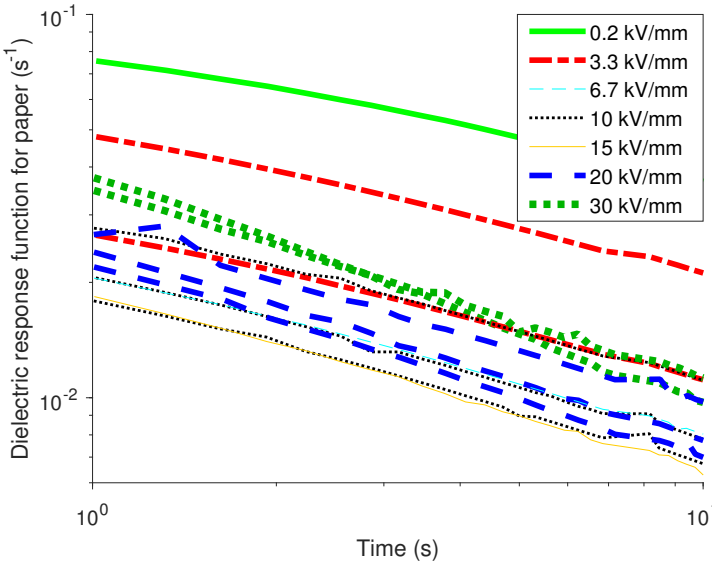

Figure 5.6: The first ten seconds of the results shown in figure 5.5, polarization only, with applied electric field strengths indicated.

5.5.2 Discussion

In figure 5.7, the median dielectric response function, which is utilized for further calculations, is compared with results obtained at 20 kV/mm by Occhini and Maschio [55]. The spread of the results in this work is also indicated. The results obtained by Occhini and Maschio approximately equal the lowest values obtained in this work.

Some plausible causes for the spread in the results are temperature fluctuations (approx. ±1 °C) and varying amount of oil in the test objects due to handling. It is less likely that remaining polarization due to insufficient depolarization time between successive voltage applications ("memory effect") is the main cause of spread. This is because the depolarization current before each new voltage application was typically less than 2 % of the steady-state current—and several orders of magnitude lower than the initial current—in the next voltage application.

A possible explanation for the differences between the dielectric response function determined from polarization and depolarization is a gradual injection of charge from the electrodes and accumulation of this charge in the test object during the course of the voltage application. The withdrawal of charge would add to the depolarization current [40], [42]. Another possible explanation for the difference is the redistribution of charge carriers in the test object during

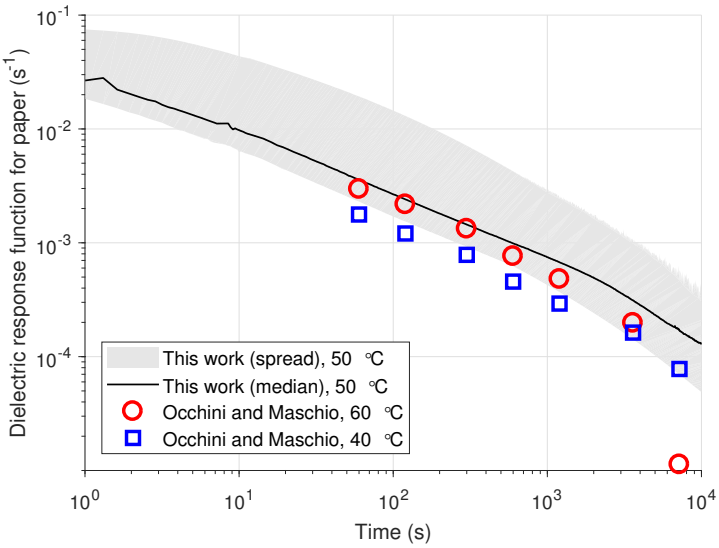

Figure 5.7: Dielectric response functions from polarization currents at 20 kV/mm.
This work: Plane-parallel test objects of mass-impregnated paper sheets.
Occhini and Maschio: Plane-parallel test objects of mass-impregnated paper tapes with butt gaps; data extracted from reference [55], ©1967 IEEE, used with permission.

polarization, regardless of any possible charge injection, causing the conductivity as well as the electric field in the test object to be inhomogeneous. Although this nonlinear behavior was statistically significant, it was not dominant, since the value of the ratio of $f_{\mathrm{pap}}(t)$ determined from depolarization currents and $f_{\mathrm{pap}}(t)$ determined from polarization current was well below 2.0.

The extrapolation backwards from $t = 1\,\mathrm{s}$ to $t = 0\,\mathrm{s}$ is an estimate of the effect of the slow polarization mechanisms before the measurements were collected. However, all the polarization at $t = 0$ is already accounted for by the permittivity, and the extrapolation back to $t = 0$ implies that some of the polarization is accounted for twice. It could thus be argued that the extrapolation should not go all the way to zero but to a time slightly larger than zero. It is not obvious, though, exactly where to stop the interpolation. However, the error made by extrapolating all the way to zero is small. The contribution from the whole second of extrapolation is

$$P_{1\,\mathrm{s}} = \varepsilon_0 \int_0^{1\,\mathrm{s}} E(\xi) f(t-\xi)\,\mathrm{d}\xi. \tag{5.3}$$

By assuming E as constant throughout the first second (which is exact in the case of a single, homogeneous material, but an approximation in the case of a

homogeneous material in a series connection), this can be simplified to

$$P_{1\,\mathrm{s}} = \varepsilon_0 E \int_0^{1\,\mathrm{s}} f(t)\,\mathrm{d}t. \tag{5.4}$$

Neither the measured nor the extrapolated $f_{\mathrm{pap}}(t)$ at any time exceeded $0.1\,\mathrm{s}^{-1}$. Therefore,

$$P_{1\,\mathrm{s}} < 0.1\varepsilon_0 E. \tag{5.5}$$

Appreciating that some of this extrapolation is probably appropriate, the error can be assumed to be lower than this value. When comparing with the contribution from the permittivity, which is $P_{\mathrm{fast}} = \varepsilon_0\varepsilon_{\mathrm{r}}E = 3.14\varepsilon_0 E$, it is evident that the error is negligible.

5.6 Dielectric Response Function for Oil

5.6.1 Results

Results from dielectric response function measurements for oil are exhibited in figure 5.8, including the median curve for both polarization and depolarization. The corresponding curve fits of a linear combination of three exponential functions (i.e., equation (4.12) with $N = 3$), utilized for the further calculations, are also illustrated. The magnitude of the results calculated from depolarization currents were approximately 1 % of those calculated from polarization currents. All the measurements were done with oil test objects (i.e., bare electrodes).

The median dielectric response functions indicated in figure 5.8 have ripples. The ripples are most easily visible in the right part of the figure due to the logarithmic time axis. The ripples in the curve obtained from *depolarization* current measurements are noise due to external disturbances, including ripples in the supplied DC voltage. Such noise caused transients that in most cases were less than $5 \times 10^{-5}\,\mathrm{s}^{-1}$ peak to peak in the estimated dielectric response function, and often much less than that. In the displayed curve, these transients were approximately $1.5 \times 10^{-5}\,\mathrm{s}^{-1}$ peak to peak. The ripples in the curve obtained from *polarization* current measurements are much larger and are due to the current fluctuations that are described for bare electrodes in section 5.4.2.

The first 100 s of the dielectric response functions estimated from current measurements at various applied electric field strengths are displayed in figure 5.9 for polarization and figure 5.10 for depolarization. No significant electric field dependency can be perceived for the polarization. For depolarization, the lowest field strengths (0.3 kV/mm and 1 kV/mm) appear to give a larger $f_{\mathrm{oil}}(t)$ than the other field strengths, but considering the spread at 2 kV/mm and 2.1 kV/mm, this should not be regarded as significant.

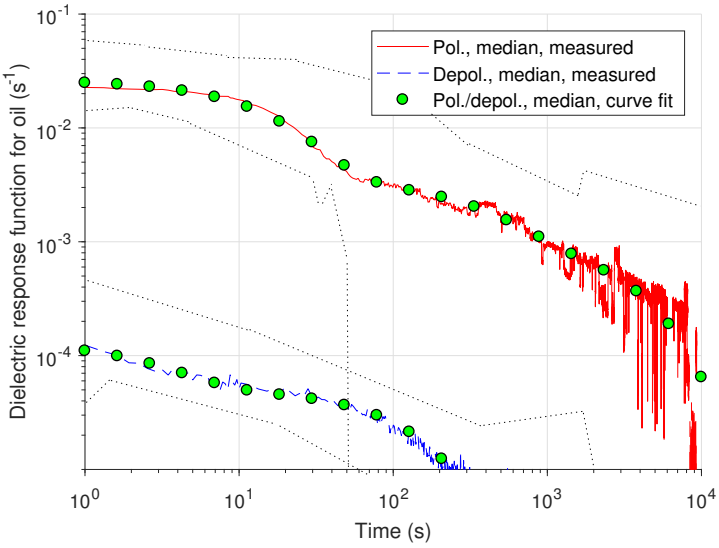

Figure 5.8: Dielectric response function $f_{\text{oil}}(t)$ for oil calculated from polarization and depolarization currents. The thin, dotted curves roughly indicate the limits of the spreads of the results.

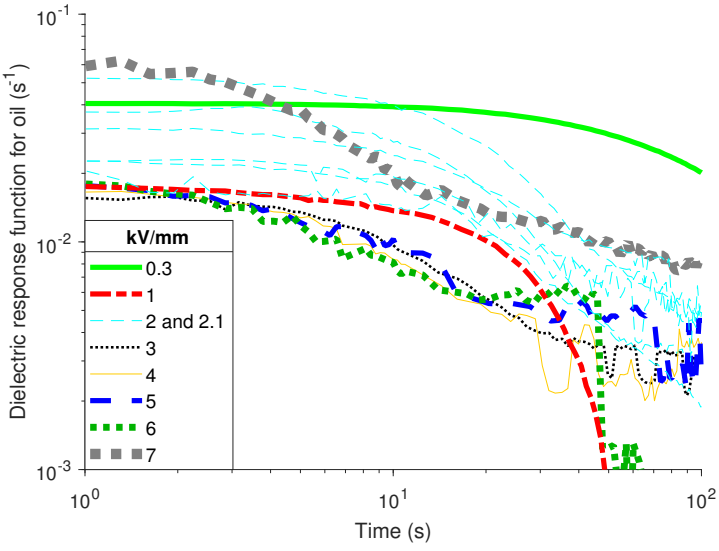

Figure 5.9: Dielectric response function from several measurements of polarization currents in oil. Applied electric field strengths are indicated. $1\,\text{s} < t < 1\,\text{s}$.

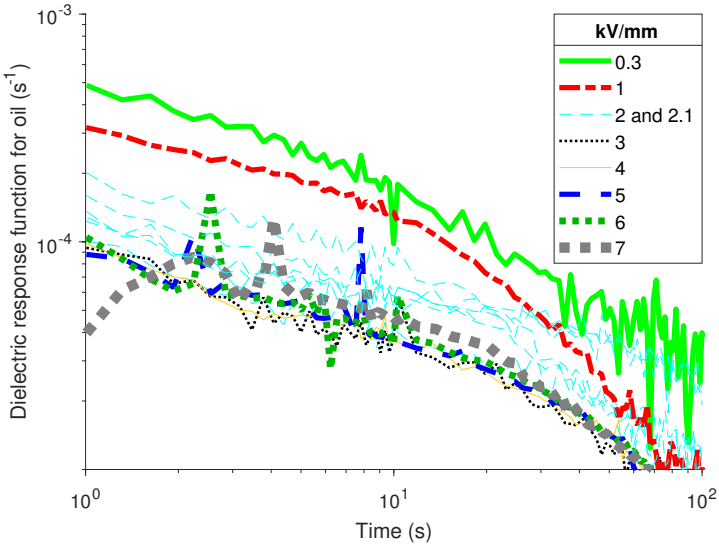

Figure 5.10: Dielectric response function from several measurements of depolarization currents in oil. Applied electric field strengths are indicated. $1\,\mathrm{s} < t < 1\,\mathrm{s}$.

5.6.2 Discussion

The dielectric response function determined from polarization was approximately 10^2 times larger than that determined from depolarization. This indicates that the polarization in oil is not linear with respect to the exciting electric field.[4] Others [78] have found similarly large differences between polarization and depolarization currents for transformer oil. At polarization, the dielectric response function contains contributions from mechanisms that can be regarded as time-dependent conduction processes. A notable example of such a process is the depletion of charge carriers (and thereby the reduction of conductivity) in the bulk of the liquid as the charge carriers drift towards the electrodes where they no longer contribute to conduction. Injection of charge from the electrodes also contributes to the conduction [35], [76], [78]. This demonstrates that $f_{\mathrm{oil}}(t)$ at polarization has contributions from both a slow, time-dependent permittivity and a time-dependent conductivity. During depolarization, the mean electric field strength (i.e., applied voltage divided by oil gap thickness) is zero, and charges that have accumulated close to the electrodes are retained by mirror charges on the electrodes. Therefore, the transport of free charges is quite limited [35]. The large difference between polarization and depolarization currents indicates

[4]The word *exciting* is used here to indicate that the polarization is excited by not only the present but also the past electric field (see section 2.3.2).

that the conduction mechanisms dominate over polarization mechanisms during voltage application [78], [79].

Despite the mentioned nonlinearity, no significant dependency on electric field strength can be observed when the results from polarization are evaluated separately from the results from depolarization. The spread in the results (except from the difference between polarization and depolarization) is mainly due to other phenomena, such as impurities, the handling of PTFE spacer between some of the measurements, and differing polarization times. The depolarization time between subsequent voltage applications in this study was always long enough for the current to decay to the noise level. Even so, the charge distribution may not have been completely reset between voltage applications. It is thus possible that too short and differing depolarization times may have contributed to the spread in the results.

Although much of the spread in the results can be attributed to the phenomena described above, there is a possibility that there is a small dependency on the electric field, masked by the mentioned sources of spread and thus rendered insignificant here. The indications that much of the contribution to the dielectric response function for oil can be regarded as time-dependent conduction, together with the fact that conduction in oil generally is field dependent, render this possibility probable. This suggests that an electric field dependency may have been observed if measurements were collected at higher field strengths.

Much of the decrease in polarization current in oil after voltage application is due to the aforementioned depletion of charge carriers. The time required for the depletion process is dependent on the thickness of the oil gap. Under a given, uniform electric field, the transit time for a charge carrier from one electrode to another is proportional to d_{oil} [76]. This demonstrates that the dielectric response function is dependent on oil gap size.

The reasoning regarding error by extrapolating $f_{\text{pap}}(t)$ back to $t = 0$ (see section 5.5.2) is valid for $f_{\text{oil}}(t)$ as well.

5.7 Structure of Paper

5.7.1 Results

Scanning electron micrographs of paper surfaces are shown in figure 5.11 and figure 5.12. Scanning electron micrographs of cross sections are shown in figures 5.13 through 5.16. For the micrographs of the cross sections, the colors can be interpreted as follows:

white roughness due to specimen preparation

light grey paper fibers

dark grey epoxy for fixating the paper fibers

black cracks in the specimen due to the specimen preparation

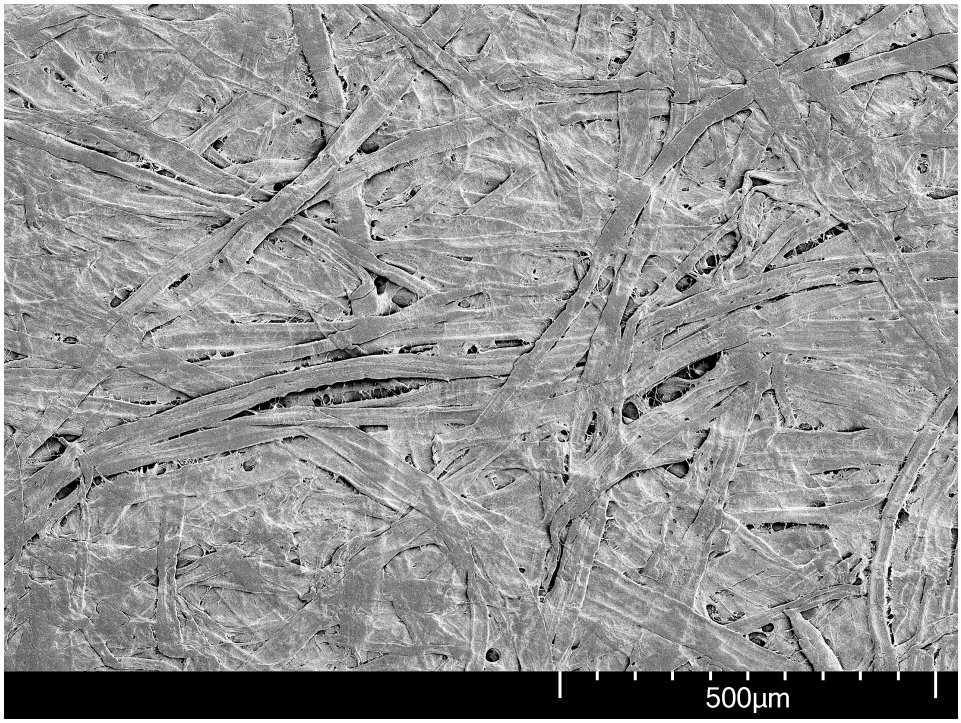

Figure 5.11: Scanning electron micrograph of cable paper surface. Original micrograph made by Per Olav Johnsen at RISE PFI AS. This edited micrograph: ©2019 IEEE, published in [16], reproduced with permission.

5.7.2 Discussion

In this chapter, the differing terms *width* and *thickness* are distinguished. The former refers to directions parallel to the plane of the investigated piece of paper (e.g., cross direction and machine direction). In contrast, the latter refers to the direction perpendicular to that plane, corresponding to the radial direction in a cable.

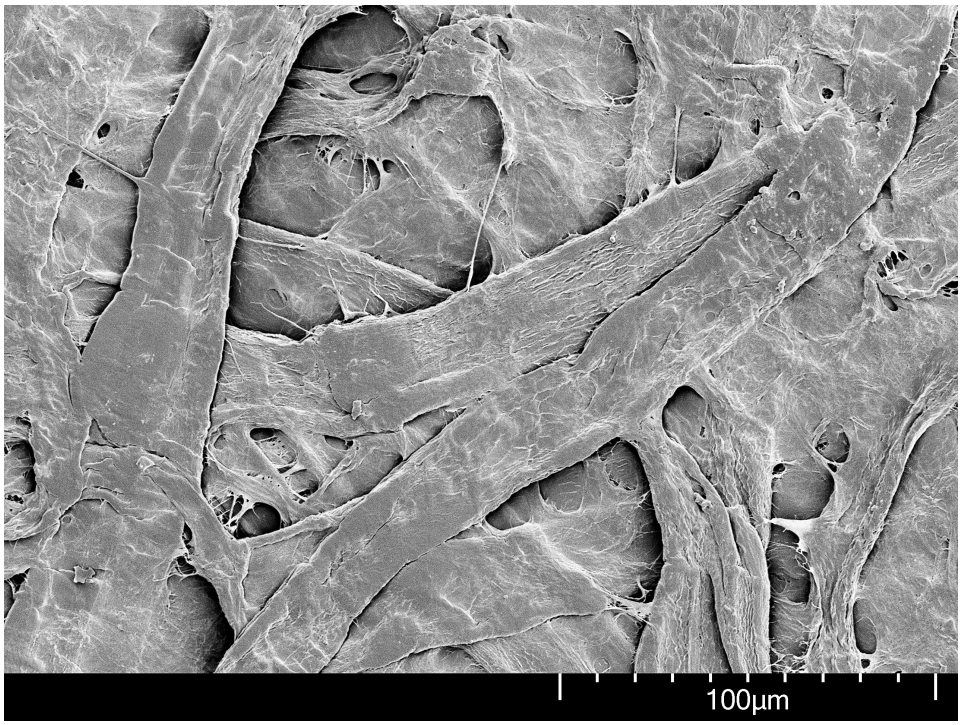

Figure 5.12: Scanning electron micrograph of cable paper surface. Original micrograph made by Per Olav Johnsen at RISE PFI AS. This edited micrograph: ©2019 IEEE, published in [16], reproduced with permission.

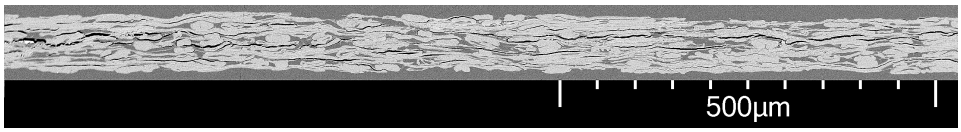

Figure 5.13: Scanning electron micrograph of cable paper cross section with angle of view in cross direction. Original micrograph made by Per Olav Johnsen at RISE PFI AS. This edited micrograph: ©2019 IEEE, published in [16], reproduced with permission.

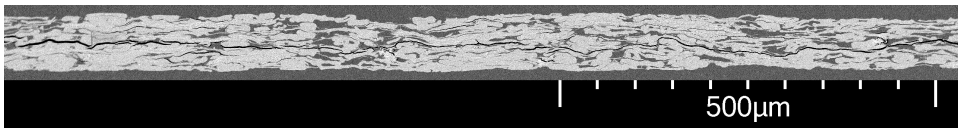

Figure 5.14: Scanning electron micrograph of cable paper cross section with angle of view in machine direction. Original micrograph made by Per Olav Johnsen at RISE PFI AS. This edited micrograph: ©2019 IEEE, published in [16], reproduced with permission.

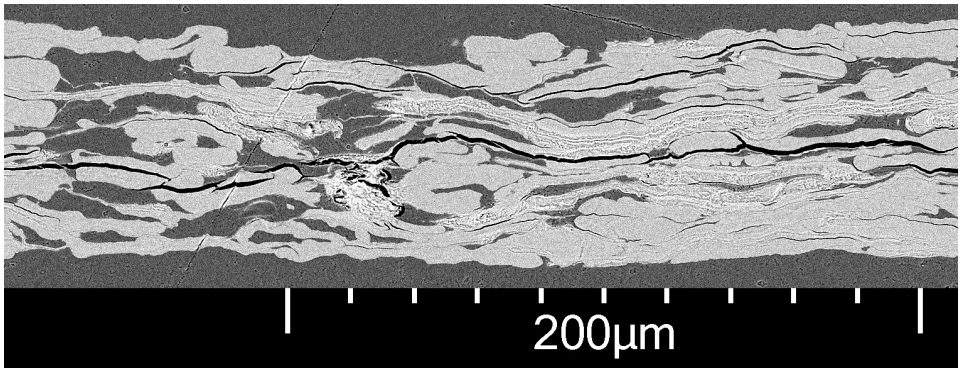

Figure 5.15: Scanning electron micrograph of cable paper cross section, zoomed in on a region corresponding to 400 µm to 700 µm to the right of the left edge of figure 5.14. Angle of view: Machine direction. Original micrograph made by Per Olav Johnsen at RISE PFI AS. This edited micrograph: ©2019 IEEE, published in [16], reproduced with permission.

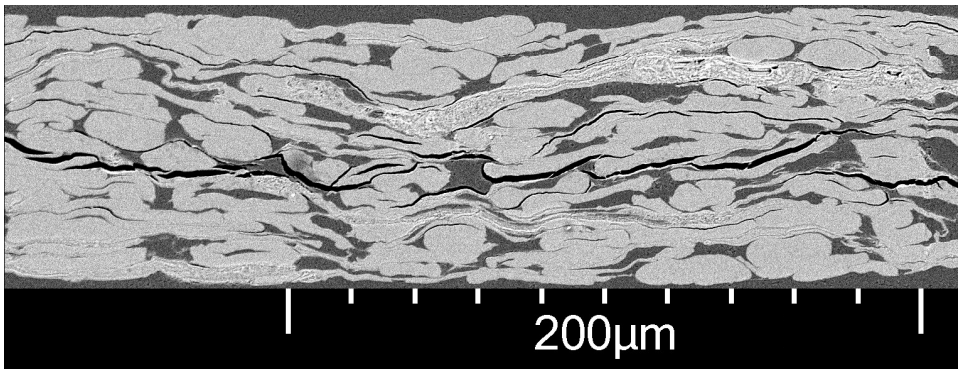

Figure 5.16: Scanning electron micrograph of cable paper cross section with angle of view in machine direction. Original micrograph made by Per Olav Johnsen at RISE PFI AS. This edited micrograph: ©2019 IEEE, published in [16], reproduced with permission.

Interfaces

The scanning electron micrographs show that there are large areas of interfaces between paper and epoxy in the specimens. This indicates that oil-impregnated paper has large areas of fiber-oil interfaces. The micrographs also demonstrate that such interfaces abound in most of the bulk of the paper tapes and is far from unique for the surfaces of the tapes. Based on this observation, the surfaces of the tapes need not be treated separately when estimating electric fields in paper-oil systems—they can simply be considered part of the paper [16].

Oil Channel Sizes

A typical butt gap is as thick as a paper tape, namely approximately 0.9 mm, and has a width of 1–4 mm [4]. The thicknesses and widths of the channels (defined in fig. 1.1) visible in the micrographs are much smaller: The thickness of most channel cross sections visible in these images are less than 15 % of the paper thickness. Some regions have channels that lie above each other in such a way that, when viewed in the direction perpendicular to the paper surface, more channel volume than fiber volume is evident. The left part of figure 5.15 exemplifies such a region. Nevertheless, the widths of such regions are negligible compared with typical butt gap widths. Therefore, it is appropriate to model the oil-filled channels as part of the paper while modeling oil-filled butt gaps as a different material [16].

Intersheet Oil

As mentioned in section 1.1.2, contacting paper tapes in mass-impregnated cables are in contact with each other at discrete spots due to the surface roughness, resulting in an *intersheet gap* filled with oil (see fig. 1.1).[5] It would be interesting to discover if typical thicknesses of intersheet gaps are comparable to channel thicknesses, or at least if typical intersheet gap thicknesses are much smaller than typical butt gap thicknesses. The roughness visible in the present micrographs is caused by at least two phenomena: individual fibers on the paper surface and varying number of fibers from one region to another. The former phenomenon manifests itself on a small length scale (i.e., up to approximately 50 µm width and 14 µm thickness); in contrast, the latter occurs on a larger scale. Which length scale is decisive for the thickness of the intersheet gap is dependent on how the surfaces yield to one another. The micrographs provide no information regarding this.

[5] It is likely that there is a thin oil layer between the papers even at these contacting spots due to the oil's ability to wet paper.

The largest and smallest thickness in these micrographs are 85 μm and 59 μm, respectively—a difference of 26 μm. Typical channel cross sections visible in the micrographs are less than 11 μm. This indicates that intersheet gaps may possibly be thicker than the channels inside the paper, but, again, this depends on the malleability of the paper surfaces.

Chapter 6

Results from Estimates and Measurements on a Series Connection Test Object

This chapter has two primary purposes: to demonstrate the role of dielectric response functions in a series connection of paper and oil, and to demonstrate the reliability of (i.e., verify) the methods for estimating electric fields in the same series connection. The role of the dielectric response functions is demonstrated by presenting estimates of electric fields and current densities with and without considering the dielectric response functions, as well as presenting a sensitivity analysis where different dielectric response functions are used as input. The reliability is demonstrated by comparing estimated current densities with measured current densities. Furthermore, results from the two-material-input method are compared with results from the one-material-input method.

All the results presented in this chapter apply to the large series connection test object ($d_{\mathrm{pap}} = 0.9\,\mathrm{mm}$, $d_{\mathrm{oil}} = 1.6\,\mathrm{mm}$) for application of a step voltage corresponding to a mean electric field strength $\overline{E} = U_0/\left(d_{\mathrm{pap}} + d_{\mathrm{oil}}\right) = 12\,\mathrm{kV/mm}$ and subsequent grounding.[1]

[1] The current measurements presented in this chapter were performed by Lars Erik Pettersen in cooperation with the author of this thesis. Data from the measurements are published in Pettersen's master's thesis [52].

6.1 Results

6.1.1 Results from the Two-Material Input Method

Voltage on

Figure 6.1 illustrates the estimated electric fields in paper and oil after turning the voltage on. Estimates where the dielectric response functions are omitted (i.e., $f_{\text{pap}}(t) = f_{\text{oil}}(t) = 0$ for all t) are also exhibited. The t_{90} is more than twice as large when dielectric response functions are considered than whey they are omitted from the estimates: with dielectric response functions, $t_{90} = 2786\,\text{s}$, whereas without, $t_{90} = 1317\,\text{s}$. Figure 6.2 illustrates the corresponding estimated current densities together with the measured current density.[2]

The estimated current density matched its measured counterpart most closely when the dielectric response functions were accounted for: when the dielectric response functions were neglected, the estimated current density was not within $\pm 20\,\%$ of the measured current density before $t = 104\,\text{s}$, whereas when the dielectric response functions were considered, the same was the case for all values of t larger than approximately 2 s.

Grounding

Figures 6.3 and 6.4 illustrate electric fields and current densities after grounding. The time $t = 0$ in these figures correspond to the limit $t \to \infty$ in figures 6.1 and 6.2.

Estimates were made with $f_{\text{oil}}(t)$ obtained both from polarization and from depolarization current measurements to see which best represented the grounding situation. The $f_{\text{oil}}(t)$ obtained from polarization provided better agreement between estimated and measured current densities. This fits well with the fact that the mean electric field strength in the oil did not become zero immediately after grounding (as it did when determining $f_{\text{oil}}(t)$ from depolarization), but changed direction and gave rise to time-dependent conduction of accumulated charges from one side of the oil gap towards the other side of the oil gap [35].

Values of t_{90} with $f_{\text{oil}}(t)$ from polarization, with $f_{\text{oil}}(t)$ from depolarization, and without and dielectric response functions were 3761 s, 4294 s, and 1613 s, respectively. The large differences between these numbers illustrate the importance of the dielectric response functions also in the case of grounding.

[2] Figures similar to figures 6.1 and 6.2 have been published in [61], though only with estimates in which the dielectric response functions were considered. Slightly different values for the electrical properties were used as input.

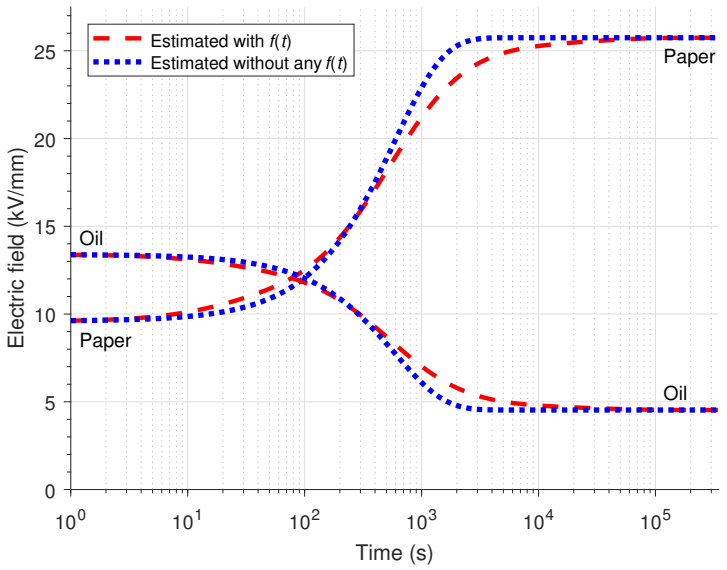

Figure 6.1: Electric fields in the large series connection test object, estimated with the two-material-input method with and without dielectric response functions taken into account. $\overline{E} = 12\,\mathrm{kV/mm}$. Voltage on. Corresponding current densities are presented in figure 6.2.

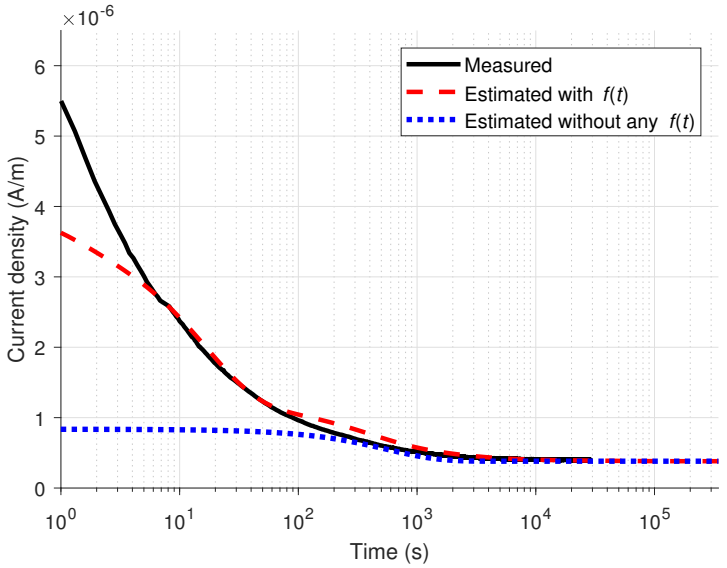

Figure 6.2: Estimated and measured current densities corresponding to figure 6.1.

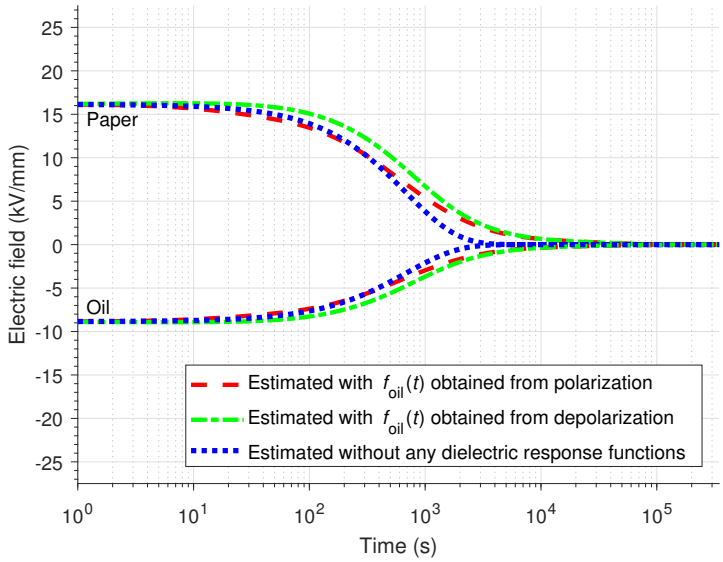

Figure 6.3: Electric fields in the large series connection test object, estimated with the two-material-input method with and without dielectric response functions taken into account. Grounding after steady-state at $\overline{E} = 12\,\mathrm{kV/mm}$. Corresponding current densities are presented in figure 6.4.

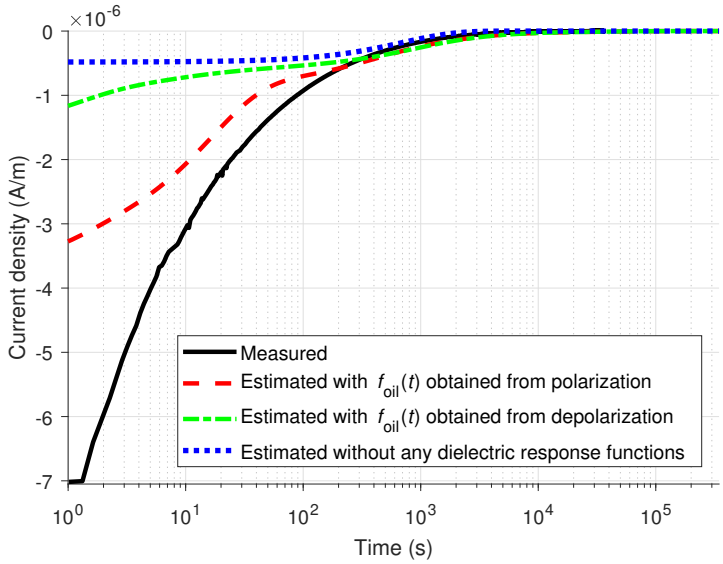

Figure 6.4: Estimated and measured current densities corresponding to figure 6.3.

For the first 86 s after grounding, the absolute value of the measured current density was larger in the case of grounding than in the case of voltage application (compare figs. 6.2 and 6.4). If the system were truly linear, the absolute value of the current density would have been largest in the case of voltage application, and the difference between the absolute values after voltage application and after grounding would have equaled the steady-state current density.

6.1.2 Results from One-Material-Input Method

The electric fields in paper estimated with the one- and two-material input methods are exhibited in figure 6.5 for turning the voltage on and in figure 6.6 for grounding. The electric field in oil is omitted for clarity. Values of t_{90} are listed in table 6.1.

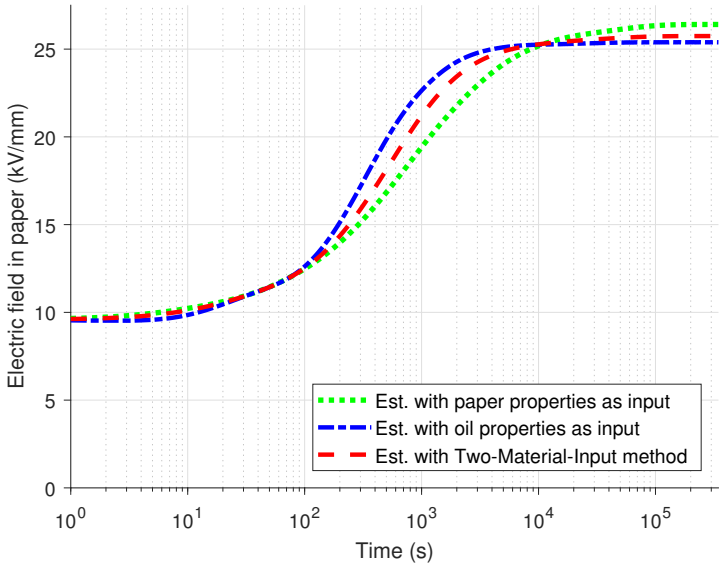

Figure 6.5: Electric fields in the large series connection test object, estimated with the one- and two-material-input methods with dielectric response functions taken into account. $\overline{E} = 12\,\mathrm{kV/mm}$. Voltage on.

Both for voltage application (fig. 6.5) and grounding (fig. 6.6), the curve describing $E_{\mathrm{pap}}(t)$ estimated with the two-material-input method mostly lie between the corresponding curves for the one-material-input method. This implies that the $E_{\mathrm{pap}}(t)$ curve obtained with the two-material-input method lies closer to the true $E_{\mathrm{pap}}(t)$ than either one or both of the corresponding curves obtained with the one-material-input method do. This indicates that although the one-material-input method avoids the uncertainties in the conductivity and

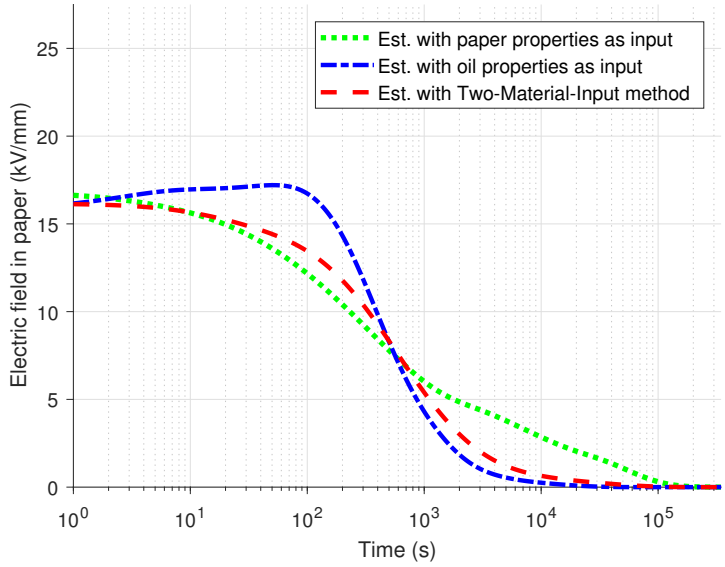

Figure 6.6: Electric fields in the large series connection test object, estimated with the one- and two-material-input methods with dielectric response functions taken into account. Grounding after steady-state at $\overline{E} = 12\,\mathrm{kV/mm}$

dielectric response function for one of the materials, it is not necessarily more a reliable method than the two-material-input method.[3]

Table 6.1: Values of t_{90} for the large series connection test object, estimated with the one- and two-material-input methods with dielectric response functions taken into account. $\overline{E} = 12\,\mathrm{kV/mm}$.

Method	Input	Voltage on t_{90} (s)	Grounding t_{90} (s)
One-material-input	Paper	7017	29 344
One-material-input	Oil	1561	2241
Two-material-input	Paper and oil	2786	3761

[3]The permittivity for one of the materials is to a large extent also unnecessary for the estimation of the electric fields, although it is needed for calculating the initial values and, through this, affects the whole transient period.

6.2 Discussion

6.2.1 Sensitivity to Dielectric Response Functions

A sensitivity analysis was performed by using combinations of maximum and minimum dielectric response functions (as defined in section 4.1.3), determined from polarization current measurements in paper and oil, as inputs for the two-material-input method. Figure 6.7 shows the resulting, estimated electric fields. Electric fields in oil are omitted for clarity, and it should kept in mind that if the electric field increases in one material, it decreases in the other. Corresponding estimated current densities are indicated in figure 6.8. Values of t_{90} are exhibited in table 6.2.

Table 6.2: Values of t_{90} for the large series connection test object, estimated with the two-material-input method. Sensitivity analysis with respect to input dielectric response functions. $\overline{E} = 12\,\mathrm{kV/mm}$. Voltage on. The figures in which the electric fields are plotted are indicated.

$f_{\mathrm{pap}}(t)$	$f_{\mathrm{oil}}(t)$	t_{90} (s)	Figure
Median	Median	2786	6.1
Zero	Zero	1317	6.1
Maximum	Maximum	11345	6.7
Maximum	Minimum	11049	6.7
Minimum	Maximum	1894	6.7
Minimum	Minimum	2214	6.7

The electric field estimates (fig. 6.7) are quite sensitive to the input dielectric response functions. The comparisons of estimated and measured current densities (figs. 6.2 and 6.8) indicate that the choice of using the median dielectric response functions in this case is suitable.

As indicated by the results presented in figure 6.7, using the maximum dielectric response function for a material resulted in a period with a low electric field strength in the same material, whereas using the minimum resulted in a period with high electric field strength in that material. This is similar to the principle that a material with high permittivity will have a low initial electric field strength and that a material with high conductivity will have a low steady-state electric field strength. [4] Moreover, in the same way that a large permittivity in any of the materials causes the initial current to be large, a "large" dielectric response function in any of the materials likewise causes the subsequent current to be large.

[4] The ratio $E_{\mathrm{pap}}(t)/E_{\mathrm{oil}}(t)$ equals $\varepsilon_{\mathrm{oil}}/\varepsilon_{\mathrm{pap}}$ immediately after voltage application and approaches $\sigma_{\mathrm{oil}}/\sigma_{\mathrm{pap}}$ as t approaches infinity [43], cf. equations (1.3) and (1.2).

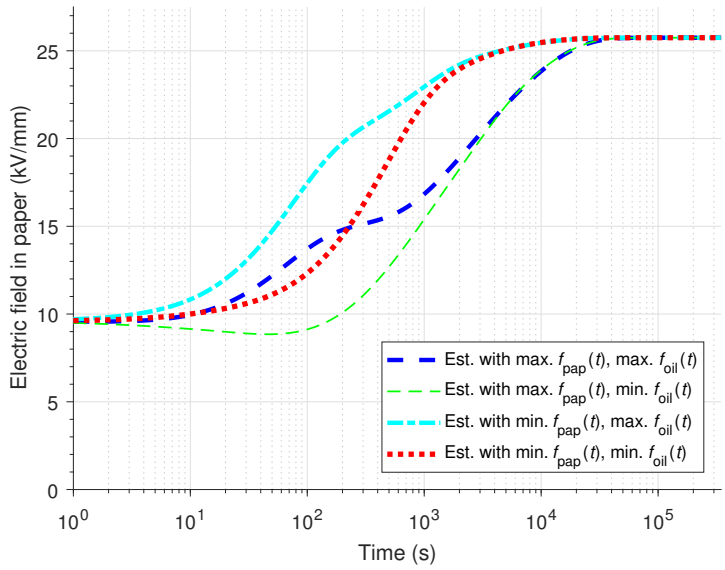

Figure 6.7: Electric fields in the large series connection test object, estimated with the two-material-input method. Sensitivity analysis with respect to input dielectric response functions. $\overline{E} = 12\,\mathrm{kV/mm}$. Voltage on. Corresponding current densities are presented in figure 6.8.

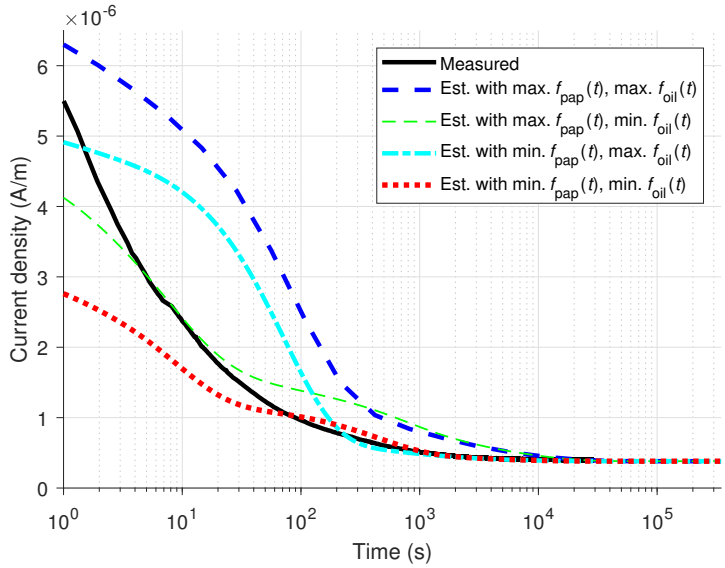

Figure 6.8: Estimated and measured current densities corresponding to figure 6.7.

However, the relationship between the dielectric response functions and the electric field strengths is more complicated than the relationships between permittivities, conductivities, initial field distributions, and steady-state field distributions. From equations (2.28)–(2.31), it can be deduced both that a large $f_{\mathrm{pap}}(0)$ contributes to a small $\frac{\mathrm{d}}{\mathrm{d}t}E_{\mathrm{pap}}(t)$ at $t = 0$ and that a large $f_{\mathrm{oil}}(0)$ contributes to a large $\frac{\mathrm{d}}{\mathrm{d}t}E_{\mathrm{pap}}(t)$ at $t = 0$. In other words, the initial values of the dielectric response functions affect the initial rate of change of the electric fields.

Whereas the effects of large and small *initial values* of the dielectric response functions can be explicated as above, the effects of the other parts of the dielectric response functions cannot be as easily deduced. This is because the dielectric response functions, or rather their time-derivatives, are convoluted with the electric fields. Consequently, the exact effects of those time-derivatives at a certain point in time are not clear unless electric fields are known for the whole period from $t = 0$ until this point in time.

From a physical perspective, the dielectric response function can be considered as a "delayed permittivity," and its Fourier transform is a frequency-dependent susceptibility. More precisely, the Fourier transform

$$\mathscr{F}[f(t)] = \varepsilon_{\mathrm{r,f}}(\omega) - \varepsilon_{\mathrm{r}}, \tag{6.1}$$

where $\varepsilon_{\mathrm{r,f}}(\omega)$ is the frequency-dependent, relative permittivity at angular frequency ω and where ε_{r} (consistent with the rest of this work) is the relative permittivity at high frequencies [42], [47]. The dielectric response function thus works like the permittivity, but in a time-delayed manner. Whether or not the "delayed permittivities" delay the transition to steady state depends on the other electrical properties of the different materials. In the series connection test object studied here, the dielectric response functions contributed to the electric field distribution in the same direction as the permittivities, opposite of the contribution from the conductivities, and thus delayed the transition to steady-state and increased t_{90}.

As figure 6.8 illustrates, a large dielectric response function, regardless of in which material, results in a high initial current density. This is as expected since the dielectric response function accounts for the displacement of charges, and a large displacement requires a large displacement current.

6.2.2 Verification of the Two-Material-Input Method

Principle for Verification

Comparison between estimated and measured current densities were used as an indirect verification of the two-material-input method. Because current densities

and electric fields are derived from the same solution to the coupled differential equations (4.25)–(4.27), a good match between the estimated and measured current density is an indication that the estimated electric fields are close to the true electric fields. For the one-material-input method, such comparison is worthless as the solution is forced to match the current density that is used as input to the estimates.

Voltage On

In the case of turning the voltage on, the difference between measured and estimated current density—with the dielectric response functions considered—was largest during the first few seconds (fig. 6.2). This was possibly due to $f_{\text{pap}}(t)$ and $f_{\text{oil}}(t)$ being extrapolated instead of measured for $t < 1$ (see section 4.1.3).[5] After the first few seconds—in the case of turning the voltage on—the match between estimated and measured current density was remarkably good. At $t = 4\,\text{s}$, the deviation from measured current density was less than 10 %. This suggests that the two-material-input method is reliable and suitable for estimating transient electric field distributions in series connections of paper and oil.

Grounding

With the dielectric response functions considered, the estimated current density matched the measured current density less closely in the case of grounding than in the case of turning the voltage on (fig. 6.4). This was due to the nonlinearity mentioned in section 6.1.1, namely that the absolute value of the measured current was larger shortly after grounding than shortly after turning the voltage on. This nonlinear behavior was confirmed by repeated experiments at various voltages. This was similar to the nonlinearity described for paper in section 5.5. However, the differences observed with the paper test objects were much smaller than the asymmetry between voltage application and grounding in the series connection. Moreover, the electric field strength in the paper was reduced at the moment of grounding, whereas the electric field the oil was increased and changed direction (cf. figs. 6.1 and 6.3). It is thus likely that the oil was the major contributor to the nonlinearity in the series connection, probably due to an increased conductivity in the oil due to injection or redistribution of charge during the voltage application. Introduction of oil gaps in paper test objects have been observed to cause similar nonlinearities in transformer insulation

[5] Although the $t < 1$ part of $f_{\text{pap}}(t)$ plays a role in the polarization as long as the electric field changes (since $f_{\text{pap}}(t)$ is convoluted with $E_{\text{pap}}(t)$ in equation (2.28)), its significance is largest for the first few seconds after application and removal of the voltage. The same applies for $f_{\text{oil}}(t)$.

[40]. This supports the hypothesis that the oil is responsible for most of the nonlinear behavior.

Assumption of Linearity

The assumption of linear polarization, which implies that dielectric response functions can be defined as in section 2.3.2 and are independent of the electric field strength, is fundamental to the methods presented in this thesis. Although a nonlinear behavior was observed as explicated above, the results indicate that using the two-material-method together with the dielectric response functions, which assumes linearity, yields more accurate results than the simpler method of neglecting the dielectric response functions. It can therefore be concluded that the system is linear enough for the estimation methods presented herein to be useful. The usefulness is emphasized by the large differences between the electric field estimates in which the dielectric response functions were taken into consideration and those in which they were neglected.

Note that the nonlinearities considered in this section 6.2.2 relate to polarization (and time-dependent conduction interpreted as polarization). Nonlinear steady-state conduction, expressed by field-dependent steady-state conductivities, is supported by both the two-material-input method and the one-material-input method.

6.2.3 Considerations regarding the One-Material-Input Method

For the case of grounding (fig. 6.6), the transient electric field estimated with oil properties as input deviates considerably from that estimated with paper properties as input. Much of the deviation for values of t larger than approximately 1000 s is probably due to an underestimated σ_{pap} for the lowest electric field strengths,[6] causing E_{pap} to be overestimated when paper properties are used as input. This heavily affects t_{90}. For smaller values of t, dielectric response functions are more important to the electric field distribution. The deviation thus indicates that one or both dielectric response functions represent the physical processes poorer in the case of grounding than in the case of voltage on. This is in line with the discussion above.

Because the nonlinearities most likely are primarily due to the oil, the one-material-method with paper properties as input may seem to be a suitable approach for determining electric field distributions. In this way, the most nonlinear parameters are literally removed from the equation. However, using the

[6] See chapter 5.3.

one-material-input method may be challenging in the case of mass-impregnated cables, as will be discussed in section 7.1.2.

6.2.4 Comparison with Literature

As indicated above, the match between estimated and measured current densities is stronger when dielectric response functions are considered than when they are neglected. This is consistent with studies of transformer insulation where estimates of current or recovery voltage[7] with and without dielectric response functions are compared [47], [79]. The same studies also show, in line with the results presented here, that the estimated approach towards steady-state is slower when dielectric response functions are taken into account.

6.2.5 Other Estimation Approaches

An alternative to using a dielectric response function for oil is to use a nonlinear oil model that considers the initial, homogeneous charge density; the decrease in charge density as the polarization current drains the oil gap for charge; and the conductivity determined by the time-dependent (and still homogeneous) charge density. The paper may still be modeled in the same way as it has been done in this work. An approach such as this has proved to be useful for estimating electric fields and currents in transformer insulation [78], [79]. Other estimation approaches are based on modeling the drift of one or several types of charge carriers, and may take into account various processes as injection, trapping, detrapping, recombination, and diffusion, as well as parameters as permittivity, charge density, and mobility [37], [80], [81]. An advantage of the dielectric response approach in this work is that only three parameters are needed for each material: Permittivity, conductivity, and dielectric response function. Approaches based on charge carriers typically involve more parameters, some of which may be challenging to determine [37].

[7] When an insulation system is charged and then to some extent discharged before the circuit is left open, a *recovery voltage* builds up across the insulation.

Chapter 7

Application to Mass-Impregnated Cables

The first part of this chapter (section 7.1) discusses how the methods for estimating electric fields can be applied to mass-impregnated cables. The second part (section 7.2) presents case studies where the two-material-input method is used to estimate electric field distributions in hypothetical, plane-parallel series connections of paper and oil—similar to the series connection used for chapter 6, but with values of the thickness ratio $d_{\mathrm{pap}}/d_{\mathrm{oil}}$ relevant to mass-impregnated cables and with two different applied mean electric field strengths.

7.1 Considerations regarding Application

7.1.1 Cylindrical Geometries and Temperature Gradients

The model used for the estimates in this thesis assumes plane-parallel and isothermal conditions. One way to include the effects of cylindrical cable geometry and temperature gradients is to combine the model of this work with estimates from other models. As explicated in section 1.2, cylindrical geometry and temperature gradients have commonly been considered in models where the two-material structure with butt gaps and paper tapes is neglected [22], [32]–[34].[1] Such models will henceforth be referred to as *structure-neglecting* models. Firstly, a structure-neglecting model can be used to estimate the time-dependent electric field strength for a certain radial position in a cable. The two-material-input method can then be used to study a thin section of insulation

[1] In such models, the insulation is considered as a single material that, apart from the effects of temperature gradients and electric field gradients, is homogeneous.

around that radial position. One of the input parameters necessary for the two-material-input method is the voltage across the considered section of insulation. This voltage approximately equals the product of the section's thickness and mean electric field strength. The time-dependent electric field strength from the structure-neglecting model can be used for this input.

Another way to include effects of cylindrical cable geometry and temperature gradients is to model the cable insulation as several concentric sections and consider each section as plane-parallel and isothermal. The insulation in each section consists of the two materials (i.e., paper and oil). The temperatures differ among the sections, causing the electrical properties to likewise differ. Consequently, the collection of sections is effectively an insulation system consisting of twice as many materials as there are sections. The two-material-input method must then be extended to systems of several materials. The principles for the two-material-input method, presented in sections 2.4.1 and 4.2.1, still apply—with adjustments for the effective area being different in the different sections. Furthermore, the equation systems become more complicated since there are more materials involved.

7.1.2 Challenges with the One-Material-Input Method

If the one-material-input method is to be used for a mass-impregnated cable, a relevant current needs to be measured in a piece of insulation small enough for it to be approximately plane-parallel (see appendix A). Moreover, the measured current needs to go through a 1–4 mm wide butt gap with minimal influence from the butt gap edges. These issues will probably be challenging to address, and might render the one-material-input method unsuitable for estimating electric fields in mass-impregnated cables. However, it may still be suitable for other types of layered insulation.

7.1.3 Edge Effects

The paper *edges* are perpendicular to the paper *surfaces* and define the widths of the butt gaps. The electric field estimates are one-dimensional and do not take into account the effects of the edges. The estimates are therefore not relevant to the regions close to the edges. An article about edge effects is reproduced in appendix F.

7.2 Case Studies

7.2.1 Description of Cases

Case studies was carried out by considering plane-parallel series connections like the one used in chapter 6 but with values of the thickness ratio $d_{\text{pap}}/d_{\text{oil}}$ relevant to mass-impregnated cables.

Two thickness ratios geometries were considered: $d_{\text{pap}}/d_{\text{oil}} = 15$, corresponding to fifteen paper tapes between each butt gap, and $d_{\text{pap}}/d_{\text{oil}} = 2$, corresponding to two paper tapes between each butt gap. The former is obtained in cables if the butt gap width is one-fifteenth of the paper tape width and each layer is staggered three-thirds of the tape width, as shown in figure 7.1. The latter is obtained if the butt gap width is one-tenth of the paper tape width and each layer is staggered one-third of the combined width of a tape and a butt gap, as illustrated in figure 7.2.

The considered voltages corresponded to two different mean electric field strengths, namely $\overline{E} = 12\,\text{kV/mm}$ and $\overline{E} = 40\,\text{kV/mm}$. The former of these mean field strengths is the same as was used in chapter 6 and is lower than typical field strengths in cables. The latter is higher than typical field strengths in cables, but is likely to occur close to the conductor at polarity reversals [4], [22]. Cases of turning the voltage on (i.e., application of a step voltage), grounding after steady state, and polarity reversal after steady state were considered.[2] The estimates were obtained by using the two-material-input method together with the electrical properties from chapter 5. This implies that the studied cases were isothermal with a temperature of 50 °C. The estimates were made with and without considering the dielectric response functions.

[2]Voltage application, grounding, and polarity reversal in real, cylindrical cables will cause any small section of the insulation to experience an abrupt voltage change followed by a gradual voltage change towards steady state. This applies both when the whole cable insulation is isothermal and when a temperature gradient is present, though the gradual part is less significant in isothermal cases [22]. For simplicity, only abrupt voltage changes were used in these cases studies. In other words, the approaches suggested in section 7.1.1 were not followed.

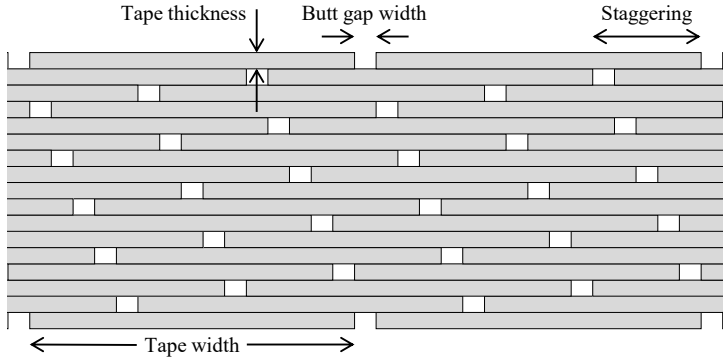

Figure 7.1: Cable insulation model with fifteen paper tapes between each butt gap. The thicknesses in this sketch are exaggerated with respect to the widths.

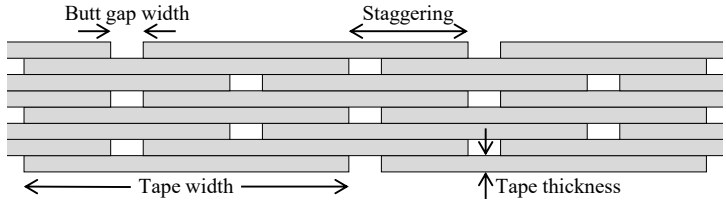

Figure 7.2: Cable insulation model with two paper tapes between each butt gap. The thicknesses in this sketch are exaggerated with respect to the widths.

7.2.2 Results

The estimated electric fields strengths are indicated in figures 7.3–7.8. When comparing graphs with each other, it is important to note that the time axes are logarithmic. Values of t_{90} are exhibited in figures 7.9–7.10.

The value of t_{90} was 1.6–2.0 times larger when dielectric response functions were taken into account than when they were neglected. By comparing values of t_{90} estimated with and without considering the dielectric response functions, it can be observed that the dielectric response functions had the largest effect on t_{90} for the lowest value of the thickness ratio, namely for $d_{\mathrm{pap}}/d_{\mathrm{oil}} = 2$. In chapter 6.1.1, where the value of the thickness ratio was even smaller ($d_{\mathrm{pap}}/d_{\mathrm{oil}} = 0.6$), the effect was even larger. This indicates a trend: The lower value of $d_{\mathrm{pap}}/d_{\mathrm{oil}}$ is, the more important it is to consider the dielectric response functions when assessing how fast steady state is approached.

Furthermore, the values of t_{90} were larger with $d_{\mathrm{pap}}/d_{\mathrm{oil}} = 2$ than with $d_{\mathrm{pap}}/d_{\mathrm{oil}} = 15$, both when dielectric response functions were considered and when they were left out of the calculations. Again, when comparing with the results in chapter 6.1.1, a trend can be identified: The lower value of $d_{\mathrm{pap}}/d_{\mathrm{oil}}$ is, the larger the t_{90} is. In two-material systems with constant permittivities, constant conductivities, and no dielectric response functions, $t_{90} = 2.3\tau$ and approaches $2.3\varepsilon_{\mathrm{oil}}/\sigma_{\mathrm{oil}}$ as the ratio $d_{\mathrm{pap}}/d_{\mathrm{oil}}$ increases (see section 2.2). With the values of the oil properties employed in this work, this corresponds to 9 min.

The values of t_{90} were larger for grounding than for turning the voltage on (though just barely for $d_{\mathrm{pap}}/d_{\mathrm{oil}} = 15$). This is because the field-dependent conductivity of paper is lower at grounding, delaying the removal of charges from the interfaces between paper and oil. If all the electrical properties for both materials were field-independent, t_{90} would be the same for turning the voltage on, grounding, and polarity reversal. It would also be independent of the magnitude of the voltage.

The electric fields in the two materials equaled each other within 2 min after turning on the voltage and within 7 min after polarity reversal.

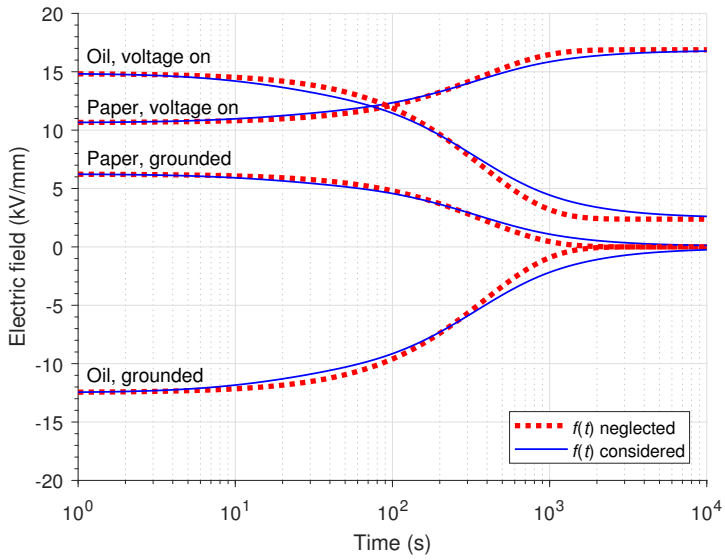

Figure 7.3: Estimated electric fields in paper and oil-filled butt gaps in cable insulation with two papers between each butt gap. The insulation is subjected to a step voltage corresponding to 12 kV/mm mean electric field strength and grounded after reaching steady-state.

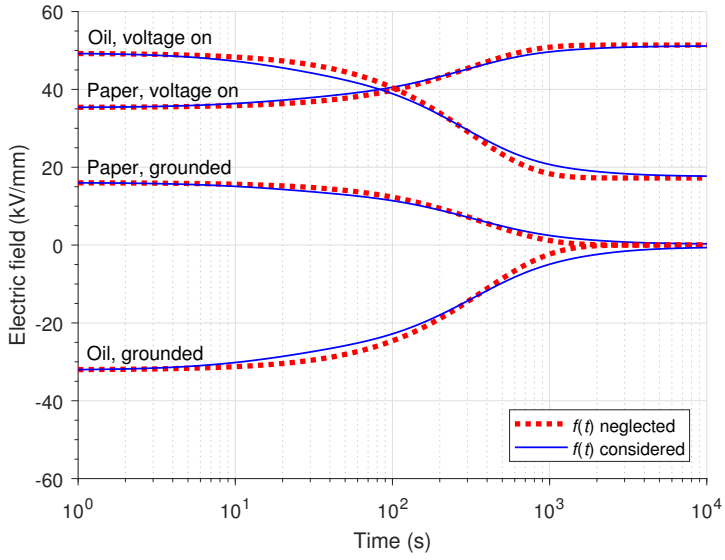

Figure 7.4: Estimated electric fields in paper and oil-filled butt gaps in cable insulation with two papers between each butt gap. The insulation is subjected to a step voltage corresponding to 40 kV/mm mean electric field strength and grounded after reaching steady-state.

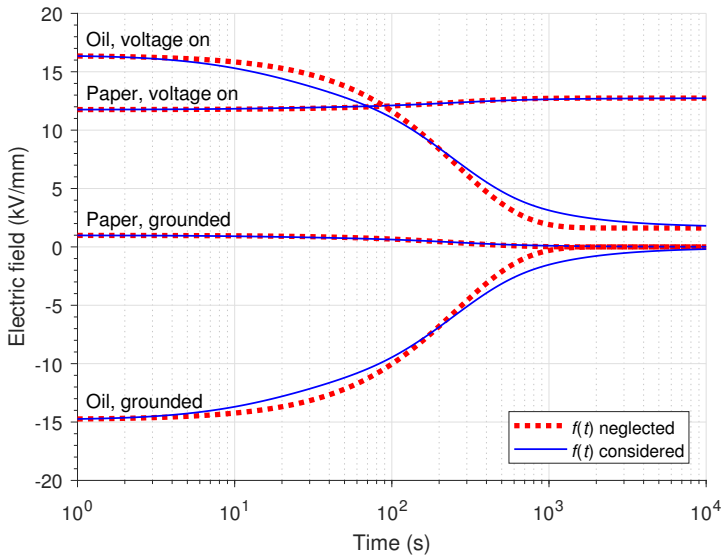

Figure 7.5: Estimated electric fields in paper and oil-filled butt gaps in cable insulation with fifteen papers between each butt gap. The insulation is subjected to a step voltage corresponding to 12 kV/mm mean electric field strength and grounded after reaching steady-state.

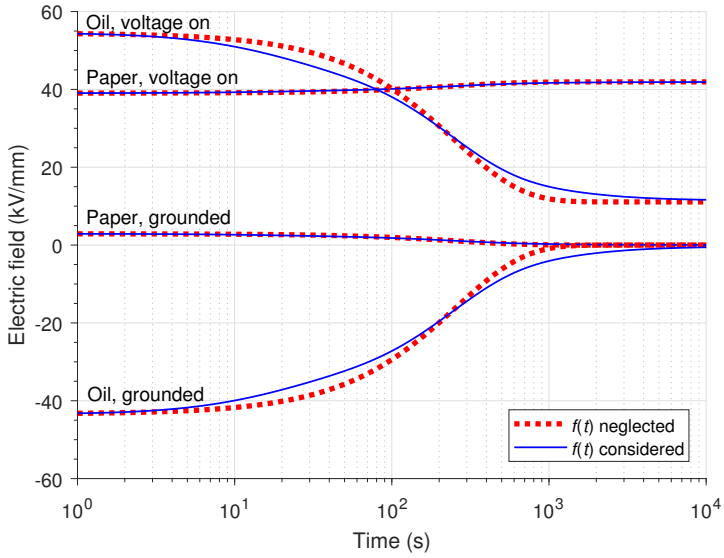

Figure 7.6: Estimated electric fields in paper and oil-filled butt gaps in cable insulation with fifteen papers between each butt gap. The insulation is subjected to a step voltage corresponding to 40 kV/mm mean electric field strength and grounded after reaching steady-state.

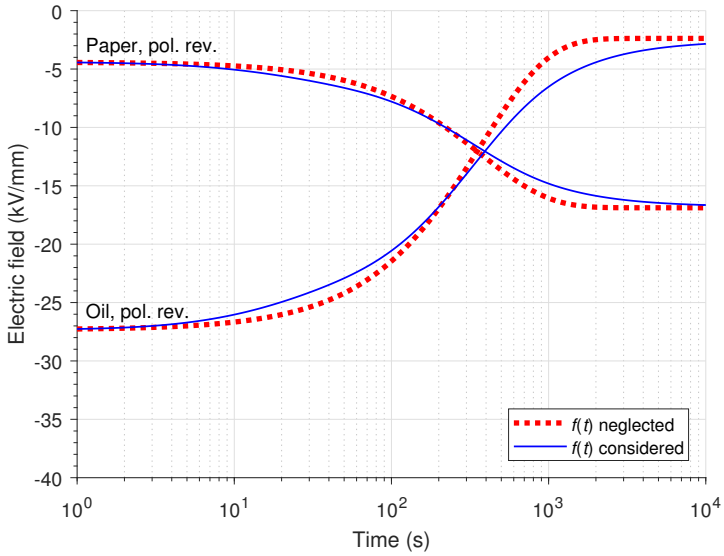

Figure 7.7: Estimated electric fields in paper and oil-filled butt gaps in cable insulation with two papers between each butt gap. The voltage corresponds to 12 kV/mm. The polarity of the applied voltage is reversed at the time $t = 0$.

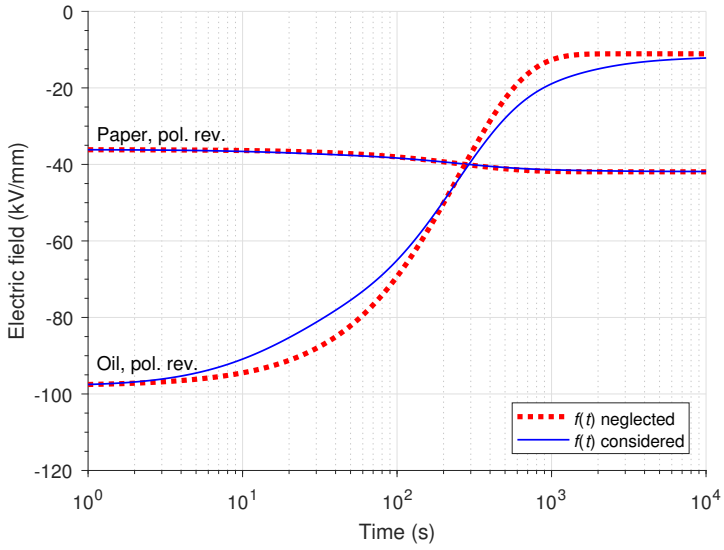

Figure 7.8: Estimated electric fields in paper and oil-filled butt gaps in cable insulation with fifteen papers between each butt gap. The voltage corresponds to 40 kV/mm. The polarity of the applied voltage is reversed at the time $t = 0$.

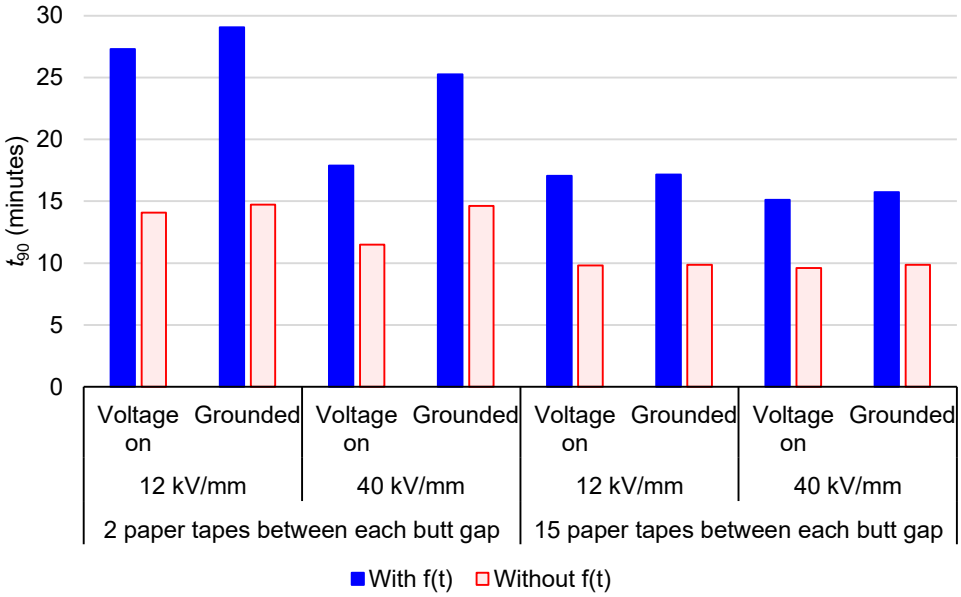

Figure 7.9: The value t_{90} calculated from the results presented in figures 7.3–7.6.

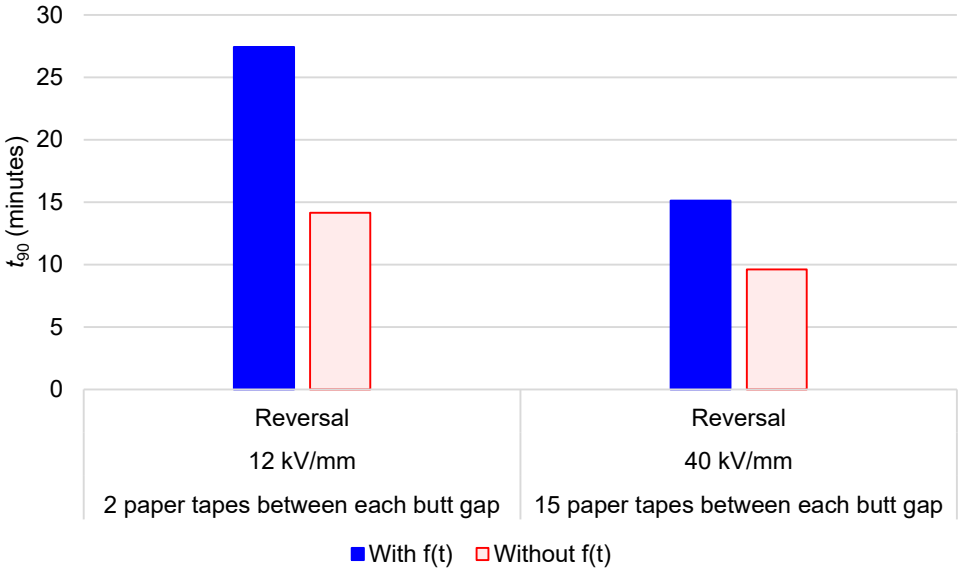

Figure 7.10: The value t_{90} calculated from the results presented in figures 7.7–7.8.

7.2.3 Discussion

Effect of Electric Field Strength

The estimates are made with the electrical properties that are presented in chapter 5 as input. That implies a field-dependent conductivity of paper and a constant conductivity of oil.[3] The conductivities determine the steady-state electric fields as described by the equation

$$\frac{E_{\text{pap}}}{E_{\text{oil}}} = \frac{\sigma_{\text{oil}}}{\sigma_{\text{pap}}}. \tag{7.1}$$

The steady-state electric fields are shown in table 7.1. It can be seen in the table that the ratio $E_{\text{pap}}/E_{\text{oil}}$ decreases with increasing mean electric field strength. However, as pointed out in section 5.4.2, the true conductivity of oil normally increases with increasing field strength as long as the field strength is above some limit. The results from the conductivity measurements indicate that this limit may be around 12 kV/mm (see results plotted as squares in fig. 5.4). This field-dependency appears to be far greater than the field-dependency in paper, and if that were included in the estimates, increasing the voltage above this limit would have increased the ratio $E_{\text{pap}}/E_{\text{oil}}$. In literature, the value of $E_{\text{pap}}/E_{\text{oil}}$ in cables is typically assumed to be 100 [5], [6], [77], although the value 10 is also used [32].

Table 7.1: Electric fields at steady state. *Low* and *high* voltage correspond to mean electric field strengths of 12 kV/mm and 40 kV/mm, respectively. *Few* and *many* tapes indicate, respectively, two and fifteen paper tapes between each butt gap.

Case	E_{pap} (kV/mm)	E_{oil} (kV/mm)	$E_{\text{pap}}/E_{\text{oil}}$
Low voltage, few tapes	17	2.4	7.1
High ——, few ——	51	17	3.0
Low ——, many ——	13	1.6	7.9
High ——, many ——	42	11	3.8

In addition to governing the steady-state electric field distribution, the conductivities affect how fast steady state is approached. (See the comment regarding difference between t_{90} for turning the voltage on and for grounding in section 7.2.2.) A higher conductivity for any of the materials imply a smaller t_{90}.

[3] The reason for regarding the conductivity of oil as constant is explained in section 5.4.2.

Effects of Oil Gap Thickness

It can be shown from equation (2.28) that for a given mean electric field strength, it is the thickness *ratio* and not the thicknesses themselves that affect the estimates.[4] However, the conductivity of oil is generally affected by the oil gap thickness [73], [76], [82]. The oil gaps from which the conductivity was estimated were eleven times as thick as a butt gap.[5] Whether or not the conductivity of butt gaps is larger or smaller than the value used here depends on the dominating conduction mechanism. In many cases, conductivities of insulating liquids decrease with decreasing gap thickness [73], [76], [82], [83]. If this is the case also with the materials, gap thicknesses, and electric field strengths involved here, the approach to steady state will be slower and the value of t_{90} larger in real cables than in the present estimates.

Also the dielectric response function for oil is likely affected by the thickness of the oil gaps. At constant electric field strength, the transit time for an ion to cross an oil gap is proportional to the gap thickness [76]. Therefore, $f_{\mathrm{oil}}(t)$ probably decays faster for thin oil gaps than for the oil gaps that here were used to determine the electrical properties. This suggests, according to section 6.2.1, that also this will contribute to a larger value of t_{90} in real cables than in the present estimates.

Lower Temperatures

Some of the insulation in mass-impregnated HVDC cables is typically colder than 50 °C during testing and operation [19], [84]. The effects of temperature on the time-dependent electric field distributions are not studied here; only these simple considerations hint at their effects:

Conductivities and dielectric response functions are affected by the temperature [55]. In cases of field-independent electrical properties and zero dielectric response functions, lower conductivities imply higher time constants. Other literature reports that the values of σ_{pap} and σ_{oil} at 40 °C are about a third of what they are at 50 °C [52], [55]. It follows from equation (2.10) that when both conductivities are reduced to a third, the time constant—and thereby also t_{90}—is tripled. Further, at 20 °C, σ_{pap} and σ_{oil} are reported to be about 15 and

[4] This can be shown by multiplying each thickness in equation (2.28) by the same factor (an operation that preserves the ratio $d_{\mathrm{pap}}/d_{\mathrm{oil}}$) and observe that the factor cancels out everywhere when the fractions are reduced. Note that the voltage U also needs to be multiplied by that factor because $U = \overline{E}\left(d_{\mathrm{pap}} + d_{\mathrm{oil}}\right)$.

[5] A butt gap is as thick as a paper tape. Where the lay direction of paper tapes is reversed, butt gaps cross each other. At the crossings, the oil gap thickness is the sum of the two butt gap thicknesses.

30 times, respectively, lower than at 50 °C [55]. This puts the value of t_{90} in the order of hours.

Regarding the dielectric response functions, it is likely that their magnitudes are lower and their decays are slower for both materials, since movement of charge in insulators is usually slower at lower temperatures.[6] If so, the effects in the different materials will likely counteract each other: A smaller (i.e., with lower magnitude) $f_{\text{pap}}(t)$ contributes to a slower transition to steady state, whereas a smaller $f_{\text{oil}}(t)$ contributes in the opposite direction (see section 6.2.1). It is hard to predict which of these effects is the stronger.

Comparison with Field Inversion due to the Temperature

Jeroense [22] has reported estimates of electric fields in a structure-neglecting model of a 450 kV mass-impregnated HVDC cable with a temperature of 50 °C at the conductor screen and 35 °C at the insulation screen. The dielectric response function for the insulation was omitted. Field- and temperature-dependencies for the conductivity were taken into account, and the field inversion caused by the temperature gradient and the cylindrical geometry was studied. It was demonstrated that in a case where the temperature gradient is established before the voltage is turned on, 63 % of the change from initial to steady-state electric field strength in the 50 °C innermost part of the insulation takes place within approximately 3 minutes after voltage application. In the cases presented in section 7.2.2, 63 % of the change took place within 4–7 minutes.

The estimates in reference [22] and section 7.2.2 relate to different phenomena occurring at different length scales. Both phenomena are kinds of field inversion: The former occurs on a large length scale and is the transition from having the highest electric field strength in the innermost part of the cable to having it in the outermost part of the cable. The latter is the transition from having the highest electric field strength in the oil to having it in the paper. This relates to a much smaller length scale. The comparisons of the estimates suggests that the latter phenomenon at least in this case is more slow-paced than the former. Considering the effects of oil gap thickness discussed above, it is likely that the latter phenomenon is even slower in real cables. Consequently, studies of the electric fields on the large scale should be accompanied by studies on the smaller scale—at least when the aim is to know when the insulation can be said have reached steady state.

[6] Both polarization and conduction involve movement of charge. Results obtained by Occhini and Maschio [85] indicate that a temperature decrease will lower the magnitude of $f_{\text{pap}}(t)$ and slow down its decay, though those results are from paper impregnated with decylbenzene (low viscosity), not mass (high viscosity).

Consequences for Mass-Impregnated Cables

All the estimates in section 7.2.2 yield a slower approach to steady state when the dielectric response functions are considered than when they are neglected. This illustrates the importance of taking dielectric response functions into account when estimating the transient electric field distribution between oil and paper. This is especially relevant when test procedures are to be evaluated: The waiting time between voltage application and polarity reversals and between subsequent polarity reversals should be long enough for the electric field distribution between butt gaps and paper to reach practically steady state. A shorter waiting time will not give enough time for the accumulation of interface charges and thus reduce the severity and relevance of the polarity reversal test (see section 2.2).

Chapter 8

Main Conclusions

The main conclusions from this work are as follows:

- By using each material's dielectric response function to represent any polarization and conduction processes that are not represented by the material's high-frequency permittivity or steady-state conductivity, the transient electric field distribution between oil and oil-impregnated paper in layered HVDC insulation can be estimated by using linear dielectric response theory.
- The high-frequency permittivity, steady-state conductivity, dielectric response function, and thickness for each material, as well as the voltage across the insulation, are input parameters for such estimates. In cases where the current density in the insulation is known from measurements, the electrical properties are needed for only one of the materials.
- The estimation process involves solving an integrodifferential equation. By expressing the dielectric response functions as linear combinations of exponential functions, the integrodifferential equation can instead be converted to a system of first-order ordinary differential equations that can be solved numerically by built-in functions in commercially available software.
- For paper, the dielectric response function can be determined from either polarization or depolarization current measurements. For oil, the dielectric response function should be determined from polarization current measurements.
- In cases where the electrical properties for both materials are used as input to the estimates, the current density can be estimated together with

the electric fields. Comparison between estimated and measured current densities has verified the electric field estimates. The agreement between estimated and measured current densities presented in this thesis supports the assumption that linear dielectric response theory is adequate for estimating the transient electric fields. Neglecting the dielectric response functions results in poorer agreement between estimated and measured current densities.

- The phenomena represented by the dielectric response functions heavily affect the approach to steady state in series connections. Whether they result in a faster or slower approach towards steady state, depends on the magnitude and shape of the dielectric response functions for the materials involved. For example, in a series connections of oil and oil-impregnated paper at 50 °C, the estimated time t_{90} needed for ninety percent of the change from initial to steady-state electric field distribution to take place can be at least twice as long when dielectric response functions are taken into account than when they are neglected.

- It is observed a trend that the value of t_{90} decreases and becomes less affected by the dielectric response functions as the ratio of total paper thickness to total oil gap thickness in the insulation is increased.

Chapter 9

Suggestions for Further Work

The following activities are suggested for further investigating the electric field distributions between oil and impregnated paper in mass-impregnated HVDC cables based on the principles presented in this thesis:

- Study intersheet gaps in cables to determine whether it is reasonable to model those gaps as part of the paper.
- Assess sources of uncertainties and develop test objects and measurement procedures that cause less variance in the results.
- Determine conductivity and dielectric response functions for oil gaps whose thicknesses are close to typical butt gap thicknesses.
- Determine electrical properties at lower temperatures than 50 °C and, for oil, at electric field strengths higher than 7 kV/mm.
- Verify the two-material-input method after completion of the abovementioned activities, using step voltage, polarity reversal, grounding, and gradually changing voltages.
- Estimate electric fields in mass-impregnated HVDC cables at relevant conditions, especially for polarity reversal tests.

Appendix A

Approximation to Plane-Parallel Geometry

This appendix explains how a cylindrical geometry can be approximated to a plane-parallel geometry.

Gauss' law

$$\nabla \cdot \boldsymbol{D} = \rho_{\text{free}} \tag{A.1}$$

inserted in the continuity equation

$$\nabla \cdot \boldsymbol{J}_{\sigma} + \frac{\partial \rho_{\text{free}}}{\partial t} = 0 \tag{A.2}$$

gives

$$\nabla \cdot \underbrace{\left(\boldsymbol{J}_{\sigma} + \frac{\partial \boldsymbol{D}}{\partial t} \right)}_{\boldsymbol{J}} = 0. \tag{A.3}$$

Here, $\boldsymbol{D}$ denotes the electric displacement, ρ_{free} is the free charge density, $\boldsymbol{J}_{\sigma}$ is the conduction current (i.e., current due to movement of free charges), $\boldsymbol{J}$ is the total current density, and t is time. Boldfaced symbols indicate vector quantities. Integrating over an arbitrary volume and applying the divergence theorem brings equation (A.3) to its integral form

$$\oiint_{Z} \boldsymbol{J} \, \mathrm{d}\boldsymbol{Z} = 0, \tag{A.4}$$

where $\mathrm{d}\boldsymbol{Z}$ is an infinitesimal surface area element and Z is an arbitrary, closed surface. For a cylindrical, symmetric cable that is homogeneous in the longitudinal direction (and, by definition of cylindrical symmetry, homogeneous also in

azimuthal direction), both $\boldsymbol{J}_\sigma$ and $\boldsymbol{D}$ are always parallel to the radial direction. Therefore, by choosing the surface Z to be a sector of the cable, as illustrated in figure A.1, the only surface segments that contribute to the integral of equation (A.4) are those at radius r_1 and r_2, facing the conductor and the insulation screen, respectively. These segments are here called Z_1 and Z_2, respectively. The area of Z_2 is r_1/r_2 times larger than that of Z_1, and $\boldsymbol{J}$ is perpendicular to both Z_1 and Z_2. Therefore, equation (A.4) can be reduced to

$$r_1 J_1 = r_2 J_2, \tag{A.5}$$

where the current densities (i.e., J_1 and J_2) are scalars. In the case of thin, adjacent layers, such as those demonstrated in figure A.2, $r_1/r_2 \approx 1$ so that

$$J_1 \approx J_2. \tag{A.6}$$

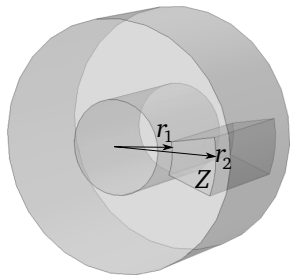

Figure A.1: Closed surface Z of a sector in a cylindrical symmetric cable.

For example, when considering one butt gap and fifteen layers of 0.09 mm thick paper tapes, $r_1/r_2 = 0.94$ if the innermost layer is at $r_1 = 24\,\text{mm}$, and $r_1/r_2 = 0.97$ if the innermost layer is at $r_1 = 42\,\text{mm}$.

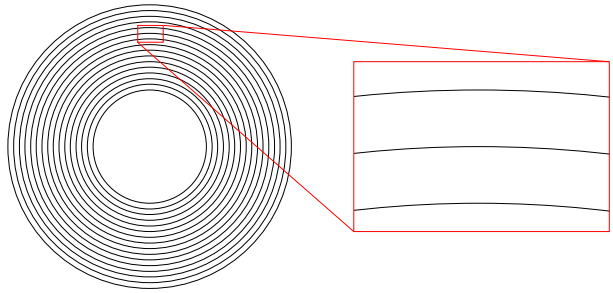

Figure A.2: Approximately plane-parallel detail of a cylindrical arrangement.

Appendix B

Derivation of Equations (4.9)–(4.11) and (5.1)–(5.2)

All quantities in this appendix relate to steady-state conditions. The parameters σ_0 and η are positive.

B.1 Derivation of Equations (4.9)–(4.11)

The principle for estimating the electric field strength and conductivity in oil in a series connection with paper is as follows: A measured current density divided by the known conductivity of paper gives the electric field strength in the paper. Multiplying this by the paper thickness yields the voltage across the paper. The total voltage across the series connection minus the voltage across the paper equals the voltage across the oil. Dividing this voltage by the oil gap thickness gives the electric field strength in the oil. The conductivity of oil is the measured current divided by the electric field strength in oil.

Assume a parallel-plane arrangement of paper and oil connected in series. Assume that the conductivity of oil satisfies equation (4.7), which is repeated here for convenience:

$$\sigma_{\text{pap}}(E_{\text{pap}}) = \sigma_0 \mathrm{e}^{\eta |E_{\text{pap}}|}. \tag{4.7}$$

Inserted in Ohm's law $J = \sigma_{\text{pap}} E_{\text{pap}}$, this becomes

$$J = \sigma_0 \mathrm{e}^{\eta |E_{\text{pap}}|} E_{\text{pap}}. \tag{B.1}$$

Multiplying both sides of equation (B.1) by η/σ_0 gives

$$\frac{\eta J}{\sigma_0} = \eta E_{\text{pap}} \mathrm{e}^{\eta |E_{\text{pap}}|}. \tag{B.2}$$

The Lambert W function is defined as the complex function $\mathrm{W}(z)$ that satisfies

$$z = \mathrm{W}(z)\mathrm{e}^{\mathrm{W}(z)}, \tag{B.3}$$

where z is a complex variable [60]. By comparing this with equation (B.2), it can be concluded that

$$\eta E_{\text{pap}} = \mathrm{W}(z) \quad \text{for} \quad E_{\text{pap}} \geq 0 \tag{B.4}$$

with

$$z = \frac{\eta J}{\sigma_0}. \tag{B.5}$$

Since $\eta > 0$, the condition that $E_{\text{pap}} \geq 0$ is fulfilled when $\mathrm{W}(z) \geq 0$. Dividing by η gives

$$E_{\text{pap}} = \frac{\mathrm{W}(z)}{\eta} \quad \text{for} \quad \mathrm{W}(z) \geq 0. \tag{B.6}$$

The Lambert W function is multivalued—it has several branches. However, both E_{pap} and η are real. $\mathrm{W}(z)$ thus must also be real, and, except for in the trivial case $E_{\text{pap}} = 0$, it must also be positive. The only branch that contains any part of the real, positive axis in its range is the principal branch W_0 [60]. Given that also z is real (as is evident from the physics in this case), $z \geq 0$ is a necessary and sufficient condition for $\mathrm{W}(z) \geq 0$. Therefore, equation (B.4) can be rewritten as

$$E_{\text{pap}} = \frac{\mathrm{W}_0(z)}{\eta} \quad \text{for} \quad z \geq 0, \tag{B.7}$$

with z as in equation (B.5). The condition that $z \geq 0$ is equivalent with $J \geq 0$. From equation (2.6), we have

$$E_{\text{oil}} = \frac{U_0 - d_{\text{pap}} E_{\text{pap}}}{d_{\text{oil}}}. \tag{B.8}$$

Inserting equation (B.7) into equation (B.8) gives

$$E_{\text{oil}} = \frac{\eta U_0 - d_{\text{pap}} \mathrm{W}_0(z)}{\eta d_{\text{oil}}} \quad \text{for} \quad z > 0. \tag{B.9}$$

Ohm's law for oil, $\sigma_{\text{oil}} = J/E_{\text{oil}}$, combined with equation (B.8) becomes

$$\sigma_{\text{oil}} = \frac{\eta d_{\text{oil}} J}{\eta U_0 - d_{\text{pap}} \mathrm{W}_0(z)} \quad \text{for} \quad z > 0. \tag{B.10}$$

Since all values here relate to steady-state, equation (B.9) is the same as equation (4.9), equation (B.5) is the same as equation (4.10), and equation (B.10) is the same as equation (4.11).

The derivaton above is previously published in less detail in reference [72].

B.2 Derivation of Equations (5.1)–(5.2)

For studying how uncertainties in the known σ_{pap} affect the estimated E_{oil} and σ_{oil}, Ohm's law $E_{\text{pap}} = J/\sigma_{\text{pap}}$ (instead of equation (B.7)) can be inserted into equation (B.8). We then obtain

$$E_{\text{oil}} = \frac{U_0 - d_{\text{pap}} J/\sigma_{\text{pap}}}{d_{\text{oil}}}, \tag{B.11}$$

instead of equation (B.9) and

$$\sigma_{\text{oil}} = \frac{d_{\text{oil}} J}{U_0 - d_{\text{pap}} J/\sigma_{\text{pap}}} \tag{B.12}$$

instead of equation (B.10). This allows for adjusting σ_{pap} and examining the effects on E_{oil} and d_{oil}. For example, in a case where the σ_{pap} that is used to estimate $\sigma_{\text{oil}}(E_{\text{oil}})$ is smaller than the true σ_{pap}, the estimated E_{oil} will be too small and the estimated σ_{oil} will be too large. Equations (B.11) and (B.12) correspond to equations (5.1) and (5.2), respectively, and do not require that the exponential relationship (i.e., equation (4.7)) between σ_{pap} and E_{pap} be valid.

Appendix C

Curve Fitting Technique

Curve fitting the right-hand side of

$$f(t) = \sum_{i=1}^{N} A_i e^{-t/t_i} \tag{C.1}$$

to the left side $f(t)$ can be demanding if the sum contains many terms (i.e., N is large). The problem can be broken up into smaller problems in the following way [62]:

Term number one, $A_1 e^{-t/t_1}$, is here defined as the term with the largest time constant t_i. The tail of $f(t)$—namely the part with the highest values of t—can be considered to be influenced only by this term, assuming that all other terms have decayed to practically zero because of their small time constants. The tail can be identified as the last, linear part in a log-lin plot.[1] The coefficient A_1 and the time constant t_1 can then be easily determined by standard curve fitting techniques (e.g., the least squares method) since there are only two parameters to fit.

Subsequently, $A_1 e^{-t/t_1}$ is subtracted from $f(t)$. The tail of the difference is assumed to be influenced by only the term with the second largest time constants, namely $A_2 e^{-t/t_2}$. This term is fitted to the tail of the difference in the same way as above. The process is repeated until a good curve fitting of the whole $f(t)$ is obtained.

[1] A plot with logarithmic f axis and linear t axis.

Appendix D

Derivation of Systems of Ordinary Differential Equations

D.1 Two-Material-Input Method

Equation (4.26) describes the rate of change of voltage across each capacitor $C_{i,\mathrm{b}}$ in figure 4.3. Similarly, in material "a",

$$\frac{\mathrm{d}(V_{i,\mathrm{a}} - V_{0,\mathrm{b}})}{\mathrm{d}t} = \frac{V_{0,\mathrm{a}} - V_{i,\mathrm{a}}}{C_{i,\mathrm{a}} R_{i,\mathrm{a}}}. \tag{D.1}$$

Isolating $\frac{\mathrm{d}V_{i,\mathrm{a}}}{\mathrm{d}t}$ above gives equation (4.26). The current I going into material "a" from an external circuit is the sum of the current going into all the branches of that material:

$$I = C_{\mathrm{fast,a}} \frac{\mathrm{d}(V_{0,\mathrm{a}} - V_{0,\mathrm{b}})}{\mathrm{d}t} + \frac{V_{0,\mathrm{a}} - V_{0,\mathrm{b}}}{R_{0,\mathrm{a}}} + \sum_{i=1}^{N_{\mathrm{a}}} \frac{V_{0,\mathrm{a}} - V_{i,\mathrm{a}}}{R_{i,\mathrm{a}}}. \tag{D.2}$$

In the same way, the current going from material "a" to material "b" is

$$I = C_{\mathrm{fast,b}} \frac{\mathrm{d}V_{0,\mathrm{b}}}{\mathrm{d}t} + \frac{V_{0,\mathrm{b}}}{R_{0,\mathrm{b}}} + \sum_{i=1}^{N_{\mathrm{b}}} \frac{V_{0,\mathrm{b}} - V_{i,\mathrm{b}}}{R_{i,\mathrm{b}}}. \tag{D.3}$$

Those two currents are equal. Subtracting equation (D.3) from equation (D.2) and isolating $\frac{\mathrm{d}V_{0,\mathrm{b}}}{\mathrm{d}t}$ gives equation (4.25). Inserting equation (4.25) into equation (D.3) gives equation (4.35).

D.2 One-Material-Input Method

The current going into the material "a" in figure 4.4 is the sum of the current going into all the branches:

$$I = C_{\text{fast,a}} \frac{\mathrm{d}}{\mathrm{d}t}\left(V_{0,\text{a}}(t) - V_{0,\text{b}}(t)\right) + \frac{V_{0,\text{a}} - V_{0,\text{b}}}{R_{0,\text{a}}} + \sum_{i=1}^{N_\text{a}} \frac{V_{0,\text{a}} - V_{i,\text{a}}}{R_{i,\text{a}}}. \tag{D.4}$$

Isolating $\frac{\mathrm{d}V_{0,\text{b}}}{\mathrm{d}t}$ in that expression gives equation (4.30). The voltage across capacitor $C_{i,\text{a}}$ is $V_{i,\text{a}} - V_{0,\text{b}}$. The current going to that capacitor is $C_{i,\text{a}} \frac{\mathrm{d}}{\mathrm{d}t}\left(V_{i,\text{a}} - V_{0,\text{b}}\right)$. This current must be the same as the current going through the connected resistor, determined by the voltage drop across the resistor and its resistance:

$$C_{i,\text{a}} \frac{\mathrm{d}}{\mathrm{d}t}\left(V_{i,\text{a}} - V_{0,\text{b}}\right) = \frac{V_{0,\text{a}} - V_{i,\text{a}}}{R_{i,\text{a}}}. \tag{D.5}$$

Isolating $\frac{\mathrm{d}V_{i,\text{a}}}{\mathrm{d}t}$ in the above expression gives equation (4.31).

Appendix E

Equivalence of Integrodifferential and Ordinary Differential Equations

In the following, it is shown that the integrodifferential equations (IDEs) are equivalent to the corresponding systems of ordinary differential equations (ODEs), both for the two-material-input method and for the one-material-input method. The deductions below are not formal mathematical proofs as this demands considerations of continuity and uniqueness of solutions.

E.1 Two-Material-Input Method

Equation (4.26) is a linear, nonhomogeneous, first-order ODE. This type of equation has a well-known general solution [44], which in this case gives

$$V_{i,\mathrm{a}}(t) = \mathrm{e}^{\frac{-t}{t_{i,\mathrm{a}}}} \left[\int_0^t \mathrm{e}^{\frac{\xi}{t_{i,\mathrm{a}}}} \left(\frac{\mathrm{d}V_{0,\mathrm{b}}(\xi)}{\mathrm{d}\xi} + \frac{V_{0,\mathrm{a}}(\xi)}{t_{i,\mathrm{a}}} \right) \mathrm{d}\xi + V_{i,\mathrm{a}}(0) \right] \tag{E.1}$$

with $t_{i,\mathrm{a}} = R_{i,\mathrm{a}} C_{i,\mathrm{a}}$ in accordance with equation (4.21). The solution can be proved by differentiating it and comparing the result with equation (4.26). Splitting the integral at the plus sign gives

$$V_{i,\mathrm{a}}(t) = \mathrm{e}^{\frac{-t}{t_{i,\mathrm{a}}}} \left(\int_0^t \mathrm{e}^{\frac{\xi}{t_{i,\mathrm{a}}}} \frac{\mathrm{d}V_{0,\mathrm{b}}(\xi)}{\mathrm{d}\xi} \mathrm{d}\xi + \int_0^t \frac{\mathrm{e}^{\frac{\xi}{t_{i,\mathrm{a}}}} V_{0,\mathrm{a}}(\xi)}{t_{i,\mathrm{a}}} \mathrm{d}\xi + V_{i,\mathrm{a}}(0) \right). \tag{E.2}$$

For the first integral in brackets, integration by parts gives

$$\begin{aligned}\int_0^t \mathrm{e}^{\frac{\xi}{t_{i,\mathrm{a}}}} \frac{\mathrm{d}V_{0,\mathrm{b}}(\xi)}{\mathrm{d}\xi}\,\mathrm{d}\xi &= \left[\mathrm{e}^{\frac{\xi}{t_{i,\mathrm{a}}}} V_{0,\mathrm{b}}(t)\right]_0^t - \int_0^t \frac{\mathrm{e}^{\frac{\xi}{t_{i,\mathrm{a}}}} V_{0,\mathrm{b}}(\xi)}{t_{i,\mathrm{a}}}\,\mathrm{d}\xi \\ &= \mathrm{e}^{\frac{t}{t_{i,\mathrm{a}}}} V_{0,\mathrm{b}}(t) - V_{0,\mathrm{b}}(0) - \int_0^t \frac{\mathrm{e}^{\frac{\xi}{t_{i,\mathrm{a}}}} V_{0,\mathrm{b}}(\xi)}{t_{i,\mathrm{a}}}\,\mathrm{d}\xi.\end{aligned} \tag{E.3}$$

Inserting equation (E.3) into equation (E.2) gives

$$\begin{aligned}V_{i,\mathrm{a}}(t) = \mathrm{e}^{\frac{-t}{t_{i,\mathrm{a}}}} \Bigg(&\mathrm{e}^{\frac{t}{t_{i,\mathrm{a}}}} V_{0,\mathrm{b}}(t) - V_{0,\mathrm{b}}(0) - \int_0^t \frac{\mathrm{e}^{\frac{\xi}{t_{i,\mathrm{a}}}} V_{0,\mathrm{b}}(\xi)}{t_{i,\mathrm{a}}}\,\mathrm{d}\xi \\ &+ \int_0^t \frac{\mathrm{e}^{\frac{\xi}{t_{i,\mathrm{a}}}} V_{0,\mathrm{a}}(\xi)}{t_{i,\mathrm{a}}}\,\mathrm{d}\xi + V_{i,\mathrm{a}}(0)\Bigg).\end{aligned} \tag{E.4}$$

Removing the big parentheses and combining the integrals gives

$$V_{i,\mathrm{a}}(t) = V_{0,\mathrm{b}}(t) + \int_0^t \frac{\mathrm{e}^{-\frac{t-\xi}{t_{i,\mathrm{a}}}} \left[V_{0,\mathrm{a}}(\xi) - V_{0,\mathrm{b}}(\xi)\right]}{t_{i,\mathrm{a}}}\,\mathrm{d}\xi + B_i(t), \tag{E.5}$$

where

$$B_i(t) = \left[V_{i,\mathrm{a}}(0) - V_{0,\mathrm{b}}(0)\right] \exp(-t/t_{i,\mathrm{a}}). \tag{E.6}$$

By using equation (E.5), the first term with a summation symbol in equation (4.25) can be rewritten as follows:

$$\begin{aligned}&\sum_{i=1}^{N_\mathrm{a}} \frac{V_{0,\mathrm{a}}(t) - V_{i,\mathrm{a}}(t)}{R_{i,\mathrm{a}}} \\ &\quad = \sum_{i=1}^{N_\mathrm{a}} \frac{V_{0,\mathrm{a}}(t) - V_{0,\mathrm{b}}(t) - \int_0^t \frac{\mathrm{e}^{-\frac{t-\xi}{t_{i,\mathrm{a}}}} \left[V_{0,\mathrm{a}}(\xi) - V_{0,\mathrm{b}}(\xi)\right]}{t_{i,\mathrm{a}}}\,\mathrm{d}\xi - B_i(t)}{R_{i,\mathrm{a}}}.\end{aligned} \tag{E.7}$$

Substituting $d_\mathrm{a}/\left(A_{i,\mathrm{a}}\varepsilon_0 S\right)$ for $R_{i,\mathrm{a}}$ (cf. equation (4.20)) and $d_\mathrm{a}E_\mathrm{a}$ for $V_{0,\mathrm{a}}-V_{0,\mathrm{b}}$ (cf. equation (4.23)) on the right-hand side of the equality sign gives

$$\sum_{i=1}^{N_\mathrm{a}} \frac{V_{0,\mathrm{a}}(t)-V_{i,\mathrm{a}}(t)}{R_{i,\mathrm{a}}} = \sum_{i=1}^{N_\mathrm{a}} \frac{A_{i,\mathrm{a}}\varepsilon_0 S}{d_\mathrm{a}} \left(d_\mathrm{a}E_\mathrm{a}(t) - \int_0^t \frac{\mathrm{e}^{-\frac{t-\xi}{t_{i,\mathrm{a}}}} d_\mathrm{a}E_\mathrm{a}(\xi)}{t_{i,\mathrm{a}}}\,\mathrm{d}\xi - B_i(t) \right), \quad \text{(E.8)}$$

and, after some rearranging,

$$\sum_{i=1}^{N_\mathrm{a}} \frac{V_{0,\mathrm{a}}(t)-V_{i,\mathrm{a}}(t)}{R_{i,\mathrm{a}}} = \varepsilon_0 S \sum_{i=1}^{N_\mathrm{a}} A_{i,\mathrm{a}}E_\mathrm{a}(t) - \varepsilon_0 S \int_0^t E_\mathrm{a}(\xi) \sum_{i=1}^{N_\mathrm{a}} \frac{A_{i,\mathrm{a}}\mathrm{e}^{-\frac{t-\xi}{t_{i,\mathrm{a}}}}}{t_{i,\mathrm{a}}}\,\mathrm{d}\xi - \frac{\varepsilon_0 S}{d_\mathrm{a}} \sum_{i=1}^{N_\mathrm{a}} A_{i,\mathrm{a}}B_i(t). \quad \text{(E.9)}$$

By comparing with equation (4.17), $\sum_{i=1}^{N_\mathrm{a}} \frac{A_{i,\mathrm{a}}\mathrm{e}^{-\frac{t-\xi}{t_{i,\mathrm{a}}}}}{t_{i,\mathrm{a}}}$ can be recognized as $\frac{\partial f_\mathrm{a}(t-\xi)}{\partial t}$. Furthermore, $\sum_{i=1}^{N_\mathrm{a}} A_{i,\mathrm{a}}$ can be recognized as $f_\mathrm{a}(0)$. Therefore,

$$\sum_{i=1}^{N_\mathrm{a}} \frac{V_{0,\mathrm{a}}(t)-V_{i,\mathrm{a}}(t)}{R_{i,\mathrm{a}}} = \varepsilon_0 S f_\mathrm{a}(0)E_\mathrm{a}(t) + \varepsilon_0 S \int_0^t E_\mathrm{a}(\xi) \frac{\partial f_\mathrm{a}(t-\xi)}{\partial t}\,\mathrm{d}\xi - \frac{\varepsilon_0 S}{d_\mathrm{a}} \sum_{i=1}^{N_\mathrm{a}} A_{i,\mathrm{a}}B_i(t). \quad \text{(E.10)}$$

Equation (4.27) is also a linear, nonhomogeneous, first-order ODE [44]. Its solution is

$$V_{i,\mathrm{b}}(t) = \mathrm{e}^{\frac{-t}{t_{i,\mathrm{b}}}} \left(\int_0^t \mathrm{e}^{\frac{\xi}{t_{i,\mathrm{b}}}} \frac{V_{0,\mathrm{b}}(\xi)}{t_{i,\mathrm{b}}}\,\mathrm{d}\xi + V_{i,\mathrm{b}}(0) \right). \quad \text{(E.11)}$$

This can be inserted into the second term with a summation symbol in equation (4.25). The term then becomes

$$\sum_{i=1}^{N_\mathrm{b}} \frac{V_{0,\mathrm{b}}(t)-V_{i,\mathrm{b}}(t)}{R_{i,\mathrm{b}}} = \sum_{i=1}^{N_\mathrm{b}} \frac{V_{0,\mathrm{b}}(t) - \mathrm{e}^{\frac{-t}{t_{i,\mathrm{b}}}} \left(\int_0^t \mathrm{e}^{\frac{\xi}{t_{i,\mathrm{b}}}} \frac{V_{0,\mathrm{b}}(\xi)}{t_{i,\mathrm{b}}}\,\mathrm{d}\xi + V_{i,\mathrm{b}}(0) \right)}{R_{i,\mathrm{b}}}. \quad \text{(E.12)}$$

After removing the brackets and writing the right-hand side of the equality sign as three sums, this becomes

$$\sum_{i=1}^{N_\mathrm{b}} \frac{V_{0,\mathrm{b}}(t)-V_{i,\mathrm{b}}(t)}{R_{i,\mathrm{b}}} = \sum_{i=1}^{N_\mathrm{b}} \frac{V_{0,\mathrm{b}}(t)}{R_{i,\mathrm{b}}} - \sum_{i=1}^{N_\mathrm{b}} \frac{\int_0^t \mathrm{e}^{-\frac{t-\xi}{t_{i,\mathrm{b}}}} \frac{V_{0,\mathrm{b}}(\xi)}{t_{i,\mathrm{b}}}\,\mathrm{d}\xi}{R_{i,\mathrm{b}}} - \sum_{i=1}^{N_\mathrm{b}} \frac{\mathrm{e}^{\frac{-t}{t_{i,\mathrm{b}}}} V_{i,\mathrm{b}}(0)}{R_{i,\mathrm{b}}}. \tag{E.13}$$

Substituting $d_\mathrm{b}/\left(A_{i,\mathrm{b}}\varepsilon_0 S\right)$ for $R_{i,\mathrm{b}}$ (according to equation (4.20)) and $U - d_\mathrm{a}E_\mathrm{a}$ for $V_{0,\mathrm{b}}$ (according to equations (2.6) and (4.24)) on the right-hand side of the equality sign give

$$\begin{aligned}\sum_{i=1}^{N_\mathrm{b}} \frac{V_{0,\mathrm{b}}(t)-V_{i,\mathrm{b}}(t)}{R_{i,\mathrm{b}}} &= \frac{\varepsilon_0 S}{d_\mathrm{b}} \sum_{i=1}^{N_\mathrm{b}} A_{i,\mathrm{b}} \left[U(t) - d_\mathrm{a}E_\mathrm{a}(t)\right] \\ &\quad - \frac{\varepsilon_0 S}{d_\mathrm{b}} \sum_{i=1}^{N_\mathrm{b}} A_{i,\mathrm{b}} \int_0^t \mathrm{e}^{-\frac{t-\xi}{t_{i,\mathrm{b}}}} \frac{U(\xi) - d_\mathrm{a}E_\mathrm{a}(\xi)}{t_{i,\mathrm{b}}}\,\mathrm{d}\xi \\ &\quad - \frac{\varepsilon_0 S}{d_\mathrm{b}} \sum_{i=1}^{N_\mathrm{b}} A_{i,\mathrm{b}} \mathrm{e}^{\frac{-t}{t_{i,\mathrm{b}}}} V_{i,\mathrm{b}}(0).\end{aligned} \tag{E.14}$$

The sum $\sum_{i=1}^{N_\mathrm{b}} \frac{A_{i,\mathrm{b}} \mathrm{e}^{-\frac{t-\xi}{t_{i,\mathrm{b}}}}}{t_{i,\mathrm{b}}}$ can now be recognized as $\frac{\partial f_\mathrm{b}(t-\xi)}{\partial t}$ and $\sum_{i=1}^{N_\mathrm{b}} A_{i,\mathrm{b}}$ as $f_\mathrm{b}(0)$. Making these substitutions and rearranging gives

$$\begin{aligned}\sum_{i=1}^{N_\mathrm{b}} \frac{V_{0,\mathrm{b}}(t)-V_{i,\mathrm{b}}(t)}{R_{i,\mathrm{b}}} &= \varepsilon_0 S f_\mathrm{b}(0) \frac{U(t) - d_\mathrm{a}E_\mathrm{a}(t)}{d_\mathrm{b}} \\ &\quad + \varepsilon_0 S \int_0^t \frac{U(\xi) - d_\mathrm{a}E_\mathrm{a}(\xi)}{d_\mathrm{b}} \frac{\partial f_\mathrm{b}(t-\xi)}{\partial t}\,\mathrm{d}\xi \\ &\quad - \frac{\varepsilon_0 S}{d_\mathrm{b}} \sum_{i=1}^{N_\mathrm{b}} A_{i,\mathrm{b}} \mathrm{e}^{\frac{-t}{t_{i,\mathrm{b}}}} V_{i,\mathrm{b}}(0).\end{aligned} \tag{E.15}$$

The other parts of equation (4.25) can be substituted as follows:

$$\frac{1}{C_{\mathrm{fast,a}} + C_{\mathrm{fast,b}}} = \frac{d_\mathrm{a} d_\mathrm{b}}{S\left(d_\mathrm{a}\varepsilon_\mathrm{b} + d_\mathrm{b}\varepsilon_\mathrm{a}\right)} \tag{E.16}$$

as per equation (4.18);

$$\frac{V_{0,\mathrm{a}}(t) - V_{0,\mathrm{b}}(t)}{R_{0,\mathrm{a}}} = S\sigma_\mathrm{a} E_\mathrm{a}(t) \tag{E.17}$$

as per equations (4.19) and (4.23);

$$\frac{V_{0,\mathrm{b}}(t)}{R_{0,\mathrm{b}}} = S\sigma_{\mathrm{b}}\frac{U(t)-d_{\mathrm{a}}E_{\mathrm{a}}(t)}{d_{\mathrm{b}}} \tag{E.18}$$

as per equations (2.6), (4.19), and (4.22);

$$C_{\mathrm{fast,a}}\frac{\mathrm{d}V_{0,\mathrm{a}}(t)}{\mathrm{d}t} = \frac{S\varepsilon_{\mathrm{a}}}{d_{\mathrm{a}}}\frac{\mathrm{d}U(t)}{\mathrm{d}t} \tag{E.19}$$

as per equations (4.18) and (4.22); and

$$\frac{\mathrm{d}V_{0,\mathrm{b}}(t)}{\mathrm{d}t} = \frac{\mathrm{d}U(t)}{\mathrm{d}t} - d_{\mathrm{a}}\frac{\mathrm{d}E_{\mathrm{a}}(t)}{\mathrm{d}t} \tag{E.20}$$

as per equations (2.6) and (4.24). Equation (4.25) then becomes

$$\begin{aligned}\frac{\mathrm{d}U(t)}{\mathrm{d}t} - d_{\mathrm{a}}\frac{\mathrm{d}E_{\mathrm{a}}(t)}{\mathrm{d}t} = \frac{d_{\mathrm{a}}d_{\mathrm{b}}}{S\left(d_{\mathrm{a}}\varepsilon_{\mathrm{b}}+d_{\mathrm{b}}\varepsilon_{\mathrm{a}}\right)}\Bigg(&S\sigma_{\mathrm{a}}E_{\mathrm{a}}(t)+\varepsilon_0 S f_{\mathrm{a}}(0)E_{\mathrm{a}}(t)\\ &+\varepsilon_0 S\int_0^t E_{\mathrm{a}}(\xi)\frac{\partial f_{\mathrm{a}}(t-\xi)}{\partial t}\,\mathrm{d}\xi - \frac{\varepsilon_0 S}{d_{\mathrm{a}}}\sum_{i=1}^{N_{\mathrm{a}}}A_{i,\mathrm{a}}B_i(t)\\ &-S\sigma_{\mathrm{b}}\frac{U(t)-d_{\mathrm{a}}E_{\mathrm{a}}(t)}{d_{\mathrm{b}}} - \varepsilon_0 S f_{\mathrm{b}}(0)\frac{U(t)+d_{\mathrm{a}}E_{\mathrm{a}}(t)}{d_{\mathrm{b}}}\\ &-\varepsilon_0 S\int_0^t \frac{U(\xi)-d_{\mathrm{a}}E_{\mathrm{a}}(\xi)}{d_{\mathrm{b}}}\frac{\partial f_{\mathrm{b}}(t-\xi)}{\partial t}\,\mathrm{d}\xi\\ &+\frac{\varepsilon_0 S}{d_{\mathrm{b}}}\sum_{i=1}^{N_{\mathrm{b}}}A_{i,\mathrm{b}}\mathrm{e}^{\frac{-t}{t_{i,\mathrm{b}}}}V_{i,\mathrm{b}}(0)+\frac{S\varepsilon_{\mathrm{a}}}{d_{\mathrm{a}}}\frac{\mathrm{d}U(t)}{\mathrm{d}t}\Bigg).\end{aligned} \tag{E.21}$$

Moving $\frac{\mathrm{d}U(t)}{\mathrm{d}t}$ from the left to the right side of the equality sign, dividing the equation by $-d_{\mathrm{a}}$, substituting $\left[V_{i,\mathrm{a}}(0)-V_{0,\mathrm{b}}(0)\right]\exp(-t/t_{i,\mathrm{a}})$ for $B_i(t)$ (cf. equa-

tion (E.6)), and simplifying the fractions give

$$\begin{aligned}\frac{\mathrm{d}E_{\mathrm{a}}(t)}{\mathrm{d}t} &= \alpha(t) - \beta E_{\mathrm{a}}(t) - \gamma \int_0^t E_{\mathrm{a}}(\xi) \frac{\partial f_{\mathrm{a}}(t-\xi)}{\partial t}\,\mathrm{d}\xi \\ &\quad + \gamma \int_0^t \frac{U(\xi) - d_{\mathrm{a}} E_{\mathrm{a}}(\xi)}{d_{\mathrm{b}}} \frac{\partial f_{\mathrm{b}}(t-\xi)}{\partial t}\,\mathrm{d}\xi \\ &\quad + \frac{\gamma}{d_{\mathrm{a}}} \sum_{i=1}^{N_{\mathrm{a}}} A_{i,\mathrm{a}} \mathrm{e}^{\frac{-t}{t_{i,\mathrm{a}}}} \left[V_{i,\mathrm{a}}(0) - V_{0,\mathrm{b}}(0) \right] \\ &\quad - \frac{\gamma}{d_{\mathrm{b}}} \sum_{i=1}^{N_{\mathrm{b}}} A_{i,\mathrm{b}} \mathrm{e}^{\frac{-t}{t_{i,\mathrm{b}}}} V_{i,\mathrm{b}}(0)\end{aligned} \tag{E.22}$$

with α, β, and γ defined as in equations (2.29), (2.30), and (2.31). Equation (E.22) is equivalent to equation (2.28) on the condition that the sum of the two last terms of equation (E.22) equals zero for all t. The condition is fulfilled when

$$V_{i,\mathrm{a}}(0) - V_{0,\mathrm{b}}(0) = V_{i,\mathrm{b}}(0) = 0. \tag{E.23}$$

This shows that the IDE (2.28) for the two-material-input method and the corresponding system of ODEs (4.25)–(4.27) are equivalent, provided that equation (E.23) holds. This provision implies that none of the capacitors $C_{i,\mathrm{a}}$ or $C_{i,\mathrm{b}}$ have any charge. This is a natural condition for the initial values; charged capacitors represent polarization, and an assumption for equation (2.28) to be valid is that no electric field nor any polarization is present in the system before $t = 0$.

Application of a step voltage and a subsequent polarity reversal or grounding can be modeled by using the initial values $V_{i,\mathrm{a}}(0) = V_{0,\mathrm{b}}(0) = V_{i,\mathrm{b}}(0) = 0$ and letting $U(t) = V_{0,\mathrm{a}}(t)$ comprise unit step functions. For modeling a step voltage applied to an initially completely discharged system, it is also possible to use use initial values described by equations (4.28)–(4.29), which are consistent with equation (E.23).

E.2 One-Material-Input Method

By moving its terms, equation (4.30) can be rewritten as

$$\frac{\mathrm{d}}{\mathrm{d}t}\left(V_{0,\mathrm{a}}(t) - V_{0,\mathrm{b}}(t)\right) = \frac{1}{C_{\mathrm{fast,a}}}\left(-I(t) - \frac{V_{0,\mathrm{a}} - V_{0,\mathrm{b}}}{R_{0,\mathrm{a}}} - \sum_{i=1}^{N_{\mathrm{a}}} \frac{V_{0,\mathrm{a}} - V_{i,\mathrm{a}}}{R_{i,\mathrm{a}}}\right). \tag{E.24}$$

The left side of the equality sign equals $-d_\mathrm{a}\frac{\mathrm{d}E_\mathrm{a}(t)}{\mathrm{d}t}$, according to equation (4.23). As already demonstrated in section E.1, the term with the summation symbol can be substituted as per equation (E.10). The term with the $R_{0,\mathrm{a}}$ can be substituted as per equation (E.17), $C_{\mathrm{fast,a}}$ as per equation (4.18), and $I(t)$ with $SJ(t)$. Performing all these substitutions and dividing the whole equation by $-d_\mathrm{a}$ gives the integrodifferential equation (2.32) with an additional term $\frac{\varepsilon_0}{\varepsilon_\mathrm{a} d_\mathrm{a}}\sum_{i=1}^{N_\mathrm{a}} A_{i,\mathrm{a}} B_i(t)$ on the right-hand side of the equality sign. Therefore, the system of ODEs is equivalent to the IDE if

$$B_i(t) = \left[V_{i,\mathrm{a}}(0) - V_{0,\mathrm{b}}(0)\right]\exp(-t/t_{i,\mathrm{a}}) = 0 \tag{E.25}$$

for all values of t. This condition is fulfilled when

$$V_{i,\mathrm{a}}(0) = V_{0,\mathrm{b}}(0), \tag{E.26}$$

which is already demanded in section 4.2.2 (cf. equation (4.32)).

Appendix F

Article on Effects of Paper Edges

Edges of paper tapes constitute edges of butt gaps. The article [86] reproduced on pages 109–114 presents a study of the effects of these edges at steady state.

The article was presented at the *25th Nordic Insulation Symposium on Materials, Components and Diagnostics*, which took place in Västerås, Sweden, on June 19–21 2017. It was published online on October 3, 2017. The author of this thesis was the main author of the article. The copyright of the article is held by the authors, and the reproduction herein is permitted by the co-authors. The main author did the simulations, data analysis, and writing of the article. The co-authors contributed with input on disposition, presentation, and how to model the paper.

A correction to the article is as follows: its equation (9) shall read

$$U(r) = -\frac{1}{2}\alpha\,(r - r_\mathrm{i})^2 - \beta\,(r - r_\mathrm{i}) + 450\,\mathrm{kV}. \tag{F.1}$$

Although an erroneous version of the equation was written in the article, the correct version was used for the simulations.

Local Electric Field in Mass-Impregnated HVDC Cables

Gunnar Håkonseth[1,2], Erling Ildstad[1], and Knut Magne Furuheim[2]

[1]*Department of Electric Power Engineering,*
Norwegian University of Science and Technology (NTNU), NO-7491 Trondheim, Norway

[2]*Nexans Norway AS, PO Box 42, NO-1751 Halden, Norway*

Abstract

Detailed knowledge of the electric field in the insulation of mass-impregnated HVDC cables is important in order to understand their breakdown mechanisms and to improve their design. When calculating the *local* electric field, the wrapped structure of paper and impregnating oil needs to be taken into account. This gives information that is lost when the insulation is treated as a single, homogeneous material, which is done when the *macroscopic* electric field is calculated.

We have modeled mass-impregnated cable insulation with finite element analysis software and subsequently calculated the local electric field with the finite element method. The wrapped structure of paper and impregnating oil was taken into account.

In our model, the magnitude of the local field in the paper was up to twice as high as the magnitude of the macroscopic field. Field enhancements came from oil-filled butt gaps, and particularly from their edges. The geometry of the insulation influenced the magnitude of the field enhancements.

1. Introduction

High voltage direct current (HVDC) cables for long lengths are traditionally insulated with mass-impregnated paper [1], and this insulation technique is still being used for new, long transmission links [2]. The insulation consists of paper strips that are helically wrapped around the conductor of the cable. The width of the strips and pitch angle are tuned to leave a gap between adjacent paper windings in order to accommodate bending of the cable. These gaps are called "butt gaps". The windings of each paper layer are staggered with respect to the previous layer so that the butt gaps are not positioned directly above each other. The butt gaps, as well as the porous structure of the paper itself, are filled with "mass", a high-viscosity impregnation compound consisting of mineral oil with additives and thickeners.

Knowledge of the electric field in the insulation is key to understanding breakdown mechanisms of such cables, which again is important when designing cables for higher voltages than the current state of the art. It has been common to view the combination of paper and oil as a single, homogeneous material, disregarding the layered structure and the butt gaps. Experimental, analytical, and numerical techniques have then been used to find the *macroscopic* electric field. The macroscopic electric field and its gradient are always pointing from the conductor to the insulation screen, or in the opposite direction. The macroscopic approach is useful in order to investigate effects of different service conditions and situations that occur during the operation of HVDC mass-impregnated cables. Such conditions and situations can be temperature gradients and rapid voltage changes [3, 4, 5].

However, the macroscopic approach neglects the effects of the wrapped geometry and the different electric properties of paper and oil. It masks the variations in the electric field due to the heterogeneity of the insulation, and therefore local peaks in the electric field strength are not discovered. The macroscopic approach also disregards the electric field components other than the radial component. A more detailed approach is necessary in order to reveal critical spots in the insulation where the *local* electric field is very high. Calculations of the local electric field need to take into account the geometry of the insulation on a millimeter scale and below. This includes paper thickness, butt gap size, and the interfaces between the paper layers.

This paper presents calculations of the local electric field at stationary, direct current (DC) conditions done with the finite element method (FEM). It shows spots where the electric field is higher than in its surroundings, indicating critical spots in the insulation.

2. Theory

If the electric potential V is known, the electric field E at DC conditions is

$$\vec{E} = -\nabla V. \tag{1}$$

The basis for calculation of the potential is, together with the equation (1) above, the continuity equation

$$\nabla \vec{J} = 0 \tag{2}$$

and Ohm's law

$$\vec{J} = \sigma E. \tag{3}$$

$\vec{J}$ is current density and σ is conductivity.

A Maxwell capacitor consists of two parallel plates with two, parallel dielectric slabs a and b with conductivities

σ_a and σ_b, respectively. At steady state, the field distribution will be resistive and independent of permittivity. The electric field E is

$$E_a = U \frac{\sigma_b}{d_a \sigma_b + d_b \sigma_a}, \tag{4}$$

where U is the voltage between the plates and $d_{a,b}$ are the thicknesses of the dielectrics [6]. If now a is impregnated paper, b is oil, and $\sigma_{\text{oil}} = k\sigma_{\text{paper}}$ where k is some constant, equation (4) becomes

$$E_{\text{paper}} = \frac{U}{d_{\text{paper}} + d_{\text{oil}}/k}. \tag{5}$$

The relationship between the electric fields in the dielectrics becomes

$$E_{\text{paper}} = kE_{\text{oil}}. \tag{6}$$

This predicts that if $k \gg 1$, meaning $\sigma_{\text{oil}} \gg \sigma_{\text{paper}}$, almost all the potential drop will be through the paper.

3. Method

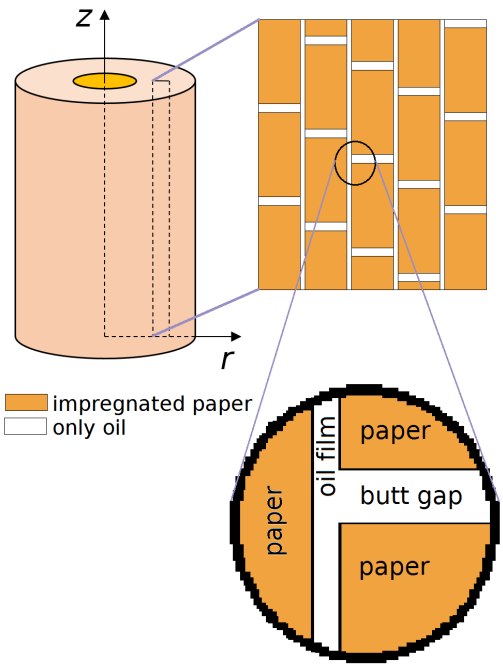

Fig. 1 – Model. Note that the detailed part of the model is heavily stretched in the r direction in order to enhance visibility of the narrow parts. Some of the subsequent figures are stretched similarly.

A two-dimensional cylindrically symmetric model of part of a paper-oil insulation system was created with the finite element analysis (FEA) software *Comsol Multiphysics* version 5.2 on a laptop computer. The symmetry axis and the radial axis are hereafter called the z and r axis respectively. A sketch of the model and its cylindrical coordinate system is shown in Figure 1. The cylindrical symmetry neglected the helical structure of the insulation by assuming that the paper strips and butt gaps are closed rings instead of helices.

The model consisted of a small section of the insulation of a 450 kV mass impregnated HVDC cable with conductor cross-section 1600 mm^2, conductor radius (including semi-conductive screen) 23.2 mm, and insulation thickness 19.2 mm. The macroscopic field of such a cable is previously studied [5].

The paper strips in our model were 20 mm wide and 100 µm thick. Neighboring layers of paper strips were staggered 30 %. The butt gaps were 2 mm wide. The interfaces between the paper layers were modelled as oil films. These oil films can be seen in Fig. 1 as long, vertical, white rectangles. Calculations were done with oil film thickness d_{film} of 1 µm and 10 µm. Calculations were also done without any oil films between the papers.

Limitations in computing memory and speed prohibited analysis of more than a small section of the insulation. The section contained five layers of paper in order to reveal effects of the staggering. This corresponded to a section thickness d_{section} of 0.500–0.540 mm. The length of the section along the z axis corresponded to the width of three paper strips and two butt gaps, which was 64 mm. The section was placed against the conductor. Thus, since the conductor radius was 23.2 mm, the left and right edges of the model were at $r = 23.2$ mm and $r = 23.2 + d_{\text{section}}$, respectively.

The paper was modeled as a solid, homogeneous material. The internal microstructure and natural residues from the wood were looked apart from. This implies that the paper in our model was to be understood as *impregnated* paper, *i.e.* paper whose pores and interstices between fibers were filled with oil. Consequently, any variations in the electric field due to the porous structure of the paper were disregarded. Furthermore, all surfaces and edges were modeled as perfectly smooth, neglecting the surface roughness of the paper. It follows that the transition between the 100 µm paper strip edges and the 20 mm paper surfaces were modeled as right-angled corners. It was assumed that the oil completely wetted the surfaces of the impregnated paper, causing close contact between the oil films and the papers. The model was free of cavities that usually form in mass-impregnated cable insulation during cooling [7, 8]. It was also free from other imperfections and contaminations.

The conductivity of impregnated paper was set to follow the relation

$$\sigma = A \exp\left(-\frac{a}{T} + b|\vec{E}|\right) \tag{7}$$

with $a = 1.10 \times 10^4$ K, $b = 0.034$ mm/kV, and $A = 4.3$ S/m. The conductivity of oil was set to be 100 times larger than the conductivity of impregnated paper, meaning $A = 430$ S/m for oil [3]. The temperature was

set to 50 °C across the whole insulation, leaving the effect of temperature gradients out of the analysis.

The finite element mesh consist of rectangular elements. The longitudinal element size was 20 µm for all the elements. The radial element size was 0.2 µm for the elements in the oil films and in the papers next to the oil–paper interfaces. It was exponentially increasing towards the middle of the paper strips, where the radial elements size was 6 µm.

The steady-state, macroscopic field in a HVDC cable varies across the insulation. In a small domain close to the conductor, it can be approximated to

$$E(r) = \alpha(r - r_\mathrm{i}) + \beta. \tag{8}$$

r_i is the conductor radius including the semi-conductive screen, and α and β are constants. With constant temperature across the insulation in a cable like the one we have modeled, $\alpha = 0.6\,\mathrm{kV/mm^2}$ and $\beta = 27.8\,\mathrm{kV/mm}$ in the innermost part of the insulation [5]. By integrating equation 8, we get the potential

$$U(r) = -\frac{1}{2}\alpha(r - r_\mathrm{i}) + \beta. \tag{9}$$

With α and β as mentioned above, this potential was used as boundary condition at the left and right boundaries of the model. This corresponded to a macroscopic field of 28 kV/mm. The boundary condition used for the top and bottom boundaries of the model were that no current could cross the boundary, meaning

$$\hat{n} \cdot \vec{J} = 0 \tag{10}$$

where $\hat{n}$ is the normal vector to the boundary.

The FEA software on the laptop computer used FEM to calculate the potential U and the field $\vec{E}$ by solving equations (1), (2), and (3) together with the boundary conditions (9) and (10).

4. Results

4.1. Field enhancement from butt gaps

Figure 2 shows the electric field in the whole model. The paper above and below the butt gaps had an electric field strength of 28 kV/mm. The paper that were directly to the left or right of a butt gap had 24–25 % higher electric field. The field in the oil was 0.8–0.9 kV/mm in the films 1.1–1.2 kV/mm in the butt gaps. This gave a value of approximately 30 for k in equations (5) and (6).

This field enhancements reached several paper layers away from the butt gaps. When our model was extended to include twelve layers of paper, areas of field enhancement coincided with each other. This is shown in Figure 3.

4.2. Field enhancement from paper edges

Paper edges, which also are butt gap edges, are defined in Figure 4. These edges induced field enhancements

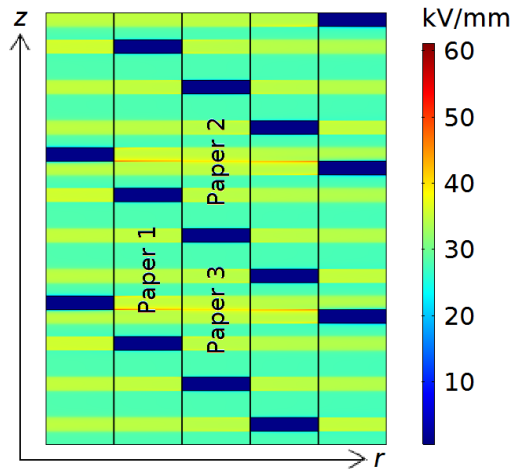

Fig. 2 – Electric field strength with $d_\mathrm{film} = 1$ µm. The dark blue areas are oil films (long, vertical) and butt gaps, and the rest is paper. Note that the figure is stretched in the r direction: The scales of the axes differ by a factor 100 so that the thickness of the papers, butt gaps, and oil films are exaggerated.

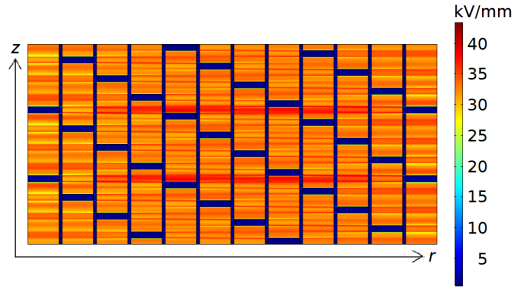

Fig. 3 – Electric field strength with $d_\mathrm{film} = 10$ µm. Note that the figure is stretched in the r direction: The scales of the axes differ by a factor 50 so that the thickness of the papers, butt gaps, and oil films are exaggerated.

that were different from the field enhancements described above. The cause of the edge-induced field can be understood by observing Figure 5, where the butt gap "pushed away" equipotential lines while Paper 3 did not. The equipotential lines were concentrated at the corner of the butt gap, and this concentration constituted an edge-induced field enhancement.

The edge-induced field enhancements can be seen as peaks in Figure 6 and Figure 7.

The edge-induced enhancements were stronger in the longitudinal than in the radial direction, but the major component of the total electric field was still radial in the peak of the enhancements. The effect of the edges was mainly seen close to the paper surface, which also was close to the edge.

The edge-induced field enhancements coincided with

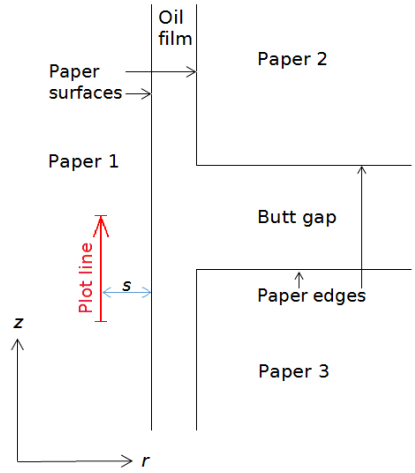

Fig. 4 – Definition of paper edges and the plot line. The plot line was placed in Paper 1, at various distances s from its right surface. The distances in the r direction are exaggerated in this figure.

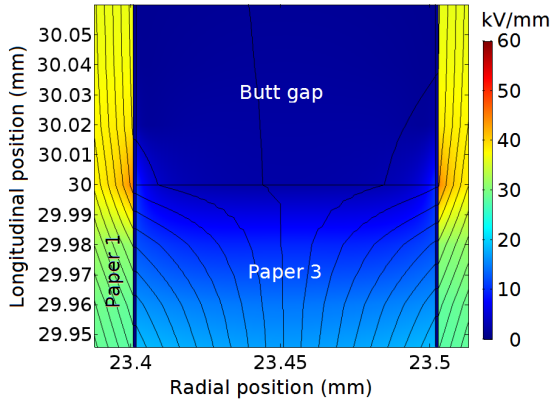

Fig. 5 – Magnitude of electric field (color surface plot) and equipotential lines (black) for each 0.1 kV. Film thickness: 1 µm. This figure is not stretched, so the scales of the r and z axes are equal.

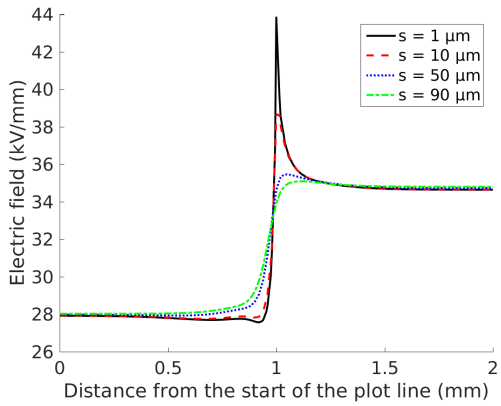

Fig. 6 – E_r along the plot line (see Figure 4) at different distances s from the paper surface. Film thickness: 1 µm.

each other in a similar manner as the field enhancements induced from butt gaps. This is visible in fig. 2.

4.3. Effect of film thickness

Except for in areas of edge-induced field enhancements, a large oil film thickness led to a high field in the paper. The radial field was 7 % higher if the oil film thickness was 10 µm than if it was 1 µm. If no oil film was present, the radial field was 0.8 % lower than if the oil film thickness was 1 µm. This can be seen in Figure 8. The longitudinal field was zero in all cases, except for in areas with edge-induced field enhancements.

In the areas affected by edge-induced field enhancements, the effect was opposite: A thicker film gave lower edge-induced field enhancements. When calculations were done without any oil film between the paper layers, the paper corners produced field enhancement not only in the adjacent paper, but also in the paper corner itself. For example: The upper left corner of Paper 3 produced field enhancement in Paper 1. When there was no oil film between Paper 1 and Paper 3, the field enhancement was observed not only in Paper 1, but also in the corner of Paper 3.

5. Discussion

Even though A in equation (7) was set to be 100 times higher for oil than for paper, $k = E_{\text{paper}}/E_{\text{oil}}$ was found to be not more than approximately 30. This was due to the conductivity's dependence on the electric field strength.

The field enhancements from butt gaps in our model agreed well with the theory of Maxwell capacitors. With $k = 30$, equation 5 predicted 24 % enhancement when the butt gap and the areas to its left and right were considered as a Maxwell capacitor. Our results showed 24–25 % enhancement. The field enhancement from the butt gaps can also be understood simply by observing that the paper takes almost the entire voltage drop across the capacitor: Since there is less paper to take this voltage drop to the left and right of a butt gap, the field is higher such regions than in the rest of the paper.

As the number of paper layers increases, the effect of field enhancements becomes more important. Virtually the whole insulation of real cables are affected by field enhancements, and areas of coinciding field enhancements are normal. Some areas will probably suffer from coinciding enhancements from more butt gaps than other areas will, even though a sound production process will spread the butt gaps as much as possible. Changes of paper strip winding directions result in overlapping butt gaps and adds to this effect. The same discussion holds for edge-induced field enhancements. Even though

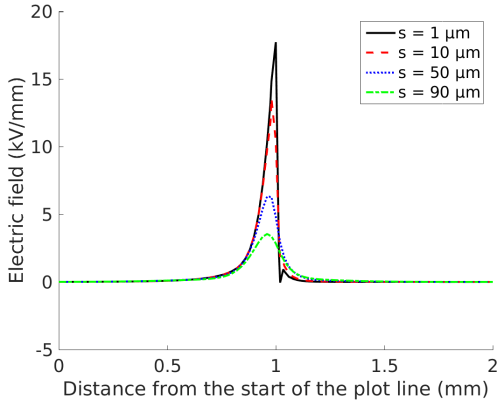

Fig. 7 – E_z along the plot line (see Figure 4) at different distances s from the paper surface. Film thickness: 1 µm.

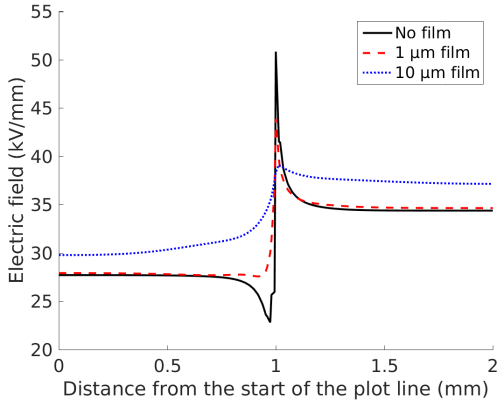

Fig. 8 – E_r along the plot line (see Figure 4) at a distances $s =$ 1 µm from the paper surface. No film, 1 µm film, and 10 µm film.

those enhancements diminish as the distance to the edge increases, they can add together, *e.g.* as shown in the middle of Paper 2 in Figure 2.

The field that we have calculated inside the paper is "macroscopic" in the sense that the effects of the internal heterogeneity of the paper is left out of the analysis. The heterogeneity, together with the surface roughness of the paper, may add further to the field enhancements in a real cable.

It can be argued that the paper–paper interfaces in reality are far more complex than an oil film with smooth surfaces. However, space charge measurements in stacked layers of mass-impregnated paper have yielded results consistent with the presence of 1–10 µm oil films between the papers [5]. Nevertheless, emphasis should be on trends rather than absolute values in our calculations—especially close to the surfaces.

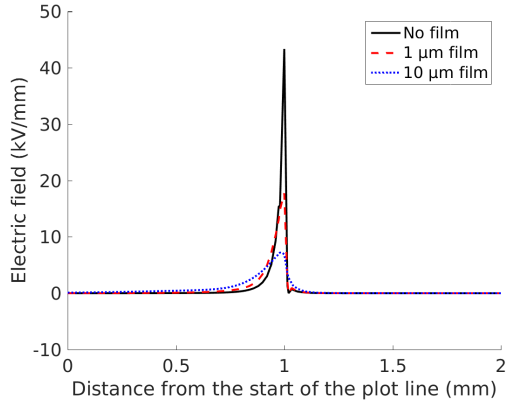

Fig. 9 – E_z along the plot line (see Figure 4) at a distances $s =$ 1 µm from the paper surface. No film, 1 µm film, and 10 µm film.

It is important to note that these considerations assume no cavities or other voids in the insulation.

6. Conclusion

In our model, the local electric field in the impregnated paper was equal to or higher than the macroscopic field. Butt gaps gave rise to field enhancements that reached far away from the butt gaps in the radial direction, but not in the longitudinal direction. Butt gaps with the same or almost the same longitudinal position intensified these enhancements.

The edges of papers and butt gaps gave rise to field enhancements that diminished as the distance from the edge increased. The only places in the model where a longitudinal component of the electric field was in such edge-induced enhancements. The radial component of the field was still the most dominant. Edges with the same or almost the same longitudinal position intensified these enhancements.

The field in the oil was negligible.

A thick oil film raised the field in the paper, except for close to paper edges where the edge-induced field enhancements were important.

Acknowledgments

This work is part of the project "Mass Impregnated Non-Draining HVDC Submarine Cables" led by Nexans Norway AS. The project is financially supported by The Research Council of Norway (Norges forskningsråd), Nexans Norway AS, Statnett SF, Affärsverket svenska kraftnät, and Fingrid Oyj, and has project number 256405/E20 within the ENERGIX program of The Research Council of Norway.

References

[1] T. Worzyk. *Submarine Power Cables: Design, Installation, Repair, Environmental Aspects*. Springer Berlin Heidelberg, 2009.

[2] Nexans (press release). NSN Link will interconnect Nordic and British energy markets with the world's longest subsea power link incorporating Nexans' HVDC cable technology, July 2015.

[3] E. Occhini and G. Maschio. Electrical Characteristics of Oil-Impregnated Paper as Insulation for HV DC Cables. *IEEE Transactions on Power Apparatus and Systems*, PAS-86(3):312–326, March 1967.

[4] Bjørn R. Nyberg. *Electrical stress in HVDC cables under stationary and transient conditions*. PhD thesis, The University of Trondheim - The Norwegian Institute of Technology, Trondheim, 1973.

[5] M.J.P. Jeroense. *Charges and discharges in HVDC cables: in particular in mass-impregnated HVDC cables*. PhD thesis, Delft University Press, Delft, 1997.

[6] F. H. Kreuger. *Industrial high DC voltage: 1. fields, 2. breakdowns, 3. tests*. Delft Univ. Press, Delft, 1995.

[7] G. Evenset. *Cavitation as a precursor to breakdown of mass-impregnated HVDC cables*. PhD thesis, Norges tekniske høgskole, Institutt for elkraftteknikk, Trondheim, 1999.

[8] M. Runde, R. Hegerberg, N. Magnusson, E. Ildstad, and T. Ytrehus. Cavity formation in mass-impregnated HVDC subsea cables-mechanisms and critical parameters. *IEEE Electrical Insulation Magazine*, 30(2):22–33, March 2014.

Appendix G

List of Publications

The work with this thesis has resulted in the following published papers in addition to the thesis:

- G. Håkonseth, E. Ildstad, and K. M. Furuheim, "Local Electric Field in Mass-Impregnated HVDC Cables," in *Proceedings of the Nordic Insulation Symposium*, vol. 25, 2017. DOI: 10.5324/nordis.v0i25.2351.
- G. Håkonseth and E. Ildstad, "Steady-State Electric Field and Conductivity in Mass-Impregnated HVDC Cable Insulation," in *2018 IEEE 2nd International Conference on Dielectrics (ICD)*, Jul. 2018. DOI: 10.1109/ICD.2018.8468346.
- G. Håkonseth and E. Ildstad, "Time-Dependent Electric Field Distribution in Layered Paper–Oil Insulation," in *Proceedings of the Nordic Insulation Symposium*, vol. 26, 2019. DOI: 10.5324/nordis.v0i26.3279.
- G. Håkonseth, K. M. Furuheim, and E. Ildstad, "Structure of Paper–Oil Insulation for Mass-Impregnated HVDC Cables," in *2019 IEEE Conference on Electrical Insulation and Dielectric Phenomena (CEIDP)*, Oct. 2019, pp. 524–527. DOI: 10.1109/CEIDP47102.2019.9009943.

Some of the contents of these papers are included in the thesis, and the papers are listed in the bibliography as references [86], [72], [61], and [16], respectively. The first paper above is reproduced in appendix F.

Bibliography

[1] B. Klebo-Espe, L. Bjerke, U. S. Gudmundsdottir, and T. Kvarts, "New Innovative Cable Installation Methods Used for the 500 kV HVDC Project, Skagerrak 4 between Denmark and Norway," presented at the Cigré 2014, Paris: Cigré, 2014 (cit. on pp. 1, 2).

[2] O. Hauge, J. N. Johnsen, T. A. Holte, and K. Bjorlolw-Larsen, "Performance of the ± 250 kV HVDC Skagerrak Submarine Cables. Further Development of the HVDC Paper-Insulated, Mass-Impregnated (Solid Type) Submarine Cable," *IEEE Transactions on Power Delivery*, vol. 3, no. 1, pp. 1–15, Jan. 1988. DOI: 10.1109/61.4221 (cit. on pp. 1, 2).

[3] E. Ildstad, "World Record HVDC Submarine Cables," *IEEE Electrical Insulation Magazine*, vol. 10, no. 4, pp. 64–, Jul. 1994. DOI: 10.1109/57.298131 (cit. on pp. 1, 2).

[4] T. Worzyk, *Submarine Power Cables: Design, Installation, Repair, Environmental Aspects*. Springer Berlin Heidelberg, 2009. DOI: 10.1007/978-3-642-01270-9 (cit. on pp. 1–3, 62, 78).

[5] M. Runde, R. Hegerberg, N. Magnusson, E. Ildstad, and T. Ytrehus, "Cavity formation in mass-impregnated HVDC subsea cables—mechanisms and critical parameters," *IEEE Electrical Insulation Magazine*, vol. 30, no. 2, pp. 22–33, Mar. 2014. DOI: 10.1109/MEI.2014.6749570 (cit. on pp. 1–3, 29, 47, 85).

[6] G. Evenset, "Cavitation as a Precursor to Breakdown of Mass-Impregnated HVDC Cables," doctoral thesis, Norges tekniske høgskole, Institutt for elkraftteknikk, Trondheim, 1999 (cit. on pp. 1–3, 85).

[7] B. Abrahamsson, L. Soderberg, and K. Lozinski, "SwePol HVDC Link," in *Seventh International Conference on AC-DC Power Transmission*, Nov. 2001, pp. 211–213. DOI: 10.1049/cp:20010544 (cit. on pp. 1, 2).

[8] L. Colla, M. Marelli, S. Lauria, M. Schembari, F. Palone, and M. Rebolini, "Mediterranean High Voltage Submarine Cable Links Technology and System Challenges," in *AEIT Annual Conference 2013*, Oct. 2013, pp. 1–5. DOI: 10.1109/AEIT.2013.6666796 (cit. on pp. 1, 2).

[9] T. Westerweller and J. Price, "Crossing the Divide," *Power Engineer*, vol. 20, no. 5, pp. 42–45, Oct. 2006. DOI: 10.1049/pe:20060508 (cit. on pp. 1, 2).

[10] C. E. Mueller, S. I. Keil, and C. Bauer, "Underground Cables vs. Overhead Lines: Quasi-Experimental Evidence for the Effects on Public Risk Expectations, Attitudes, and Protest Behavior," *Energy Policy*, vol. 125, pp. 456–466, Feb. 1, 2019. DOI: 10.1016/j.enpol.2018.10.053 (cit. on p. 1).

[11] J. Song-Manguelle, M. Harfman Todorovic, S. Chi, S. K. Gunturi, and R. Datta, "Power Transfer Capability of HVAC Cables for Subsea Transmission and Distribution Systems," *IEEE Transactions on Industry Applications*, vol. 50, no. 4, pp. 2382–2391, Jul. 2014. DOI: 10.1109/TIA.2013.2291934 (cit. on p. 1).

[12] L. Colla and E. Zaccone, "HVDC Land and Submarine Cables in the Mediterranean Area," in *2018 AEIT International Annual Conference*, Oct. 2018, pp. 1–6. DOI: 10.23919/AEIT.2018.8577424 (cit. on p. 1).

[13] T. Worzyk. (Nov. 1, 2007). "100 Years of High Voltage DC Links," [Online]. Available: https://www.modernpowersystems.com/features/feature100-years-of-high-voltage-dc-links/ (visited on Jan. 28, 2020) (cit. on p. 1).

[14] R. Liu, "Long-Distance DC Electrical Power Transmission," *IEEE Electrical Insulation Magazine*, vol. 29, no. 5, pp. 37–46, Sep. 2013. DOI: 10.1109/MEI.2013.6585855 (cit. on p. 1).

[15] N. Garoff, "The Friction between Paper Surfaces," doctoral thesis, KTH Royal Institute of Technology, Stockholm, Sweden, 2002 (cit. on p. 2).

[16] G. Håkonseth, K. M. Furuheim, and E. Ildstad, "Structure of Paper–Oil Insulation for Mass-Impregnated HVDC Cables," in *2019 IEEE Conference on Electrical Insulation and Dielectric Phenomena (CEIDP)*, Oct. 2019, pp. 524–527. DOI: 10.1109/CEIDP47102.2019.9009943 (cit. on pp. 3, 30, 59–62, 115).

[17] G. Hyson, "Power Cables: Ancient and Modern," *Electronics and Power*, vol. 20, no. 11, pp. 450–453, Jun. 1974. DOI: 10.1049/ep.1974.0327 (cit. on p. 2).

[18] M. Jeroense, M. Bergkvist, and P. Nordberg, "Partial Discharges in High Voltage Direct Current Mass-Impregnated Cables," in *1999 Eleventh International Symposium on High Voltage Engineering*, vol. 5, Aug. 1999, 53–57 vol.5. DOI: 10.1049/cp:19990884 (cit. on p. 3).

[19] P. Szabo, O. Hassager, and E. Strobech, "Modeling of Pressure Effects in HVDC Cables," *IEEE Transactions on Dielectrics and Electrical Insulation*, vol. 6, no. 6, pp. 845–851, Dec. 1999. DOI: 10.1109/94.822026 (cit. on pp. 3, 86).

[20] G. Chen, M. Hao, Z. Xu, A. Vaughan, J. Cao, and H. Wang, "Review of High Voltage Direct Current Cables," *CSEE Journal of Power and Energy Systems*, vol. 1, no. 2, pp. 9–21, Jun. 2015. DOI: 10.17775/CSEEJPES.2015.00015 (cit. on p. 3).

[21] K. M. Furuheim, "Aging of Oil Impregnated Insulation Paper of Subsea HV Cables in Decades of Service," presented at the 10th International Conference on Insulated Power Cables (Jicable'19), Paris, 2019 (cit. on p. 3).

[22] M. J. P. Jeroense, "Charges and Discharges in HVDC Cables: In Particular in Mass-Impregnated HVDC Cables," doctoral thesis, Delft University of Technology, Delft, The Netherlands, 1997 (cit. on pp. 3–7, 47, 76, 78, 87).

[23] M. P. Bahrman and B. K. Johnson, "The ABCs of HVDC Transmission Technologies," *IEEE Power and Energy Magazine*, vol. 5, no. 2, pp. 32–44, Mar. 2007. DOI: 10.1109/MPAE.2007.329194 (cit. on p. 4).

[24] D. Jovcic, "Bidirectional, High-Power DC Transformer," *IEEE Transactions on Power Delivery*, vol. 24, no. 4, pp. 2276–2283, Oct. 2009. DOI: 10.1109/TPWRD.2009.2028600 (cit. on p. 4).

[25] I. M. de Alegría, J. L. Martín, I. Kortabarria, J. Andreu, and P. I. Ereño, "Transmission Alternatives for Offshore Electrical Power," *Renewable and Sustainable Energy Reviews*, vol. 13, no. 5, pp. 1027–1038, Jun. 1, 2009. DOI: 10.1016/j.rser.2008.03.009 (cit. on p. 4).

[26] R. L. Sellick and M. Åkerberg, "Comparison of HVDC Light (VSC) and HVDC Classic (LCC) Site Aspects, for a 500MW 400kV HVDC Transmission Scheme," in *10th IET International Conference on AC and DC Power Transmission (ACDC 2012)*, Dec. 2012, pp. 1–6. DOI: 10.1049/cp.2012.1945 (cit. on p. 4).

[27] S. Rüberg, A. L'Abbate, G. Fulli, and A. Purvins, "High-Voltage Direct-Current Transmission," in *Advanced Technologies for Future Transmission Grids*, ser. Power Systems, G. Migliavacca, Ed., London: Springer, 2013, pp. 157–213. DOI: 10.1007/978-1-4471-4549-3_5 (cit. on p. 4).

[28] D. O. Adeuyi, N. Jenkins, and J. Wu, "Topologies of the North Sea Supergrid," in *2013 48th International Universities' Power Engineering Conference (UPEC)*, Sep. 2013, pp. 1–6. DOI: 10.1109/UPEC.2013.6714967 (cit. on p. 4).

[29] O. Vestergaard, B. Westman, G. McKay, P. Jones, J. Fitzgerald, and B. Williams, "HVDC – Enabling the Transition to an Energy System Based on Renewables," in *9th IET International Conference on AC and DC Power Transmission (ACDC 2010)*, Oct. 2010, pp. 1–6. DOI: 10.1049/cp.2010.0970 (cit. on p. 4).

[30] K. L. Västermark, M. Hofmann, E.-A. Bergmann, and A. Kringstad, "A European Energy-Only Market in 2030," Statnett SF, Oct. 2015 (cit. on p. 4).

[31] I. Graabak, S. Jaehnert, M. Korpås, and B. Mo, "Norway as a Battery for the Future European Power System—Impacts on the Hydropower System," *Energies*, vol. 10, no. 12, p. 2054, Dec. 2017. DOI: 10.3390/en10122054 (cit. on p. 4).

[32] B. R. Nyberg, "Electrical Stress in HVDC Cables nder Stationary and Transient Conditions," doctoral thesis, University of Trondheim – Norwegian Institute of Technology, Trondheim, Norway, 1973 (cit. on pp. 4, 5, 7, 21, 43, 76, 85).

[33] C. K. Eoll, "Theory of Stress Distribution in Insulation of High-Voltage DC Cables: Part I," *IEEE Transactions on Electrical Insulation*, vol. EI-10, no. 1, pp. 27–35, Mar. 1975. DOI: 10.1109/TEI.1975.297853 (cit. on pp. 4, 76).

[34] Z. Huang, "Rating Methodology of High Voltage Mass Impregnated DC Cable Circuits," doctoral thesis, University of Southampton, Southampton, United Kingdom, 2014 (cit. on pp. 4, 43, 76).

[35] A. Küchler, *High Voltage Engineering: Fundamentals – Technology – Applications*, ser. VDI-Buch. Berlin, Germany: Springer Vieweg, 2018. DOI: 10.1007/978-3-642-11993-4 (cit. on pp. 5, 6, 11, 44, 50, 57, 65).

[36] D. Fabiani *et al.*, "HVDC Cable Design and Space Charge Accumulation. Part 3: Effect of Temperature Gradient [Feature article]," *IEEE Electrical Insulation Magazine*, vol. 24, no. 2, pp. 5–14, Mar. 2008. DOI: 10.1109/MEI.2008.4473049 (cit. on p. 5).

[37] Y. Zhan *et al.*, "Comparison of Two Models on Simulating Electric Field in HVDC Cable Insulation," *IEEE Transactions on Dielectrics and Electrical Insulation*, vol. 26, no. 4, pp. 1107–1115, Aug. 2019. DOI: 10.1109/TDEI.2019.007878 (cit. on pp. 5, 75).

[38] E. W. G. Bungay and D. McAllister, *Electric Cables Handbook*. Oxford: BSP Professional Books, 1990 (cit. on p. 5).

[39] Z. Y. Huang, J. A. Pilgrim, P. L. Lewin, S. G. Swingler, and G. Tzemis, "Thermal-Electric Rating Method for Mass-Impregnated Paper-Insulated HVDC Cable Circuits," *IEEE Transactions on Power Delivery*, vol. 30, no. 1, pp. 437–444, Feb. 2015. DOI: 10.1109/TPWRD.2014.2359772 (cit. on pp. 5, 6).

[40] V. D. Houhanessian, "Measurement and Analysis of Dielectric Response in Oil-Paper Insulation Systems," doctoral thesis, Swiss Federal Institute of Technology in Zurich, Zurich, Switzerland, 1998 (cit. on pp. 12, 15, 18, 19, 37, 38, 53, 74).

[41] D. J. Griffiths, *Introduction to Electrodynamics*, 3rd. San Francisco, CA, USA: Pearson Benjamin Cummings, 2008 (cit. on p. 12).

[42] A. K. Jonscher, *Dielectric Relaxation in Solids*. London: Chelsea Dielectrics Press Limited, 1983 (cit. on pp. 12, 16–18, 53, 72).

[43] F. H. Kreuger, *Industrial High DC Voltage: 1. Fields, 2. Breakdowns, 3. Tests*. Delft: Delft Univ. Press, 1995 (cit. on pp. 13, 15, 70).

[44] E. Kreyszig, *Advanced Engineering Mathematics*, 8th ed. John Wiley & Sons, 1999 (cit. on pp. 13, 52, 101, 103).

[45] R. A. Adams, *Calculus. A Complete Course*, 6th ed. Toronto: Pearson/Addison Wesley, 2006 (cit. on pp. 13, 21).

[46] V. D. Houhanessian and W. S. Zaengl, "Application of Relaxation Current Measurements to On-Site Diagnosis of Power Transformers," in *IEEE 1997 Annual Report Conference on Electrical Insulation and Dielectric Phenomena*, vol. 1, Oct. 1997, pp. 45–51. DOI: 10.1109/CEIDP.1997.634555 (cit. on pp. 15, 18, 38).

[47] U. Gäfvert and E. Ildstad, "Modelling Return Voltage Measurements of Multi-Layer Insulation Systems," in *Proceedings of 1994 4th International Conference on Properties and Applications of Dielectric Materials (ICPADM)*, vol. 1, Jul. 1994, pp. 123–126. DOI: 10.1109/ICPADM.1994.413926 (cit. on pp. 15, 72, 75).

[48] E. Kuffel, W. S. Zaengl, and J. Kuffel, *High Voltage Engineering: Fundamentals*, 2nd ed. Oxford; Boston: Butterworth-Heinemann, 2000 (cit. on pp. 15, 22).

[49] H. Flanders, "Differentiation Under the Integral Sign," *The American Mathematical Monthly*, vol. 80, no. 6, pp. 615–627, 1973. DOI: 10.2307/2319163 (cit. on p. 18).

[50] P. Linz, *Analytical and Numerical Methods for Volterra Equations*, ser. Studies in Applied and Numerical Mathematics. Society for Industrial and Applied Mathematics, Jan. 1, 1985. DOI: 10.1137/1.9781611970852 (cit. on p. 21).

[51] *Paper and Board – Determination of Thickness, Density and Specific Volume*, ISO 534:2011, 2011 (cit. on p. 23).

[52] L. E. Pettersen, "Dielectric Response and Electrical Conductivity of Mass Impregnated HVDC Cable Insulation," Master's thesis, Norwegian University of Science and Technology, Trondheim, Norway, 2018 (cit. on pp. 24, 43, 64, 86).

[53] F. Vahidi, S. Haegele, S. Tenbohlen, K. Rapp, and A. Sbravati, "Study on Moisture Influence on Electrical Conductivity of Natural Ester Fluid and Mineral Oil," in *2017 IEEE Electrical Insulation Conference (EIC)*, Jun. 2017, pp. 290–293. DOI: 10.1109/EIC.2017.8004614 (cit. on p. 25).

[54] T. A. Ve, F. Mauseth, and E. Ildstad, "Effect of Water Content on the Conductivity of XLPE Insulation," in *2012 Annual Report Conference on Electrical Insulation and Dielectric Phenomena (CEIDP)*, Oct. 2012, pp. 649–653. DOI: 10.1109/CEIDP.2012.6378864 (cit. on p. 28).

[55] E. Occhini and G. Maschio, "Electrical Characteristics of Oil-Impregnated Paper as Insulation for HV DC Cables," *IEEE Transactions on Power Apparatus and Systems*, vol. PAS-86, no. 3, pp. 312–326, Mar. 1967. DOI: 10.1109/TPAS.1967.291959 (cit. on pp. 29, 33, 47, 48, 51, 53, 54, 86, 87).

[56] Keysight Technologies. (Oct. 12, 2018). "U1730C Series Handheld LCR Meters: Data Sheet," [Online]. Available: http://literature.cdn.keysight.com/litweb/pdf/5990-7778EN.pdf (visited on May 21, 2019) (cit. on p. 29).

[57] D. R. Roisum, *The Mechanics of Winding*. Atlanta, GA, USA: TAPPI, 1994 (cit. on p. 30).

[58] *Paper, Board, Pulps and Related Terms – Vocabulary – Part 3: Paper-Making Terminology*, ISO 4046-3:2016, 2016 (cit. on p. 30).

[59] M. J. P. Jeroense and F. H. Kreuger, "Electrical Conduction in HVDC Mass-Impregnated Paper Cable," *IEEE Transactions on Dielectrics and Electrical Insulation*, vol. 2, no. 5, pp. 718–723, Oct. 1995. DOI: 10.1109/94.469968 (cit. on pp. 33, 47).

[60] R. M. Corless, G. H. Gonnet, D. E. G. Hare, D. J. Jeffrey, and D. E. Knuth, "On the Lambert W function," *Advances in Computational Mathematics*, vol. 5, no. 1, pp. 329–359, Dec. 1, 1996. DOI: 10.1007/BF02124750 (cit. on pp. 34, 96).

[61] G. Håkonseth and E. Ildstad, "Time-Dependent Electric Field Distribution in Layered Paper–Oil Insulation," in *Proceedings of the Nordic Insulation Symposium*, vol. 26, 2019, pp. 58–63. DOI: 10.5324/nordis.v0i26.3279 (cit. on pp. 37, 41, 65, 115).

[62] T. K. Saha, P. Purkait, and F. Müller, "Deriving an Equivalent Circuit of Transformers Insulation for Understanding the Dielectric Response Measurements," *IEEE Transactions on Power Delivery*, vol. 20, no. 1, pp. 149–157, Jan. 2005. DOI: 10.1109/TPWRD.2004.835436 (cit. on pp. 37, 98).

[63] *Matlab*, version 9.2 (release R2017a), The MathWorks, Inc., 2017 (cit. on p. 41).

[64] L. F. Shampine and M. W. Reichelt, "The MATLAB ODE Suite," *SIAM Journal on Scientific Computing*, vol. 18, no. 1, pp. 1–22, Jan. 1, 1997. DOI: 10.1137/S1064827594276424 (cit. on p. 41).

[65] M. J. P. Jeroense and P. H. F. Morshuis, "Electric Fields in HVDC Paper-Insulated Cables," *IEEE Transactions on Dielectrics and Electrical Insulation*, vol. 5, no. 2, pp. 225–236, Apr. 1998. DOI: 10.1109/94.671940 (cit. on p. 43).

[66] P. Gazzana Priaroggia, P. Metra, and G. Miramonti, "Dielectric Phenomena in the Breakdown of Non Pressure Assisted, Impregnated Paper Insulated, HVDC Cables," in *[1992] Proceedings of the 4th International Conference on Conduction and Breakdown in Solid Dielectrics*, Jun. 1992, pp. 407–417. DOI: 10.1109/ICSD.1992.225002 (cit. on p. 43).

[67] H. P. Moser, V. Dahinden, and H. Brechna, *Transformerboard II: Properties and Application of Transformerboard of Different Fibres*. Rapperswil, Switzerland: H. Weidmann AG, 1987 (cit. on p. 43).

[68] *Product Data Sheet: T 2015 Impregnating Compound*, version 0/02/98, Dussek Campbell (now H&R ChemPharm (UK) Ltd.) (cit. on p. 44).

[69] C. Tang, B. Huang, M. Hao, Z. Xu, J. Hao, and G. Chen, "Progress of Space Charge Research on Oil-Paper Insulation Using Pulsed Electroacoustic Techniques," *Energies*, vol. 9, no. 1, article no. 53, Jan. 2016. DOI: 10.3390/en9010053 (cit. on p. 47).

[70] K. Wu and C. Cheng, "Interface Charges between Insulating Materials," *IEEE Transactions on Dielectrics and Electrical Insulation*, vol. 24, no. 4, pp. 2633–2642, 2017. DOI: 10.1109/TDEI.2017.006442 (cit. on p. 47).

[71] B. R. Nyberg, K. Herstad, and K. Bjørløw-Larsen, "Numerical Methods for Calculation of Electrical Stresses in HVDC Cables with Special Application to the Skagerrak Cable," *IEEE Transactions on Power Apparatus and Systems*, vol. 94, no. 2, pp. 491–497, Mar. 1975. DOI: 10.1109/TPAS.1975.31876 (cit. on p. 48).

[72] G. Håkonseth and E. Ildstad, "Steady-State Electric Field and Conductivity in Mass-Impregnated HVDC Cable Insulation," in *2018 IEEE 2nd International Conference on Dielectrics (ICD)*, Jul. 2018. DOI: 10.1109/ICD.2018.8468346 (cit. on pp. 49, 97, 115).

[73] A. A. Zaky, H. Tropper, and H. House, "Electrical Conduction in Organic Liquids," *British Journal of Applied Physics*, vol. 14, no. 10, pp. 651–656, 1963. DOI: 10.1088/0508-3443/14/10/313 (cit. on pp. 49, 50, 86).

[74] K. C. Kao, *Dielectric Phenomena in Solids: With Emphasis on Physical Concepts of Electronic Processes*. San Diego / London: Elsevier Academic Press, 2004 (cit. on p. 49).

[75] K. Wu, Q. Zhu, H. Wang, X. Wang, and S. Li, "Space Charge Behavior in the Sample with Two Layers of Oil-Immersed-Paper and Oil," *IEEE Transactions on Dielectrics and Electrical Insulation*, vol. 21, no. 4, pp. 1857–1865, Aug. 2014. DOI: 10.1109/TDEI.2014.004241 (cit. on p. 49).

[76] M. Hilaire, C. Marteau, and R. Tobazeon, "Apparatus Developed for Measurement of the Resistivity of Highly Insulating Liquids," *IEEE Transactions on Electrical Insulation*, vol. 23, no. 4, pp. 779–789, Aug. 1988. DOI: 10.1109/14.7352 (cit. on pp. 50, 57, 58, 86).

[77] P. Gazzana Priaroggia, P. Metra, and G. Miramonti, "Research on the Breakdown under Type Test of Non-Pressurized Paper-Insulated HVDC Cables," *European Transactions on Electrical Power*, vol. 3, no. 5, pp. 321–330, Sep. 1, 1993. DOI: 10.1002/etep.4450030502 (cit. on pp. 51, 85).

[78] A. Küchler *et al.*, "Evaluation of Conductivities and Dielectric Properties for Highly Stressed HVDC Insulating Materials," presented at the Cigré Session 2010, Cigré, 2010 (cit. on pp. 57, 58, 75).

[79] M. Liebschner, *Interaktion von Ölspalten und fester Isolation in HVDC-Barrierensystemen*, ser. Fortschritt-Berichte VDI. Düsseldorf: VDI-Verlag, 2009 (cit. on pp. 58, 75).

[80] U. Gäfvert, A. Jaksts, C. Törnkvist, and L. Walfridsson, "Electrical Field Distribution in Transformer Oil," *IEEE Transactions on Electrical Insulation*, vol. 27, no. 3, pp. 647–660, Jun. 1992. DOI: 10.1109/14.142730 (cit. on p. 75).

[81] U. Gäfvert, O. Hjortstam, Y. Serdyuk, C. Törnkvist, and L. Walfridsson, "Modeling and Measurements of Electric Fields in Composite Oil/Cellulose Insulation," in *2006 IEEE Conference on Electrical Insulation and Dielectric Phenomena*, Oct. 2006, pp. 154–157. DOI: 10.1109/CEIDP.2006.312084 (cit. on p. 75).

[82] M. E. Zein Eldine, A. A. Zaky, R. Hawley, and M. C. Cullingford, "Influence of Insulating Films on Conduction," *Proceedings of the Institution of Electrical Engineers*, vol. 112, no. 3, pp. 580–585, Mar. 1965. DOI: 10.1049/piee.1965.0098 (cit. on p. 86).

[83] Y. Sha, Y. Zhou, D. Nie, Z. Wu, and J. Deng, "A Study on Electric Conduction of Transformer Oil," *IEEE Transactions on Dielectrics and Electrical Insulation*, vol. 21, no. 3, pp. 1061–1069, Jun. 2014. DOI: 10.1109/TDEI.2014.6832249 (cit. on p. 86).

[84] Cigré Working Group 21.02, "Recommendations for Tests of Power Transmission DC Cables for a Rated Voltage up to 800 kV," *Electra*, vol. 189, pp. 39–55, Apr. 2000 (cit. on p. 86).

[85] E. Occhini and G. Maschio, "Transient and Steady-State Electrical Conductivity of Paper Impregnated with Synthetic Oil as Insulation for Extra-High-Voltage Direct-Current Oil-Filled Cables," in *Conference on Electrical Insulation Dielectric Phenomena — Annual Report 1967*, Sep. 1967, pp. 178–186. DOI: 10.1109/CEIDP.1967.7736340 (cit. on p. 87).

[86] G. Håkonseth, E. Ildstad, and K. M. Furuheim, "Local Electric Field in Mass-Impregnated HVDC Cables," in *Proceedings of the Nordic Insulation Symposium*, vol. 25, 2017. DOI: 10.5324/nordis.v0i25.2351 (cit. on pp. 108, 115).

ISBN 978-82-326-5030-9 (printed ver.)
ISBN 978-82-326-5031-6 (electronic ver.)
ISSN 1503-8181

NTNU

Norwegian University of
Science and Technology